USDOT Tier 1
University Transportation Center
on Improving Rail Transportation
Infrastructure Sustainability and Durability

Final Report UD-10

DETERMINING TRACK-INDUCED LATERAL THERMAL EXPANSION FORCES ON A CURVED RAILWAY BRIDGE

By

Jubair Ahmad Musazay
Graduate Research Assistant
Department of Civil and Environmental Engineering
University of Delaware
musazay@udel.edu

Professor Allan Zarembski PhD, PE, FASME, Hon. Mbr. AREMA
Professor and Director of Railroad Engineering and Safety Program
Department of Civil Engineering and Environmental
University of Delaware
dramz@udel.edu

Dr. Joseph Palese, PhD, MBA, PE
Senior Scientist
Department of Civil Engineering and Environmental
University of Delaware
palesezt@udel.edu

October 5, 2020

Grant Number: 69A3551747132

DISCLAIMER

The contents of this report reflect the views of the authors, who are responsible for the facts and the accuracy of the information presented herein. This document is disseminated in the interest of information exchange. The report is funded, partially or entirely, by a grant from the U.S. Department of Transportation's University Transportation Centers Program. However, the U.S. Government assumes no liability for the contents or use thereof.

ABSTRACT

This research studies the development of lateral thermal expansion forces[1] on a curved railway track in general and specifically when the curved track is located on a railway bridge. Geometric alignment of railways often requires railway tracks to be curved for alignment of the right of way as well as safety and ride quality. This curvature is usually defined either by a radius of curvature or by a corresponding degree of curvature. Curved tracks constitute a higher level of complexity in the track's analysis and design process. Particularly, presence of curvature on the track introduces multiple sources of force in the lateral (radial) direction, including, but not limited to, lateral thermal expansion, centrifugal action, lateral components of vertical loads, hunting and nosing effects of locomotives, and vehicle curving dynamics. When a curved railway track is constructed on the ground like most curved tracks are, these forces are absorbed by the ballast shoulder and tie-ballast friction or interlocking. However, when a curved track is carried by a curved railway bridge, these forces will be transferred to the bridge in the lateral direction. While some of these forces are well known and defined, such as centrifugal forces, others are not as well known or analyzed. This is particularly true in the case of lateral forces generated by constrained thermal expansion on curves. To bridge this gap, this research studies the development of track-induced lateral thermal expansion forces on a curved railway bridge. In this research, the curved track is assumed to be an arbitrary arc section of a circular track and is modeled as an equivalent idealized circular ring for analysis. Owing to its importance, three analytical methods are used such as 1) Timoshenko thermoelastic stress analysis in cylindrical coordinate system, 2) Application of the mechanics of thin wall cylinders and 3) adaptation of a variational calculus formulation method from a previous comparable study. A fourth analysis, consisting of a finite element model using a commercially available finite element software package was also performed and used to compare and validate the results from these three methods. The results show good agreement between the four analytical approaches with respect to the generated lateral forces.

[1] The thermal forces referred to here-in are due to constrained thermal expansion of the rail, i.e. when the rail is welded in track and is unable to expand and contract to relive the building of thermal forces in the rail.

TABLE OF CONTENTS

LIST OF FIGURES

LIST OF FIGURES

LIST OF APPENDIX FIGURES

LIST OF TABLES (APPENDIX)

INTRODUCTION

Introduction to Curved Railway Track

A section of a railway track that has a radius of curvature is referred to as a curved track. The curvature of the track can be defined either by its radius of curvature or, as commonly used in North American railway systems, by its degree of curvature which is the measure of a central angle to the ends of a chord with a predetermined length in a circular section. In North America, for railroad geometric design purposes, this chord length is conventionally taken as 100 ft (Figure 1) with the resulting relationship between degree of curvature and radius of curvature given by the equation:

$$D = 5730/R$$

Where,
D is the degree of curvature (in degrees)
R is the radius of curvature in feet.

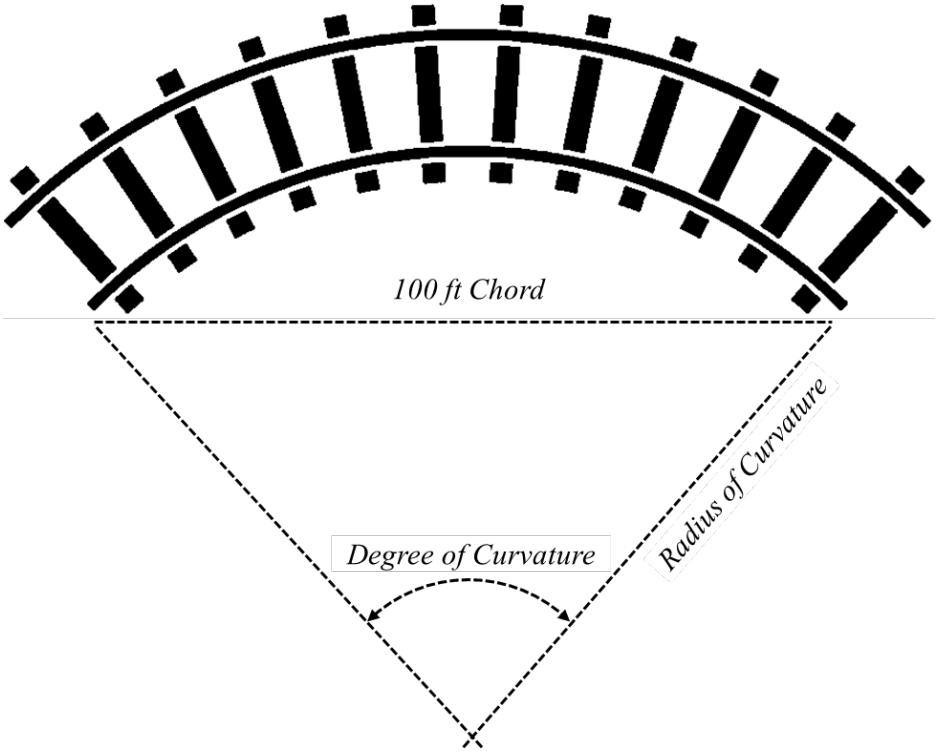

Figure 1: A representation of a typical curved track

Likewise, a railway bridge carrying a curved track is referred to as a curved railway bridge. Sometimes, a curved railway bridge is made up of straight girders, curved in overall profile (Figure 2).

Geometric alignment requirements for railway right of way often requires railway tracks and bridges to be curved by a certain degree of curvature. Unlike straight bridges, their curved

counterparts experience a combined action of forces that introduce further levels of complexity in their analysis and design process (Deng et al. 2015, Unsworth 2010, Nakai, and Yoo 1988, Heins and Firmage 1979, Shanmugam et al. 2003, Practical Guide to Railway Engineering 2003). Additionally, when a curved bridge carries a curved railway track (or tracks), it will be required to withstand further load complexities that are induced by the curved track itself. Particularly, presence of curvature on the track introduces multiple sources of force in the lateral (radial) direction, including, but not limited to the following:

1. Lateral forces due to constrained thermal expansion
2. Vehicle centrifugal action
3. Lateral components of vertical vehicle dynamic loads
4. Hunting and nosing effects of locomotives, and
5. Vehicle curving dynamics.

This study will be limited to the first of these, lateral forces due to constrained thermal expansion. When a curved railway track is constructed on the ground like most curved tracks are, these forces are absorbed by the track lateral resistance mechanism such as ballast shoulder and tie-ballast friction and interlocking. However, when a curved track is carried by a curved railway bridge, these forces will be transferred (partially or fully) to the bridge in the lateral direction through track-bridge connection and are considered in the bridge design process. While some of these forces are well known and defined, such as centrifugal forces, others are not as well known or analyzed. This is particularly true in the case of lateral forces generated by constrained thermal expansion on curves. To bridge this gap, this research studies the development of track-induced lateral thermal expansion forces on a curved railway bridge since current bridge design relies on approximated lateral loads (Unsworth 2010) based on engineering experience, finite-element-based modeling and simulations and where applicable. While railway bridge designers attempt to avoid curvature on bridges or try to introduce large radii of curvature as an attempt to minimize the development of lateral forces due to curvature effects, circumstances sometimes require the presence of a significant degree of curvature. This in turn can result in the generation of significant levels of lateral force.

In this research, the curved track is assumed to be an arbitrary arc section of a circular track and is modeled as an equivalent idealized circular ring for analysis. Owing to its importance, three analytical methods are used such as 1) Timoshenko thermoelastic stress analysis in cylindrical coordinate system, 2) Application of mechanics of thin wall cylinders and 3) adaptation of a variational formulation method from a previous comparable study. A fourth analysis, consisting of a finite element model using a commercially available finite element software package was also performed and used to compare and validate the results from these three methods. It should be noted that although a curved track usually consists of a circular section with constant radius and two transition sections on each end of the curved section which transition into the tangent (straight) track sections, the methodology used in this study is only applied to the circular section of the curve.

Research Objectives

The primary objective of this research is to determine the track-induced lateral thermal expansion forces on a curved railway bridge. This is done by using three different analytical approaches and is then compared with and validated to a finite element model through a parametric study.

Research Scope

The scope of this research is limited only to the determination of lateral forces due to thermal expansion of a curved track. These forces are of particular interest in the design of curved railway bridges. Additionally, defining the dynamic impact factor for the calculated lateral load, load transfer path from the track to the bridge and load transfer mechanism are also within the scope of this research.

Introduction to Curved Railway Bridge

Generally, curved railway bridges are girder bridges (steel or concrete) with common cross sections such as box, I and T. As curved bridges also experience large torsional loads (Unsworth 2010) box girders are often preferred and typically are constructed as segmental prestressed concrete box girder bridges. Curved bridges are made up of either curved girders or straight girders, curved in plan (Figure 2). There is also precedence for curved cable stayed railway bridges, however, for the purpose of this study, it is assumed that the track is carried by a curved girder bridge.

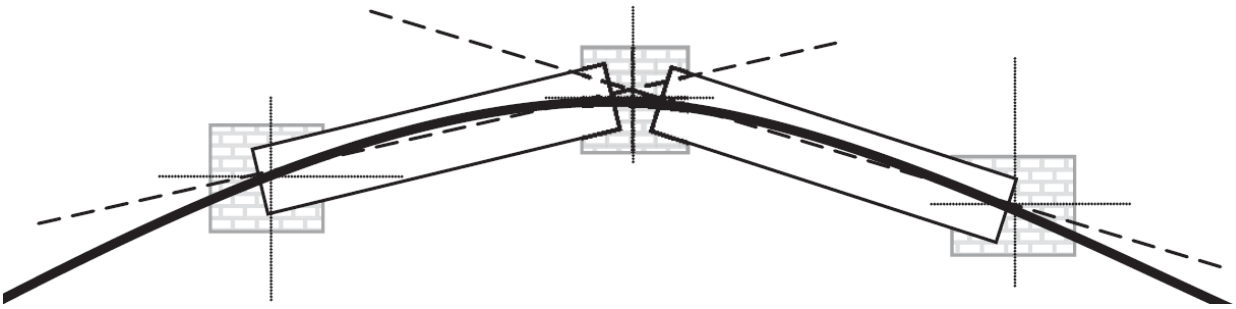

Figure 2: Plan of a curved track (bold line) carried by straight girder bridge curved in plan (Unsworth 2010).

Bridge-Track Connection

Load transfer from a track to the bridge is affected by how the track is connected to the bridge which is typically done by various methods. Commonly practiced methods are listed below (Practical Guide to Railway Engineering, 2003). It should be noted, however, that regardless of the connection method, the forces will still develop on the track and transferred to the bridge. The lateral load transfer path and transfer mechanism will depend on types of bridge–track connection systems. For the purpose of this research, it is assumed that the track is connected to the bridge slab with direct fixation and the developed load is fully transferred to the bridge.

Open Deck Bridge

In an open deck railway bridge, the track is connected directly to the bridge girders. Open deck bridges provide free drainage and better short to medium term economics (Practical Guide to Railway Engineering 2003) and hence may be construed as an attractive design option for certain projects. Should this be the case, it should be noted that in such bridges, the lateral thermal loads (and other lateral loads that are not considered in this study) are directly and fully transferred to the girder and therefore the girder design should incorporate provision to resist the total of lateral loads developed in this study.

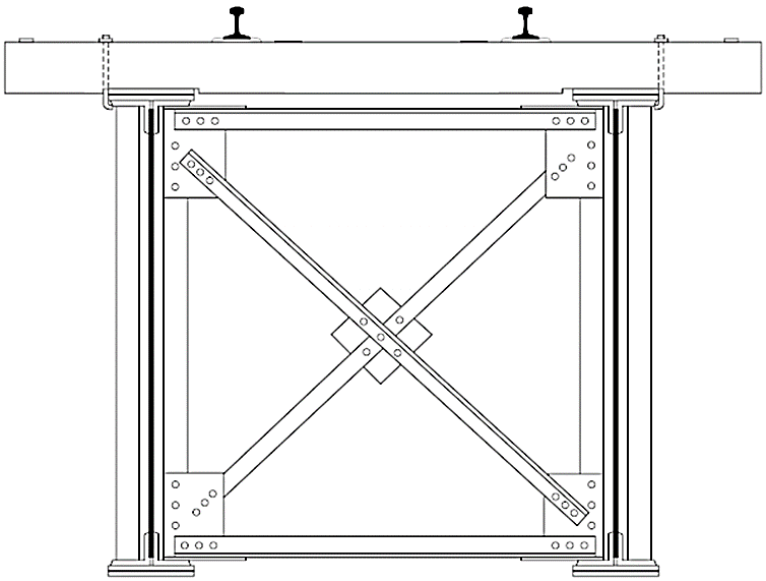

Figure 3: Open deck bridge [6]

Slab Track with Direct Fixation

Slab track with direct fixation is another option that is used in railway bridges. In this type of bridges, the loads are transferred to the slab through the fastening system and subsequently to the girder. The slab may be designed so to resist some of the loads and transfer the remaining to the next medium, in this case, girder.

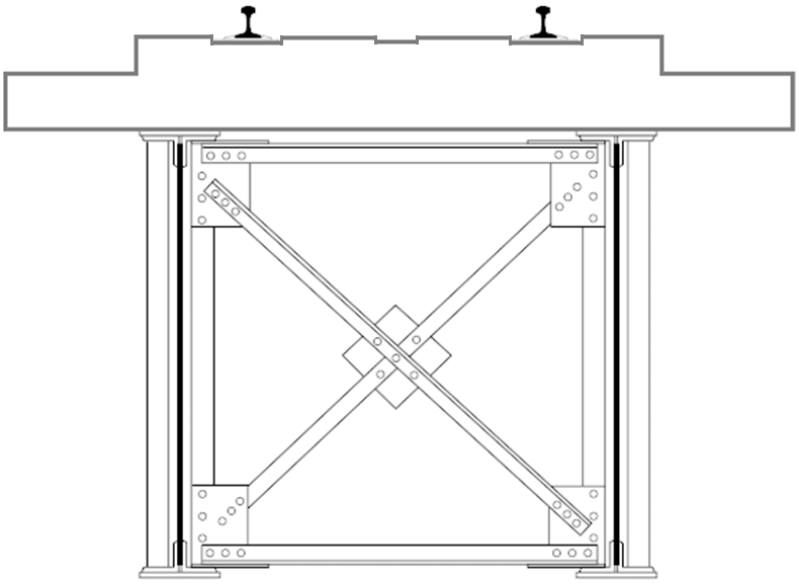

Figure 4: Slab track with direct fixation [6]

Ballasted Track

Regular ballasted tracks are also used on railway bridges. A “ballast plate” is placed or constructed on the bridge deck and the track sits on the ballast similar to a regular ballasted track. Likewise, resistance to the lateral movement of the track is provided by the ballast shoulder and ballast-tie friction. In this type, the track is “discretely connected” with the bridge.

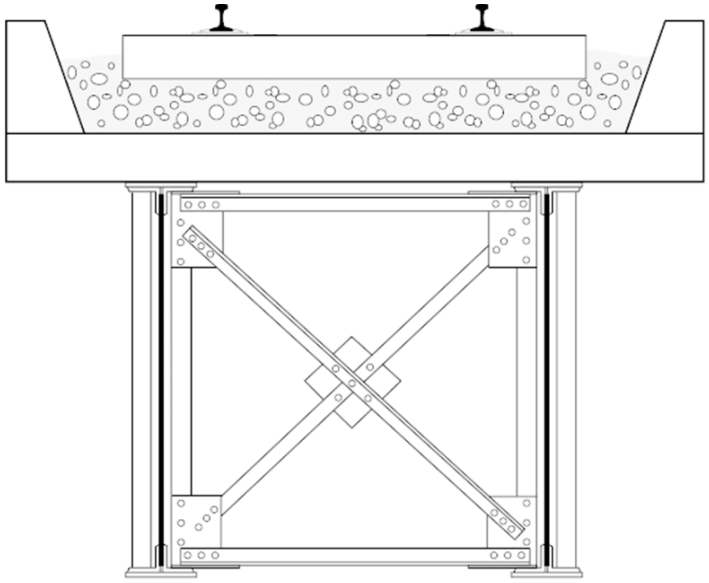

Figure 5: Ballasted track [6]

METHODOLOGY

Problem Formulation

The overarching methodology used to conduct this research is categorized into five general steps as shown in Figure 6 below. Initially, the circular track problem is formulated based on other mechanical principles (ring analogy and thin walled cylinder). Subsequently, simplifications such as taking constant cross section, defining height and width of the ring are made. Then, the developed models are compared with previous comparable literature and eventually verified with the finite element model also developed in this activity.

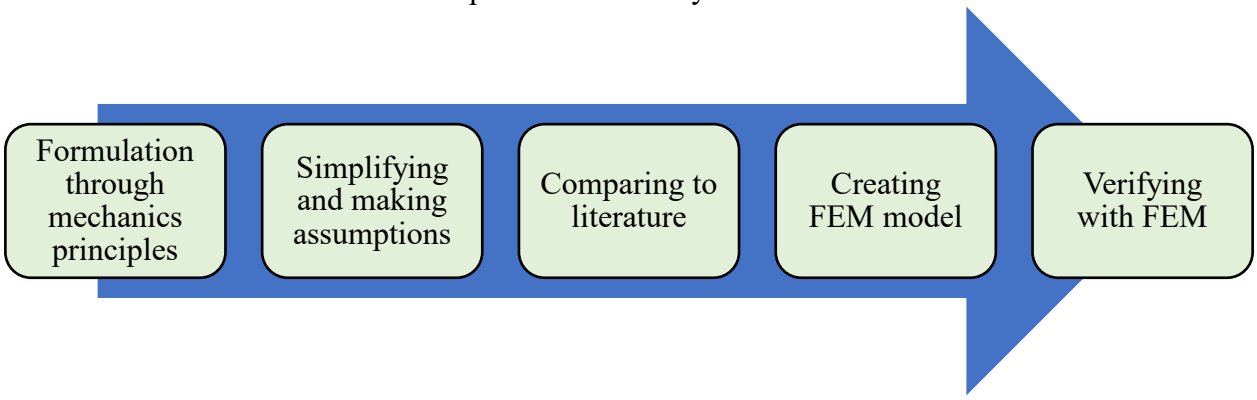

Figure 6: The research overall approach

Idealized Circular Track

As mentioned above, a curved track consists of a circular section, a transition (a.k.a. spiral or clothoid) and a tangent section. The methods and equations used in this study are applied only to the circular section of the curve. To formulate the problem, the circular section of the curve is assumed to be an arbitrary arc section of a circular track (Figure 7) with a constant cross section and radius subjected to a temperature difference. This can be modeled as an equivalent idealized circular ring, and therefore, analyzed for lateral forces (radial direction), axial forces (hoop or circumferential direction) and as well as vertical forces (vertical direction) due to thermal expansion. The thermal forces in the vertical and circumferential directions are not covered in this study. The methods presented in the following sections are used to determine forces for lateral direction.

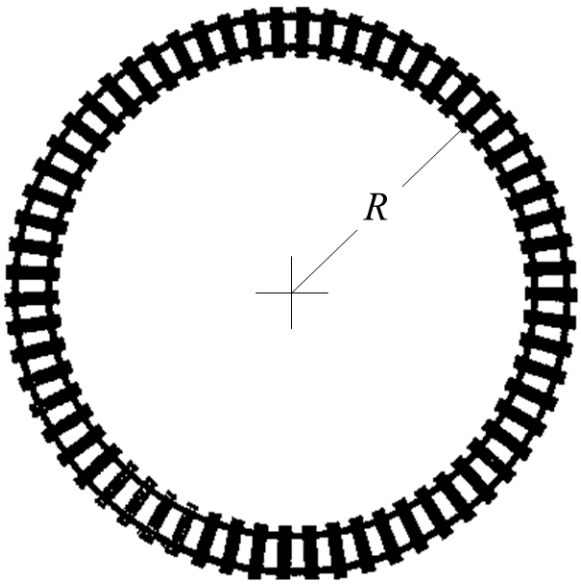

Figure 7: The curved track is taken as an arbitrary arc section of a circular track

For each of the aforementioned methods, the governing equation is initially derived for free lateral thermal expansion as a function of force in the radial direction, assuming that the idealized ring is initially allowed to expand freely as it is subjected to a temperature difference. Subsequently, the radial expansion is set to zero to simulate a condition whereby a continuous resisting medium is confining the idealized ring from radial expansion along the circumference. This agrees with the way the fastening system is restraining or confining the rail from lateral displacement or the way ballast resistance is restraining the track against lateral displacement.

Confining the idealized ring from radial expansion results in the development of pressure between the idealized ring and the resisting medium. Since the height of the idealized ring could be defined (e.g. taken as the height of the base of the rail for the parametric study under this research), the developed pressure could be converted into force per unit length (a.k.a. ring load), uniformly distributed along the idealized ring as shown in Figure 8a and 8b. For an actual track, since the resisting medium is not continuous but discrete (e.g. fastening system), the calculated force per unit length may be multiplied by the fasters longitudinal spacing (sleeper spacing) to obtain the lateral force on each of the fasteners.

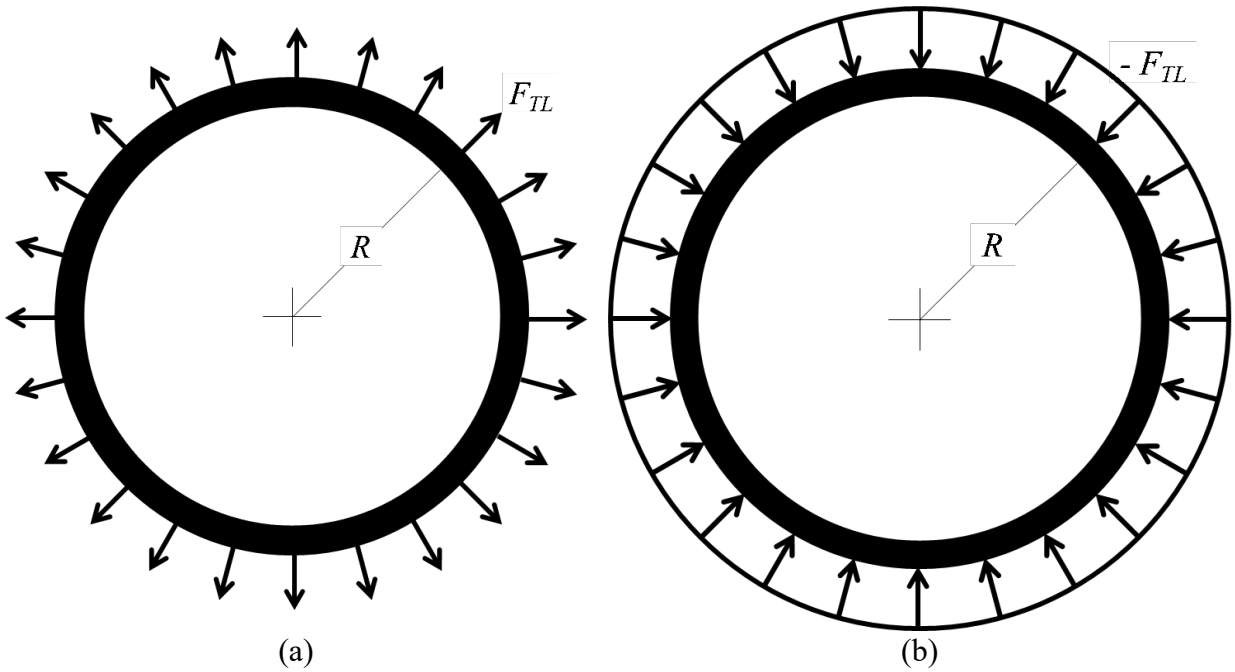

Figure 8: (a) Lateral forces shown as F_{TL}, and (b) lateral resistance shown as reaction

It should be noted that, this may be construed as a conservative approach because when a curved railway bridge is subjected to a temperature difference, the rails are not the only part of the structure that will experience thermal expansion. Other members that the rails are connected to, such as fastening system and bridge deck, will also experience thermal expansion and hence the actual magnitude of the developed pressure between the idealized ring and the resisting medium could be smaller as they will expand relative to one another.

Analytical Methods

In this study, three analytical methods are used to calculate the lateral forces due to thermal expansion of curved railway tracks. The results from these methods are compared against one another through a wide range of parametric studies and are then verified by their equivalent finite element model using a commercially available finite element software package. The methods are listed below.

1. Timoshenko thermoelastic stress analysis in cylindrical coordinate system (developed for this research)
2. Applying the concept of mechanics of thin wall cylinders, and
3. Adaptation of a variational formulation method from a previous comparable study on the thermal buckling of a curved railway track which also includes a section for analysis of lateral thermal expansion before buckling. This section of the study is used to back calculate the distribution of lateral thermal forces per unit length (as in ballast resistance) assuming that thermal expansion is confined in the lateral direction

These are then compared with a finite element model that is also developed as part of this activity.

Timoshenko Thermoelastic Stress Analysis

In this section, the idealized ring is analyzed using Timoshenko thermoelastic stress analysis in a cylindrical coordinate system (r, θ, z) as shown in Figure 9a. A small element from the idealized ring is considered and the stresses on the element is shown for the analysis (Figure 9b). Subsequently, the governing equations that are presented under this section are developed based on the assumptions, principles and relationships presented in (Timoshenko and Goodier, 1951, Boresi et al. 2011, Barron and Barron 2013, Eslami et al. 2018, Blosser 1988, Fukui and Fukui 1969). It should be noted that these referenced sources here do not include a direct or detailed analysis and hence the derivation of the governing equations is the result of a comprehensive study and correlation of the methods presented in these sources.

Using Timoshenko stress analysis, initially the equations are developed based on a single idealized circular ring. Subsequently, to simulate fastener or ballast resistance (Figure 10), a double ring approach is used where an outer idealized ring is confining an inner idealized ring from expansion. This approach creates lateral stresses at the contact surface of both rings and this stress can be converted to force per unit length or force per fastening system in the lateral direction.

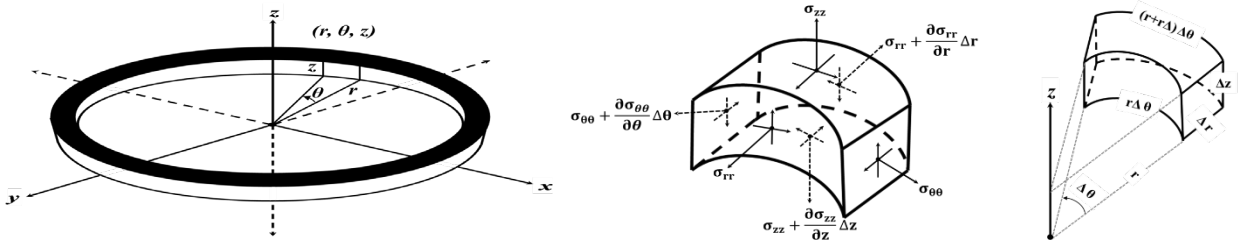

Figure 9: (a) An idealized ring shown in a cylindrical coordinate, and (b) a small element considered in the idealized ring for the stress analysis *(Shear stresses and body forces are not shown in the figure)*

Considering the small element in the idealized ring in Figure 8, the force equilibrium equations for radial, circumferential, and vertical directions can be written as follows:

$$\sum \mathrm{F_r} = 0$$

$$\frac{\partial \sigma_{rr}}{\partial r} + \frac{1}{r}\frac{\partial \sigma_{\theta r}}{\partial \theta} + \frac{\partial \sigma_{rz}}{\partial z} + \frac{\sigma_{rr} - \sigma_{\theta\theta}}{r} + \mathrm{F_r} = 0 \tag{1}$$

$$\sum \mathrm{F_z} = 0$$

$$\frac{\partial \sigma_{rz}}{\partial r} + \frac{1}{r}\frac{\partial \sigma_{\theta z}}{\partial \theta} + \frac{\partial \sigma_{zz}}{\partial z} + \frac{\sigma_{rz}}{r} + \mathrm{F_z} = 0 \tag{2}$$

$$\sum \mathrm{F_\theta} = 0$$

$$\frac{\partial \sigma_{r\theta}}{\partial r} + \frac{1}{r}\frac{\partial \sigma_{\theta\theta}}{\partial \theta} + \frac{\partial \sigma_{\theta z}}{\partial z} + 2\frac{\sigma_{r\theta}}{r} + \mathrm{F_\theta} = 0 \tag{3}$$

For a railway track however, the stresses in the vertical direction are of no consequence here and can be ignored. This will significantly simplify the problem and a polar coordinate system (r and θ) can be used to analyze the radial and tangential stresses. In a polar coordinate system, the vertical components of Equation (1) and (3) and the entire Equation (2) will be omitted which will result in Equations (4) and (5).

$$\frac{\partial \sigma_{rr}}{\partial r} + \frac{1}{r}\frac{\partial \sigma_{\theta r}}{\partial \theta} + \frac{\sigma_{rr} - \sigma_{\theta\theta}}{r} + F_r = 0 \tag{4}$$

$$\frac{\partial \sigma_{r\theta}}{\partial r} + \frac{1}{r}\frac{\partial \sigma_{\theta\theta}}{\partial \theta} + 2\frac{\sigma_{r\theta}}{r} + F_\theta = 0 \tag{5}$$

Furthermore, since the focus of this study is to analyze lateral stresses (radial direction), only Equation (4) will be used. Equating the body force Fr to zero as there are no body forces present, the following relationships (Airy Stress Functions) satisfy Equation (4).

$$\sigma_{rr} = \frac{1}{r}\frac{\partial \varphi}{\partial r} + \frac{1}{r^2}\frac{\partial^2 \varphi}{\partial \theta^2} \tag{6}$$

$$\sigma_{\theta\theta} = \frac{\partial^2 \varphi}{\partial r^2} \tag{7}$$

$$\sigma_{\theta r} = \frac{1}{r^2}\frac{\partial \varphi}{\partial \theta} - \frac{1}{r}\frac{\partial^2 \varphi}{\partial r\, \partial \theta} = -\frac{\partial}{\partial r}\left(\frac{1}{r}\frac{\partial \varphi}{\partial \theta}\right) \tag{8}$$

Using Timoshenko approach, to yield a possible solution or a stress function, the function must satisfy the conditions of compatibility. In the next steps, the general condition of compatibility from a Cartesian coordinate system is transformed to a polar coordinate system following Timoshenko approach. Hence,

$$\frac{\partial^4 \varphi}{\partial x^4} + 2\frac{\partial^4 \varphi}{\partial x^2\, \partial y^2} + \frac{\partial^4 \varphi}{\partial y^4} = 0 \tag{9}$$

$$r^2 = x^2 + y^2 \tag{10}$$

$$\theta = \arctan\left(\frac{y}{x}\right) \tag{11}$$

$$\frac{\partial r}{\partial x} = \frac{x}{r} = \cos\theta, \quad \frac{\partial r}{\partial y} = \frac{y}{r} = \sin\theta \tag{12}$$

$$\frac{\partial \theta}{\partial x} = -\frac{y}{r^2} = -\frac{\sin\theta}{r}, \quad \frac{\partial \theta}{\partial y} = \frac{x}{r^2} = \frac{\cos\theta}{r} \tag{13}$$

$$\frac{\partial \varphi}{\partial x} = \frac{\partial \varphi}{\partial r}\frac{\partial r}{\partial x} + \frac{\partial \varphi}{\partial \theta}\frac{\partial \theta}{\partial x} = \frac{\partial \varphi}{\partial r}\cos\theta - \frac{1}{r}\frac{\partial \varphi}{\partial \theta}\sin\theta \tag{14}$$

$$\begin{aligned}\frac{\partial^2 \varphi}{\partial x^2} &= \left(\frac{\partial}{\partial r}\cos\theta - \frac{1}{r}\sin\theta\frac{\partial}{\partial \theta}\right)\left(\frac{\partial \varphi}{\partial r}\cos\theta - \frac{1}{r}\frac{\partial \varphi}{\partial \theta}\sin\theta\right) \\ &= \frac{\partial^2 \varphi}{\partial r^2}\cos^2\theta - 2\frac{\partial^2 \varphi}{\partial \theta\ \partial r}\frac{\sin\theta\ \cos\theta}{r} + \frac{\partial \varphi}{\partial r}\frac{\sin^2\theta}{r} + 2\frac{\partial \varphi}{\partial \theta}\frac{\sin\theta\ \cos\theta}{r^2} \\ &\quad + \frac{\partial^2 \varphi}{\partial \theta^2}\frac{\sin^2\theta}{r^2}\end{aligned} \tag{15}$$

$$\frac{\partial^2 \varphi}{\partial y^2} = \frac{\partial^2 \varphi}{\partial r^2}\sin^2\theta + 2\frac{\partial^2 \varphi}{\partial \theta\ \partial r}\frac{\sin\theta\ \cos\theta}{r} + \frac{\partial \varphi}{\partial r}\frac{\cos^2\theta}{r} - 2\frac{\partial \varphi}{\partial \theta}\frac{\sin\theta\ \cos\theta}{r^2} + \frac{\partial^2 \varphi}{\partial \theta^2}\frac{\sin^2\theta}{r^2} \tag{16}$$

Adding together Equations (15) and (16), the following equation is obtained.

$$\frac{\partial^2 \varphi}{\partial x^2} + \frac{\partial^2 \varphi}{\partial y^2} = \frac{\partial^2 \varphi}{\partial r^2} + \frac{1}{r}\frac{\partial \varphi}{\partial r} + \frac{1}{r^2}\frac{\partial^2 \varphi}{\partial \theta^2} \tag{17}$$

On the other hand, using the identity Equation (17), the compatibility equation for Cartesian coordinate system which is given as Equation (9) will be reduced to that of a polar coordinate system, given below as Equation (18).

$$\frac{\partial^4 \varphi}{\partial x^4} + 2\frac{\partial^4 \varphi}{\partial x^2\ \partial y^2} + \frac{\partial^4 \varphi}{\partial y^4} = \left(\frac{\partial^2}{\partial x^2} + \frac{\partial^2}{\partial y^2}\right)\left(\frac{\partial^2 \varphi}{\partial x^2} + \frac{\partial^2 \varphi}{\partial y^2}\right) \tag{18}$$

$$\left(\frac{\partial^2}{\partial r^2} + \frac{1}{r}\frac{\partial}{\partial r} + \frac{1}{r^2}\frac{\partial^2}{\partial \theta^2}\right)\left(\frac{\partial^2 \varphi}{\partial r^2} + \frac{1}{r}\frac{\partial \varphi}{\partial r} + \frac{1}{r^2}\frac{\partial^2 \varphi}{\partial \theta^2}\right) = 0 \tag{19}$$

When evaluating the stresses in the radial direction only, the stress function will only depend on r and hence the compatibility equation becomes

$$\begin{aligned}\left(\frac{d^2}{dr^2} + \frac{1}{r}\frac{d}{dr}\right)\left(\frac{d^2 \varphi}{dr^2} + \frac{1}{r}\frac{d\varphi}{dr}\right) &= 0 \\ \frac{\partial^4 \varphi}{\partial r^4} + \frac{2}{r}\frac{\partial^3 \varphi}{\partial r^3} - \frac{1}{r^2}\frac{\partial^2 \varphi}{\partial r^2} + \frac{1}{r^3}\frac{\partial \varphi}{\partial r} &= 0\end{aligned} \tag{20}$$

Equation (20) which is now an ordinary differential equation has a solution in the form of Equation (21) that, depending on the boundary condition, maybe used to approximate the radial stresses and displacement for a given problem in polar coordinate system.

$$\varphi = r^n \tag{21}$$

After substituting Equation (21) into Equation (20), the following general solution is obtained.

$$\varphi = \mathrm{A}\ln(\mathrm{r}) + \mathrm{B}\,\mathrm{r}^2\ln(\mathrm{r}) + \mathrm{C}\,\mathrm{r}^2 + \mathrm{D} \tag{22}$$

Substituting Equation (22) into Equations (6), (7) and (8) will result in the following equations:

$$\begin{aligned}\sigma_{\mathrm{rr}} = \frac{1}{\mathrm{r}}\frac{\partial}{\partial \mathrm{r}}[\mathrm{A}\ln(\mathrm{r}) + \mathrm{B}\,\mathrm{r}^2\ln(\mathrm{r}) + \mathrm{C}\,\mathrm{r}^2 + \mathrm{D}] \\ + \frac{1}{\mathrm{r}^2}\frac{\partial^2}{\partial\theta^2}[\mathrm{A}\ln(\mathrm{r}) + \mathrm{B}\,\mathrm{r}^2\ln(\mathrm{r}) + \mathrm{C}\,\mathrm{r}^2 + \mathrm{D}] \\ = \frac{\mathrm{A}}{\mathrm{r}^2} + 2\mathrm{B}\ln(\mathrm{r}) + \mathrm{B} + 2\mathrm{C}\end{aligned} \tag{23}$$

$$\sigma_{\theta\theta} = \frac{\partial^2}{\partial \mathrm{r}^2}[\mathrm{A}\ln(\mathrm{r}) + \mathrm{B}\,\mathrm{r}^2\ln(\mathrm{r}) + \mathrm{C}\,\mathrm{r}^2 + \mathrm{D}] = -\frac{\mathrm{A}}{\mathrm{r}^2} + 2\mathrm{B}\ln(\mathrm{r}) + 3\mathrm{B} + 2\mathrm{C} \tag{24}$$

$$\sigma_{\mathrm{r}\theta} = -\frac{\partial}{\partial \mathrm{r}}\left(\frac{1}{\mathrm{r}}\frac{\partial}{\partial\theta}[\mathrm{A}\ln(\mathrm{r}) + \mathrm{B}\,\mathrm{r}^2\ln(\mathrm{r}) + \mathrm{C}\,\mathrm{r}^2 + \mathrm{D}]\right) = 0 \tag{25}$$

Now, strain in polar coordinate system, Equation (26) through Equation (28) can be used for the calculations of displacement.

$$\varepsilon_{\mathrm{rr}} = \frac{\partial u_{rr}}{\partial \mathrm{r}} \tag{26}$$

$$\varepsilon_{\theta\theta} = \frac{u_{rr}}{\mathrm{r}} + \frac{1}{r}\frac{\partial u_{\theta\theta}}{\partial\theta} \tag{27}$$

$$\varepsilon_{r\theta} = \frac{1}{2}\left(\frac{\partial u_{\theta\theta}}{\partial \mathrm{r}} - \frac{u_{\theta\theta}}{r} + \frac{1}{r}\frac{\partial u_{rr}}{\partial\theta}\right) \tag{28}$$

Taking advantage of the stress – strain relationship for an isotropic material and Hooke's Law, Equations (26) – (28) can also be written as below.

$$\varepsilon_{\mathrm{rr}} = \frac{1}{E}(\sigma_{\mathrm{rr}} - \nu\,\sigma_{\theta\theta}) \tag{29}$$

$$\varepsilon_{\theta\theta} = \frac{1}{E}(\sigma_{\theta\theta} - \nu\,\sigma_{\mathrm{rr}}) \tag{30}$$

$$\varepsilon_{r\theta} = \frac{1+\nu}{E}\sigma_{\mathrm{r}\theta} \tag{31}$$

By equating Equations (26) and (27) with Equations (29) and (30) respectively and solving the resulting equations subsequently, equations for calculation of displacement in radial direction can be determined as shown below.

$$\varepsilon_{rr} = \frac{\partial u_{rr}}{\partial r} = \frac{1}{E}\left(\frac{A\,(1+\nu)}{r^2} + 2\,C\,(1-\nu) + B(1-\nu)[2\,ln(r)+1] - 2\,\nu\,B\right) \tag{32}$$

$$\varepsilon_{\theta\theta} = \frac{u_{rr}}{r} = \frac{1}{E}\left(-\frac{A\,(1+\nu)}{r^2} + 2\,C\,(1-\nu) + B(1-\nu)[2\,ln(r)+1] - 2\;B\right) \tag{33}$$

And the two expressions for the radial displacement produced by Equations (32) and Equation (33) are given as follows:

$$u_{rr1} = \frac{1}{E}\left(-\frac{A\,(1+\nu)}{r} + 2\,C\,(1-\nu)\,r + B(1-\nu)[2\,r\,ln(r) - r] - 2\,\nu\,B\,r\right) \tag{34}$$

$$u_{rr2} = \frac{1}{E}\left(-\frac{A\,(1+\nu)}{r} + 2\,C\,(1-\nu)\,r + B(1-\nu)[2\,r\,ln(r) + r] + 2\;B\,r\right) \tag{35}$$

To be applied for a problem with a hole in the origin (e.g. the idealized ring), Equation (34) and (35) must be consistent and for them to be so, the constant B in the equation must be zero. Equating B to zero, the expression for stresses given in Equations (23) and Equation (24) will be reduced to the following:

$$\sigma_{rr} = \frac{A}{r^2} + 2C \tag{36}$$

$$\sigma_{\theta\theta} = -\frac{A}{r^2} + 2C \tag{37}$$

Now, Equations (34) and (35) can be used to write the expression for the radial displacement as follows:

$$u_{rr} = \frac{1}{E}\left(-\frac{A\,(1+\nu)}{r} + 2\,C\,(1-\nu)\,r\right) \tag{38}$$

On the other hand, the thermal displacement is proportional to the radial position and hence by superposition (Blosser 1988) the thermal expansion term is added to the equation above to produce the following equation for total thermal displacement.

$$u_{rr} = \frac{1}{E}\left(-\frac{A\,(1+\nu)}{r} + 2\,C\,(1-\nu)\,r\right) + r\alpha\Delta T \tag{39}$$

Now, this equation could be used to analyze a double ring approach where an outer idealized ring is confining an inner idealized ring to simulate fastener or ballast resistance (Figure 10). While using this approach for the parametric study, the thermal properties and the dimensions of the outer ring will be modified such that it does not allow thermal expansion.

This will make sure that the inner ring is fully confined and hence the desired radial stress is developed at the contact surface as the inner ring tries to expand under a temperature difference but it is restricted against such expansion. Accordingly, the radial stress in the inner radius of inner idealized ring is equal to zero and the radial stress at the interaction surface of the two rings (outer

radius of the inner ring and inner radius of the outer ring) is equal to the contact pressure, P between the two rings.

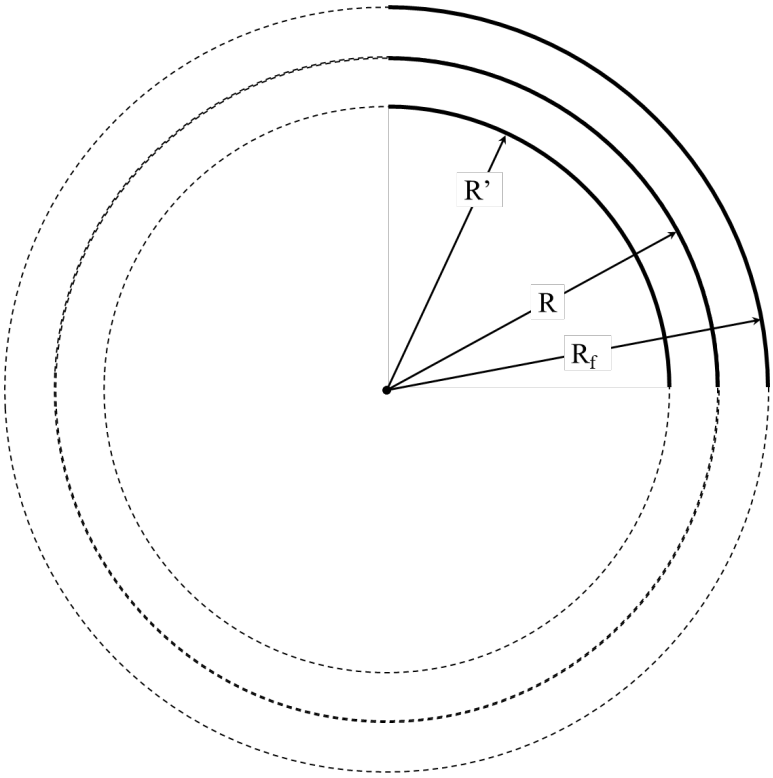

Figure 10: Idealized double rings to simulate the fastener/ballast resistance

Likewise, since the height of the idealized ring could easily be defined, the contact pressure between the rings could be converted into a ring load or force per unit length. Now, assuming that the inner radius of the inner ring is denoted with R' and the outer radius of the inner ring (also equal to inner radius of the outer ring) is denoted with R and the outer radius of the outer ring is denoted with Rf, the following boundary conditions apply.

$$\begin{aligned} at\ r\ &=\ R', \quad \sigma_{rr}(R') = 0 \\ at\ r\ &=\ R, \quad \sigma_{rr}(R) = -P \end{aligned} \tag{40}$$

Applying these boundary conditions into Equations (36) and (37), the constant A and C are found to be

$$0 = \frac{A}{R'^2} + 2C \tag{41}$$

$$-P = \frac{A}{R^2} + 2C \tag{42}$$

Equating Equations (41) and (42) and solving for A and C, the following expressions are obtained

$$A = \frac{P\,R^2\,R'^2}{R^2 - R'^2} \tag{43}$$

$$C = \left(-\frac{P\,R^2}{2\,(R^2 - R'^2)}\right) \tag{44}$$

Substituting the constant A and C into Equation (39), the resulting equation can be used to calculate for the radial displacement for the idealized ring.

$$u_{rr} = \frac{1}{E}\left(-\frac{\left(\frac{P\,R^2\,R'^2}{R^2 - R'^2}\right)(1+\nu)}{r} + 2\left(-\frac{P\,R^2}{2 * (R^2 - R'^2)}\right)(1-\nu)\,r\right) + r\alpha\Delta T \tag{45}$$

To differentiate between the inner and the outer ring, a subscript OR is used for the outer ring in Equation (47) where applicable.

$$u_{rr(outer)} = \frac{1}{E_{OR}}\left(-\frac{\left(\frac{P\,R^2\,{R_f}^2}{R^2 - {R_f}^2}\right)(1+\nu_{OR})}{r} + 2\left(-\frac{P\,R^2}{2 * (R^2 - {R_f}^2)}\right)(1-\nu_{OR})\,r\right) + r\alpha_{OR}\Delta T \tag{46}$$

Now, based on the concept of displacement compatibility between the two idealized rings, Equations (46) and (47) can be equated to solve for the interface pressure, P which is given below.

$$\frac{1}{E}\left(-\frac{\left(\frac{P\,R^2\,R'^2}{R^2 - R'^2}\right)(1+\nu)}{r} + 2\left(-\frac{P\,R^2}{2 * (R^2 - R'^2)}\right)(1-\nu)\,r\right) + r\alpha\Delta T = \frac{1}{E_{OR}}\left(-\frac{\left(\frac{P\,R^2\,{R_f}^2}{R^2 - {R_f}^2}\right)(1+\nu_{OR})}{r} + 2\left(-\frac{P\,R^2}{2 * (R^2 - {R_f}^2)}\right)(1-\nu_{OR})\,r\right) + r\alpha_{OR}\Delta T \tag{47}$$

$$P = \frac{E_{OR}\left(\left(\frac{R_f}{R}\right)^2 - 1\right)(\alpha - \alpha_{OR})(\Delta T)}{\left(\frac{R_f}{R}\right)^2(1+\nu_{OR}) + (1-\nu_{OR}) + \frac{E_{OR}}{E}\left(\frac{{R_f}^2 - R^2}{R'^2 - R^2}\right)\left(\left(\frac{R'}{R}\right)^2(1-\nu) - (1-\nu)\right)} \tag{48}$$

Equation (48) will be substituted for the interface pressure, P in Equation (46) to solve for the radial thermal displacement. Likewise, if the mentioned displacement is set to zero and the properties of the outer ring is adjusted such that it does not expands under thermal action, the

maximum interface pressure, P that can be developed between the two rings can be obtained. As previously stated, since the height of the idealized ring can easily be defined, the interface pressure, P can be converted into force per unit length and subsequently to force on a given fastener.

Mechanics of Thin Wall Cylinders

In order to derive the equations using this method, it is assumed that the idealized ring, which was discussed in previous section, is a cut section from an open ended, thin–walled cylinder with an assumed internal pressure as shown in Figure 11 below. This internal pressure causes stresses in circumferential direction of the idealized ring. To calculate this stress, assume that an arbitrary section is cut through the idealized ring such that the cross-sectional area of the thickness, t is exposed.

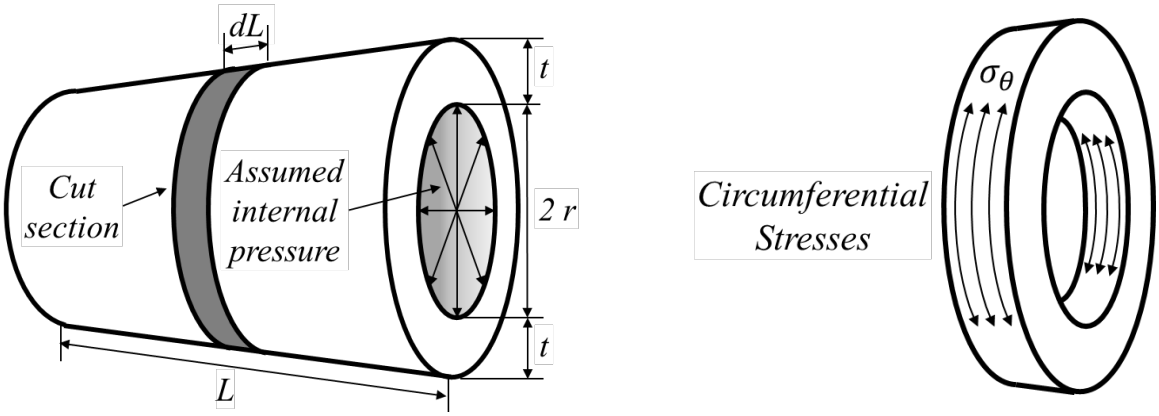

Figure 11: (a) A thin–walled cylinder, and (b) a cut idealized ring with hoop stresses

The circumferential stress (σ_θ) acts perpendicular on this area ($t \cdot dL$). Similarly, the internal pressure (P) acts on an area ($2r \cdot dL$) along the internal diameter in the opposite direction (Blosser 1988, Hibbeler 2011, Sinclair and Helms 2015, Campos and Hall 2019). Now, summing up forces in the direction perpendicular to ($t \cdot dL$), the follow equation of equilibrium is obtained. which can be solved for stresses in the circumferential direction (hoop stresses) presented in Equation (50).

$$2[\sigma_\theta(t \cdot dL)] - P(2r \cdot dL) = 0 \tag{49}$$

$$\sigma_\theta = \frac{P \cdot r}{t} \tag{50}$$

The stresses in the circumferential direction (σ_θ) are then related to the strain in the mentioned direction using Hooke's Law which can be written as:

$$\epsilon_\theta = \frac{\sigma_\theta}{E} = \frac{Pr}{Et} \tag{51}$$

Subsequently, since strain in the circumferential direction is change in circumference, this is related to change in radius to derive an equation for the idealized ring's radial expansion under the given internal pressure, Equation (54).

$$\Delta_C = C \cdot \epsilon_\theta = 2\pi r * \frac{Pr}{Et} \tag{52}$$

$$\Delta_r = \frac{\Delta_C}{2\pi} \tag{53}$$

$$\Delta_r = \frac{Pr^2}{Et} \tag{54}$$

Likewise, by the principles of linear superposition (Blosser 1988), a thermal expansion term for the assumed ring is added to Equation (54) to obtain:

$$\Delta_r = \frac{Pr^2}{Et} + r\alpha T \tag{55}$$

Where,

Δ_r = Thermal expansion in the radial direction
P = Idealized internal pressure
r = Radius of curvature of the idealized ring
E = Modulus of elasticity of rail
t = Wall thickness of the idealized ring
α = Coefficient of thermal expansion of rail steel
T = Change in temperature

Similar to previous method, the radial expansion can then be set to zero to solve for the pressure. Again, since the height of the section of the cylinder under consideration can be defined, the developed pressure can then be converted into force per unit length or force per fastener if so desired.

Variational Formulation Method

In the study of *Thermal Buckling of Curved Railway Tracks*, Donley and Kerr (1987) developed a model using a variational calculus formulation approach. Unlike previous studies on thermal buckling of curved railway tracks, these equations can be used to calculate pre-buckling thermal expansion of a curved railway track for different temperature, radii and track properties. In derivation of the equation, the authors have assumed that before the buckling takes place, the radial displacement is uniform along the length of the arc for the circular section of the curve (excluding the transition and tangent tracks), and based on this assumption, the authors have derived the governing equation, assuming that the track is a circular ring, embedded in a ballast layer.

Since the current research is studying the development of lateral forces on a curved railway track before buckling, their equation is adopted to cross check the models developed in this study for

the lateral forces due to thermal expansion. A summarized version of the equation's derivation is given in Donley and Kerr (1987) while the complete and step by step derivation is presented in Donley (1981). Although, they use a mathematically comprehensive approach, their final equation for radial expansion of the idealized ring is eventually the same as that of the thin wall cylinder method discussed in previous section.

Using their equation for this study, the pre-buckling lateral thermal displacement is set to zero and the equation is solved for ballast resistance, rho which is also equivalent to the total lateral force due to thermal expansion in the ring, uniformly distributed along the curve as shown in Figure 8 above.

$$u = \frac{EA\alpha T - R\rho}{\frac{EA}{R}} \tag{56}$$

Where,
u = Pre-buckling thermal lateral displacement (in / mm)
E = Modulus of elasticity of rail (psi / MPa)
A = Cross sectional area of rail (in^2 / mm^2)
α = Coefficient of thermal expansion of rail steel (/F or /C)
T = Change in temperature
R = Radius of curvature of the curved track (ft / m)
ρ = Ballast resistance (lb/ft or N/m)

Setting the pre-buckling thermal lateral displacement to zero and solving for ballast resistance (force per unit length), gives the following equation:

$$0 = \frac{EA\alpha T - R\rho}{\frac{EA}{R}} \tag{58}$$

$$\rho = \frac{EA\alpha T}{R} \tag{59}$$

Finite Element Models

To verify the models analyzed in the parametric study, a finite element model was also created using a commercially available finite element analysis software package[2]. Before comparing the FEM results with the analytical models, the development of the FEM model and the associated inputs, assumptions and outputs are presented. The model was developed as shown in Figure 12. Since multiple curvatures were analyzed, with the corresponding need for different numbers of meshes along the circumference of the rail, a mesh size of 1.0 which represents 1.0 ft was adopted. This allowed for consistency between the different circumferential versions of the FEM models, For the purpose of consistency between the FEM models, a mesh size of 1.0 which represents 1.0 ft is adopted. Given that the height (base of the rail) and width (length of gage) of all of the models

[2] The ABAQUS Finite Element package was used.

in the parametric study are the same, a 1.0 ft mesh will create five elements across the width, one element along the height and since the radii of the models are not the same, a variable number of elements along the circumference.

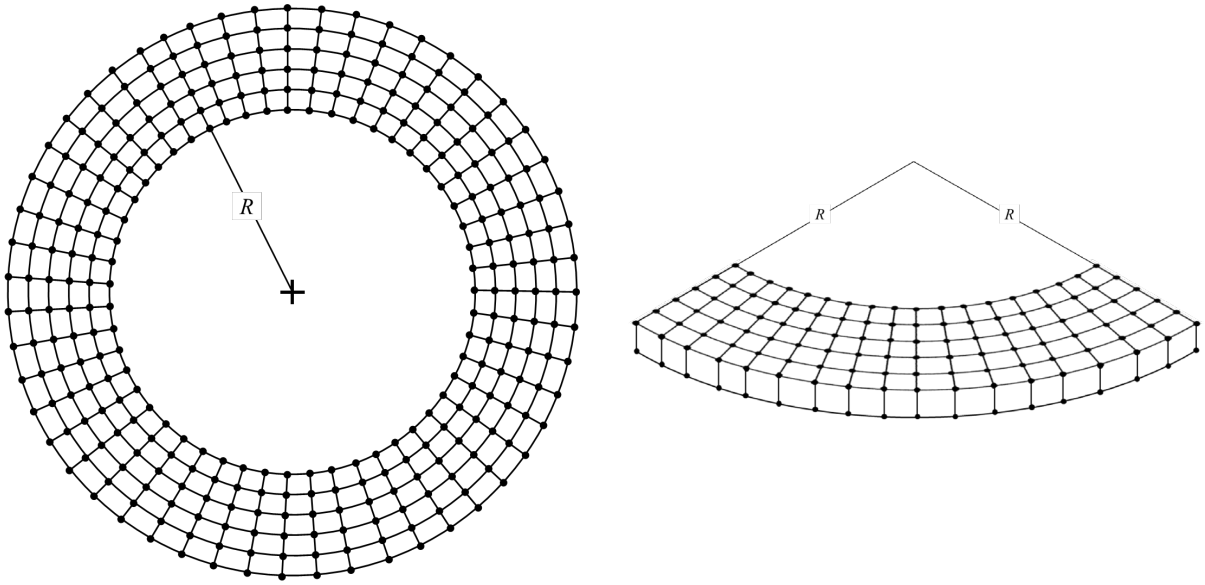

(a) (b)

Figure 12: (a) Diagram of the finite element model, (b) an arbitrary arc section of the finite element model with the sideview

The finite element models are restrained (confined) against lateral expansion at the surface of the outer radius using boundary conditions as they are subjected to a temperature difference. This ensures that a stress is generated at the surface of the outer radius.

To compare this stress with the results from the analytical models, it can either be compared with forces that are generated directly on the nodes (nodal forces) at the surface of the outer radius or with the forces that are calculated based on the element area and stress on any given element along the surface of the outer radius.

If comparison is to be made with nodal forces, it should be noted that the total force on the element face is shared by all nodes in that particular face and hence only the magnitude can be compared with the analytical models. On the other hand, the forces that are calculated based on the element area and stress can be directly compared with analytical models.

Theoretically, whether the forces are obtained from the element nodes or from the product of element stress and area, should be the same. However, for this study, it was initially noticed that the nodal forces were slightly different from their equivalent forces calculated from element stress and area. This was also true in comparison with the results from the analytical models.

Therefore, the model was reevaluated, and it was found that this effect was caused by the use of linear elements to represent a curved section. In order to overcome this issue, a finer mesh was used. As the mesh gets finer, it reduces the curvature effect and make the element area more precise. Consequently, the results converge and the previous differences become negligible.

This was tested on 100 ft and a 1000 ft radius curves by changing the mesh size from 1.00 ft to 0.50 ft and eventually to 0.25 ft. Graphical results and accompanying explanations for the 100 ft model are presented below. The results for the 1000 ft model are similar, however a limit in the number of allowable elements was encountered so that the lowest mesh size that could be used in this particular finite element software for the 1000 ft model was 0.28 ft.

In the comparisons that follow, the 100 ft curve model is first analyzed using a 1.00 ft mesh size. As it can be noticed from Figure 13, the nodal forces and stresses in the radial direction using a cylindrical coordinate system are shown on a zoomed arc section of the idealized ring. The figure is from the analysis of the 100 ft radius curve with a 1.00 ft mesh size subjected to a 100 F temperature difference. The unit for the forces (indicated as RF, FR1 (CSYS-1) in the figure) is pounds and that of stresses (indicated as S, S11 (CSYS-1) in the figure) is pounds per square foot. Surface area of each element in the outer radius for this particular model is 0.0370 square feet. As shown in the figure, the maximum force on each node of the outer radius is 2506 lbs. while it is equivalent calculated from stress on the element face and area of element is 2197 lbs. As it can be seen in Figure 14, the values get closer as the mesh size get finer and similarly their percentage differences diverges from as high as about 14% for a mesh size of 1.00 to as low as 3% for a mesh size of 0.25 ft (Figure 15).

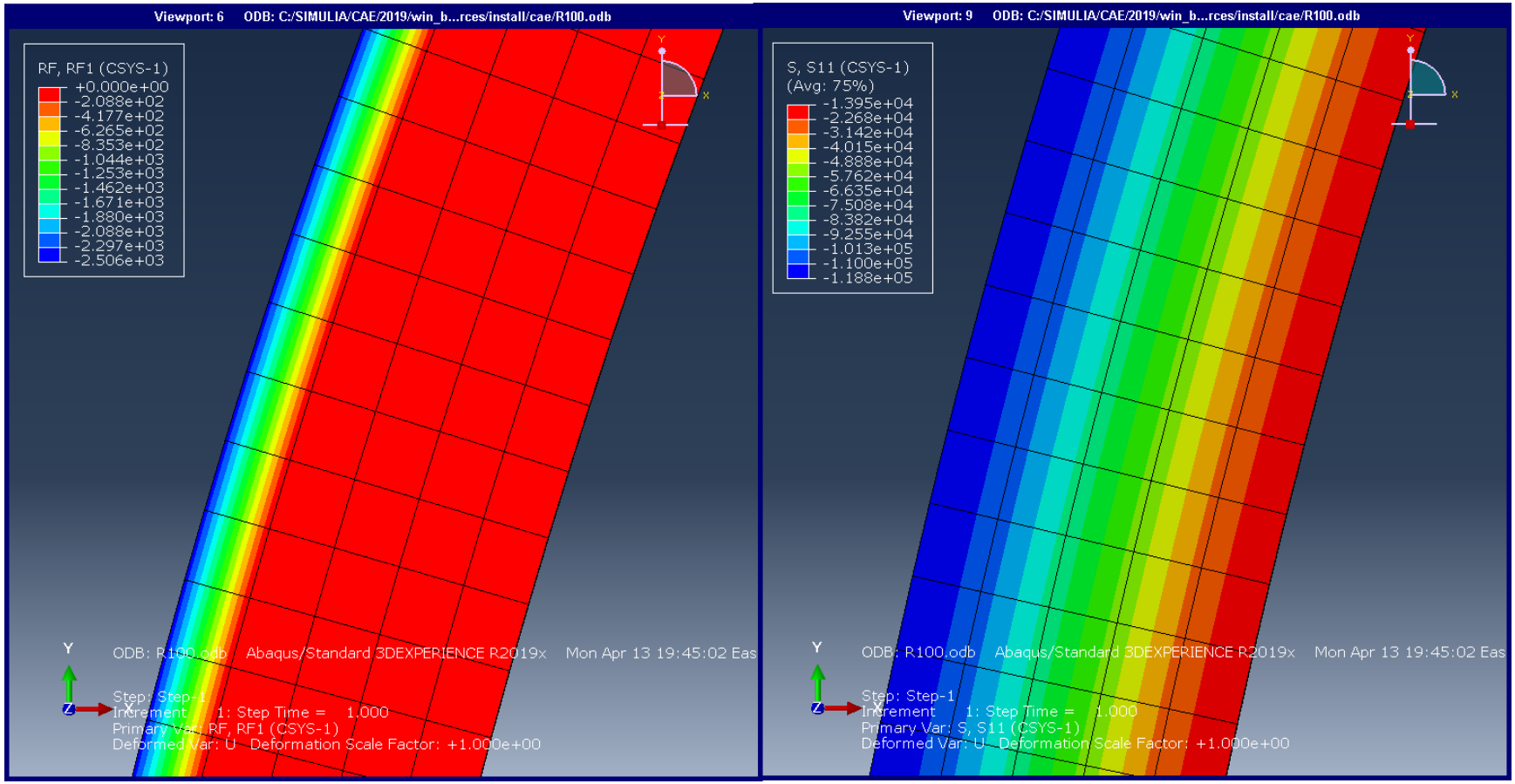

Figure 13: A zoomed arc section of the ideal ring from the finite element software with nodal forces and radial stress. Screenshots for the rest of FEM models are reported in the Appendix section

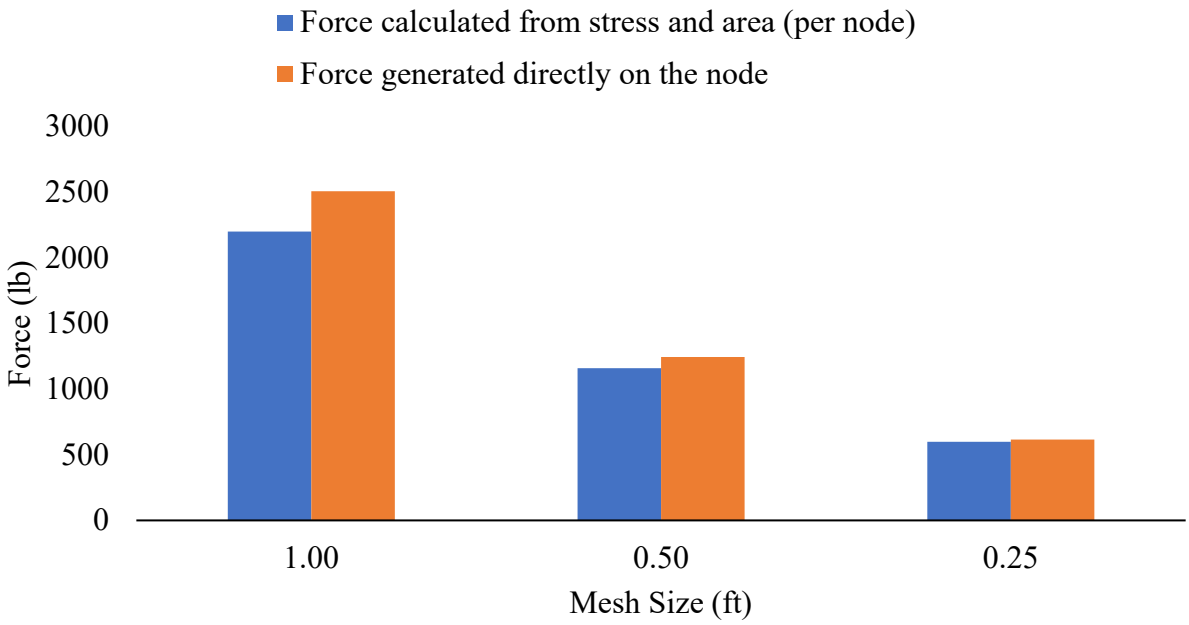

Figure 14: Comparison of forces calculated from stress and area and their equivalent generated directly on the element nodes (100 ft curve)

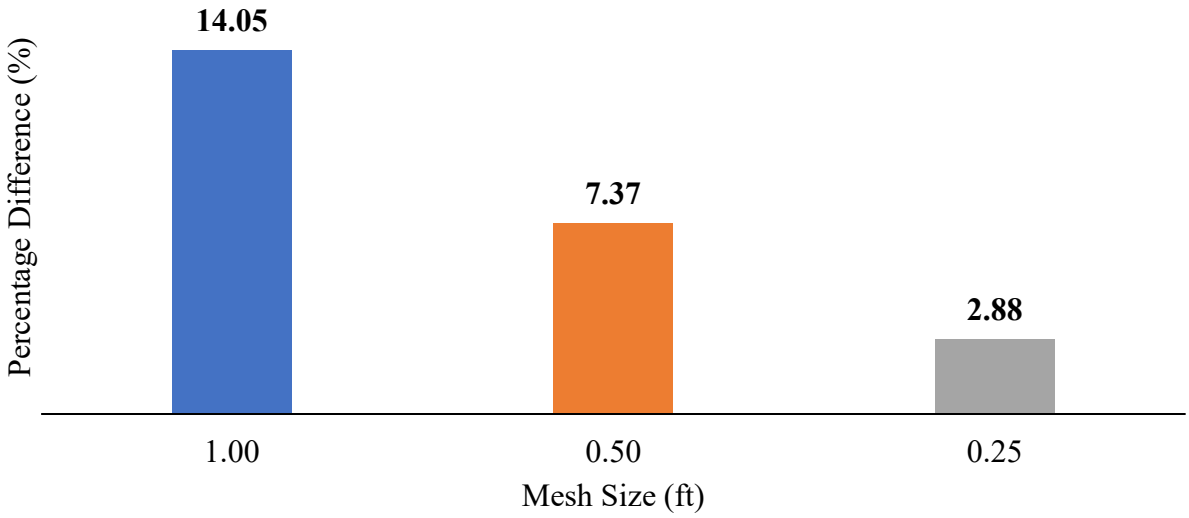

Figure 15: Percentage difference between forces calculated from stress and area and their equivalent generated directly on the element nodes (100 ft curve)

Similarly, while comparing the finite element results with the analytical models, the percentage differences reduces significantly as the mesh gets finer (Figure 16).

\The abbreviations in Figure 16 and the subsequent figures are TM = Timoshenko method, CM = Cylinder mechanics, VM = Variational method and FEM = Finite Element Method.

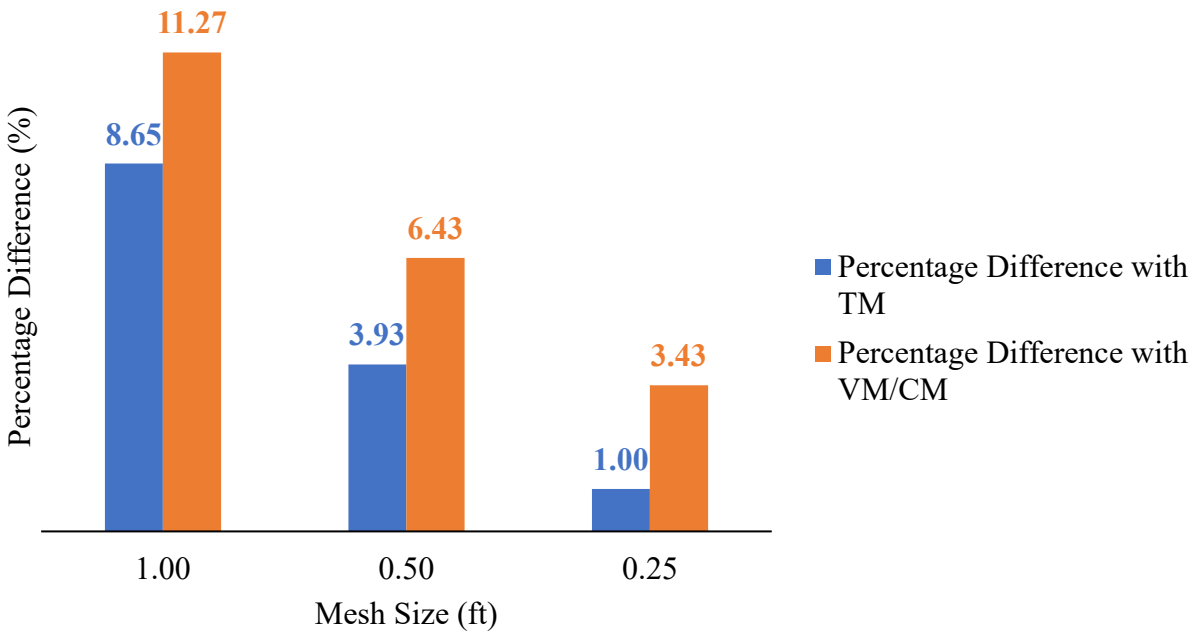

Figure 16: Comparing the results from the FEM methods with the analytical models for a 100 ft radius curve, subjected to a 100 F temperature difference (100 ft curve)

Likewise, the behavior of the 1000 ft radius curve is similar as the mesh size gets smaller. The results are graphically presented in Figure 17 and 18. As it can be observed, the figures are identical to that of 100 ft radius curve, however, with different values.

Furthermore, even if the model with 1.00 ft mesh size is considered, the average percentage difference between the radial stresses from the finite element model and that of analytical models are still about 10%

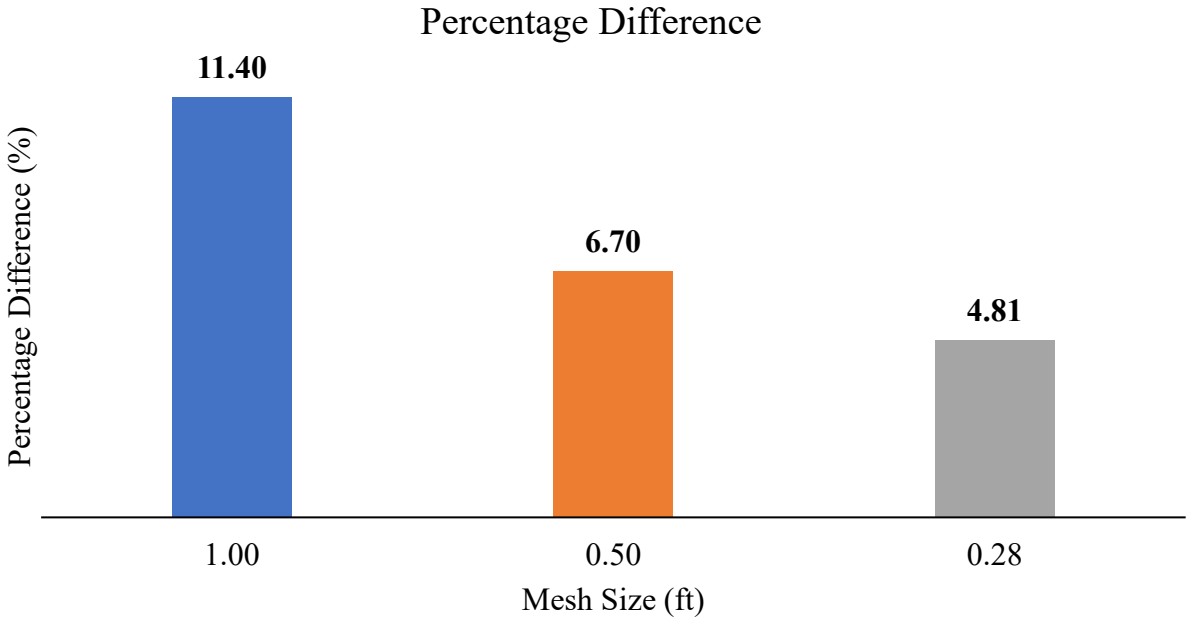

Figure 17: Percentage difference between forces calculated from stress and area and their equivalent generated directly on the element nodes (1000 ft curve)

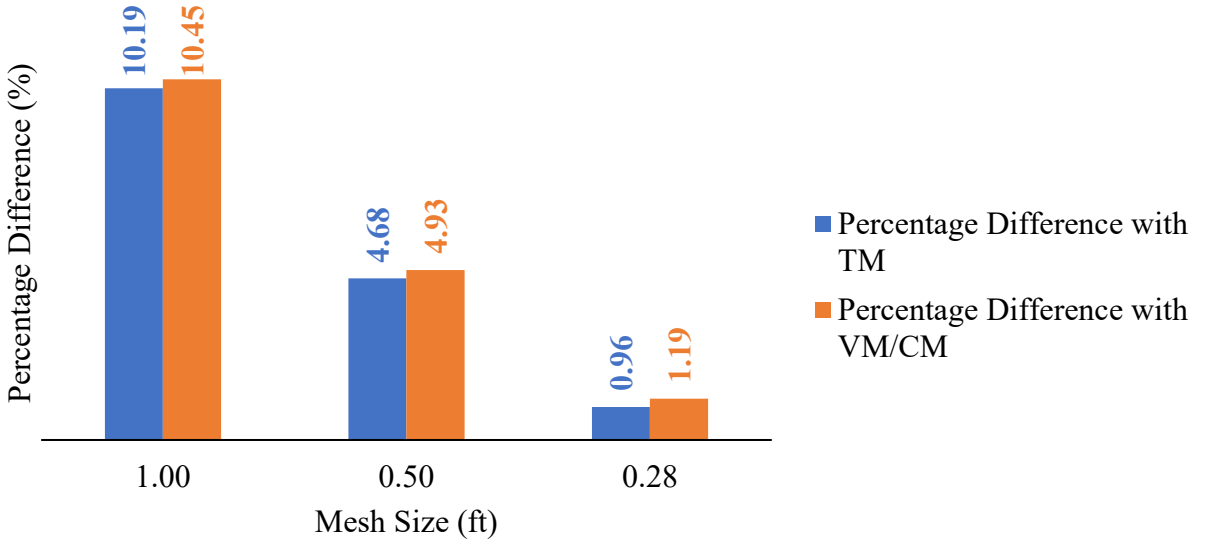

Figure 18: Comparing the results from the FEM methods with the analytical models for a 1000 ft radius curve, subjected to a 100 F temperature difference (1000 ft curve)

PARAMETRIC STUDY

In order to examine lateral forces generated in a curved track, and to validate the different models, a parametric study was performed over a broad range of curvature (radii), temperature changes, and other key inputs. Thus, for each of the key input variables, the following input value or range of values was used.

- Range of temperature changes, T = 0, 20, 40, 60, 80, and 100 degrees Fahrenheit
- Range of radius of curvature, R, or r = 100, 250, 500, 750, 1000, 1500, 2000, 2500 and 3000 ft radii curves
- Elastic modulus, E = 4,320,000,000 lb/ft^2 (30m psi),
- Thermal expansion coefficient, α = 0.0000065 /F
- Poisson ratio = 0.30
- Model height is taken as height of the base of a typical rail = 0.0365 ft (0.438 inches)
- Model thickness is taken as length of a standard gage = 4.7083 ft (56.5 inches)
- Forces are calculated per unit length
- Tie spacing (fastener's longitudinal spacing) is considered as to 2 ft
- Since axle loading and train speed is not involved in the derivation of radial thermal expansion forces, the dynamic impact factor for the thermal expansion is approximated as 1.00

RESULTS AND DISCUSSION

The results obtained from the parametric study under this research are presented graphically from Figure 19 to Figure 31 in the following section. For the first analytical method (Timoshenko stress analysis), Equations (45) and (48) are used to calculate the values in the figures. As stated above, to use these equations, the thermal properties and the dimensions of the outer ring will be modified such that it does not allow thermal radial expansion. This will ensure that the inner ring is fully confined and hence the desired radial stress is developed at the contact surface. This can be obtained through trial and error by either changing the coefficient of thermal expansion or increasing the outer radius of the outer ring. This a computationally exhaustive process as Equations (45) and (48) are quite involved.

The second and third analytical methods are essentially the same. The difference is that the second method is derived using the classic mechanics technique of thin walled cylinders while the third method uses a mathematically advanced and comprehensive approach based on a variational calculus formulation.

The results of the parametric study for the research are graphically presented below.

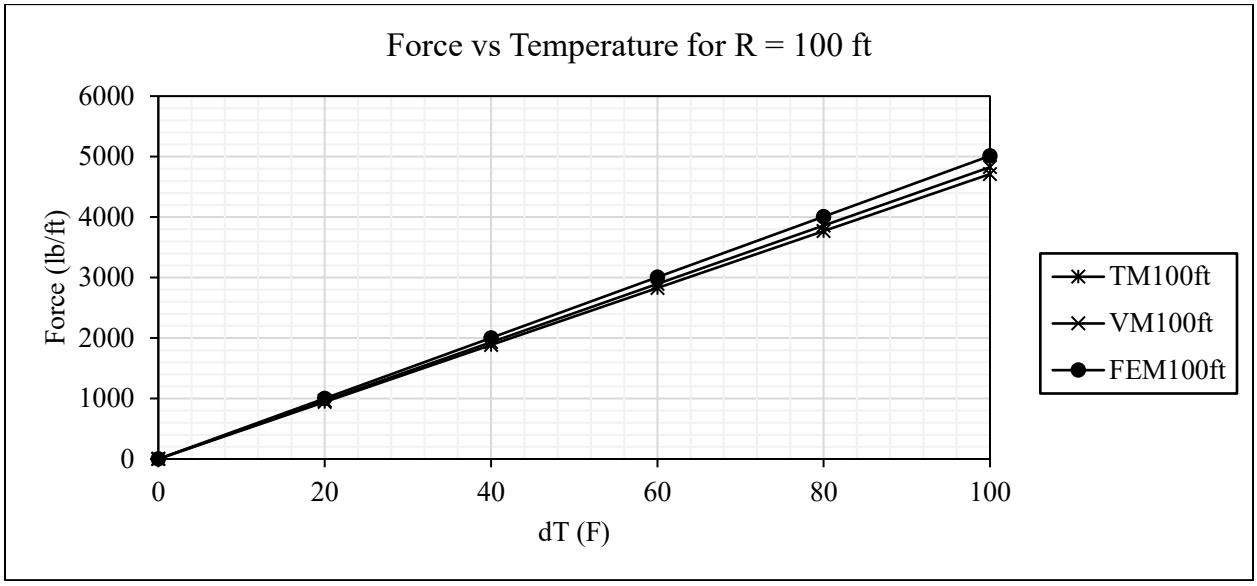

Figure 19: Force per unit length vs temperature difference for different methods (100 ft)

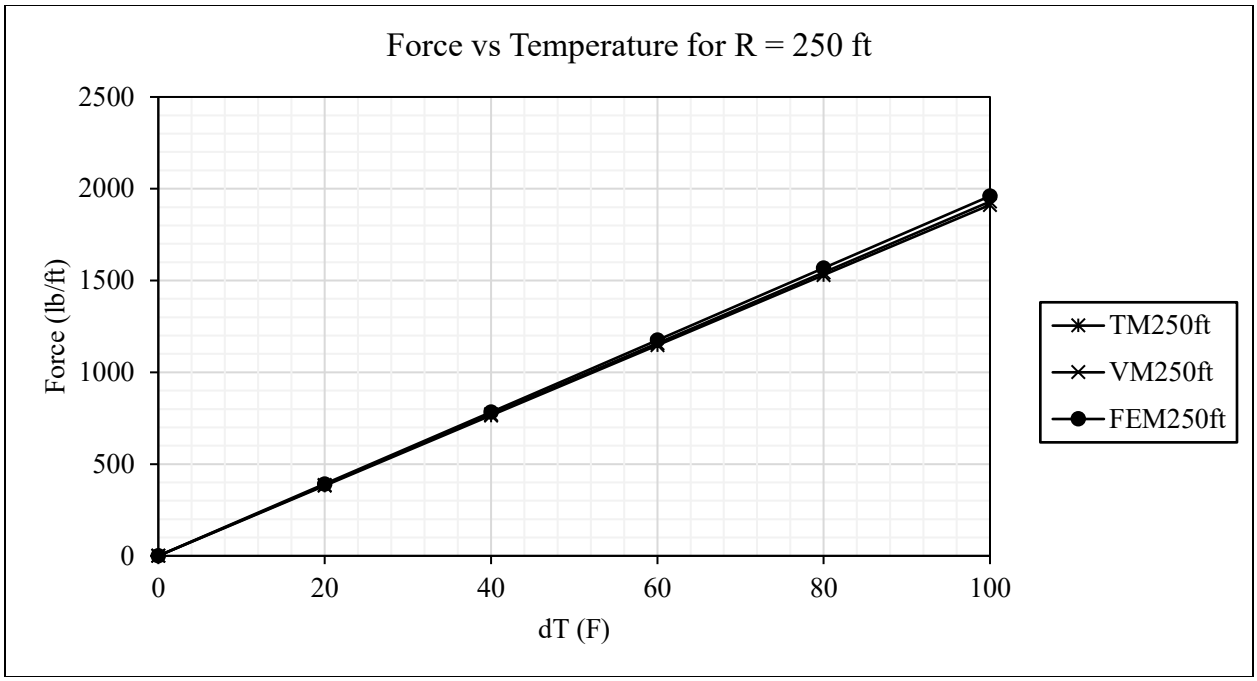

Figure 20: Force per unit length vs temperature difference for different methods (250 ft)

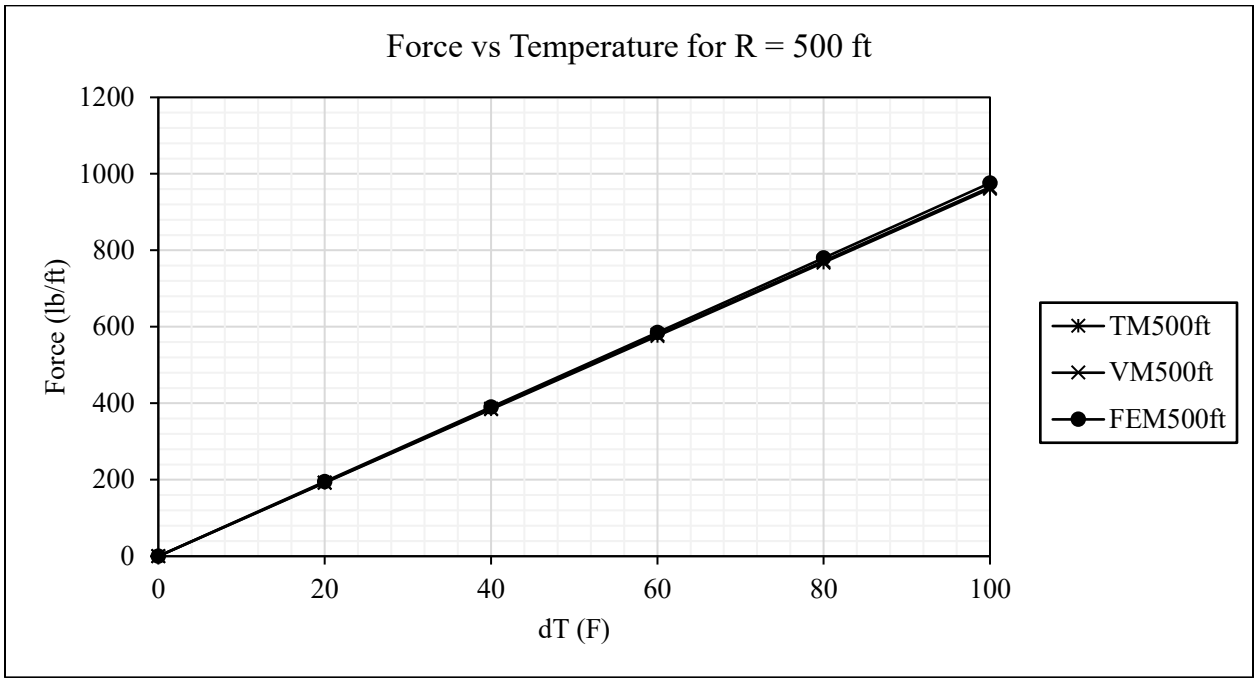

Figure 21: Force per unit length vs temperature difference for different methods (500 ft)

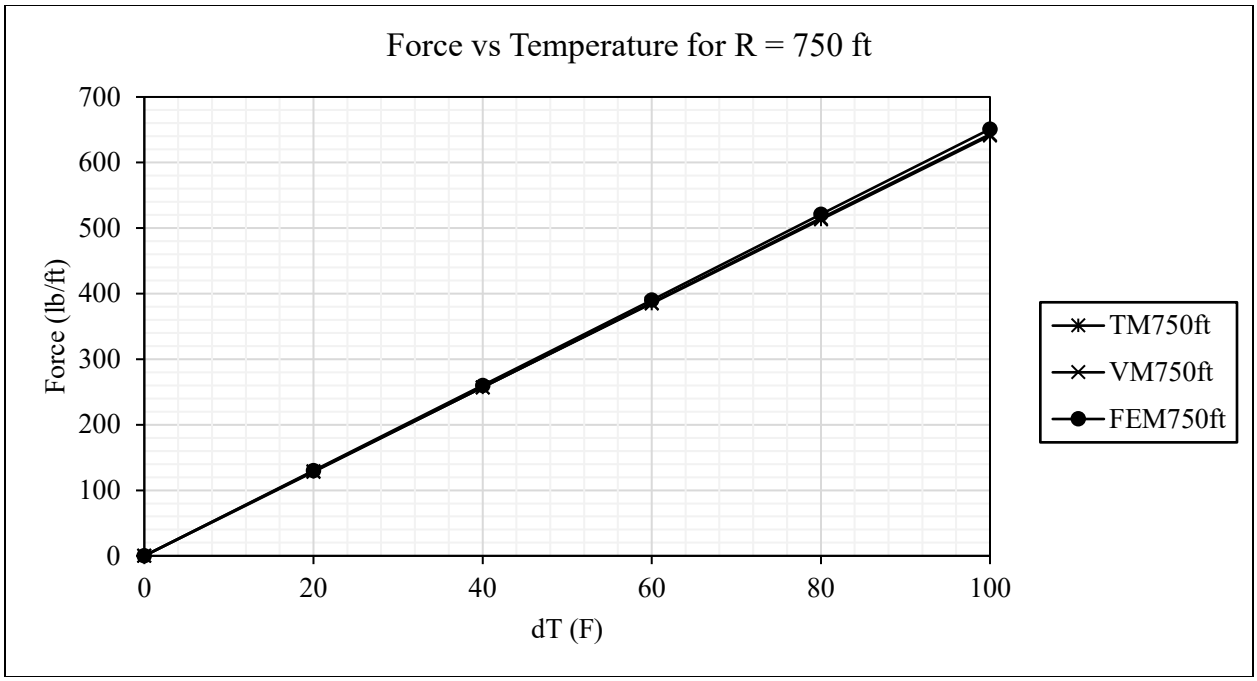

Figure 22: Force per unit length vs temperature difference for different methods (750 ft)

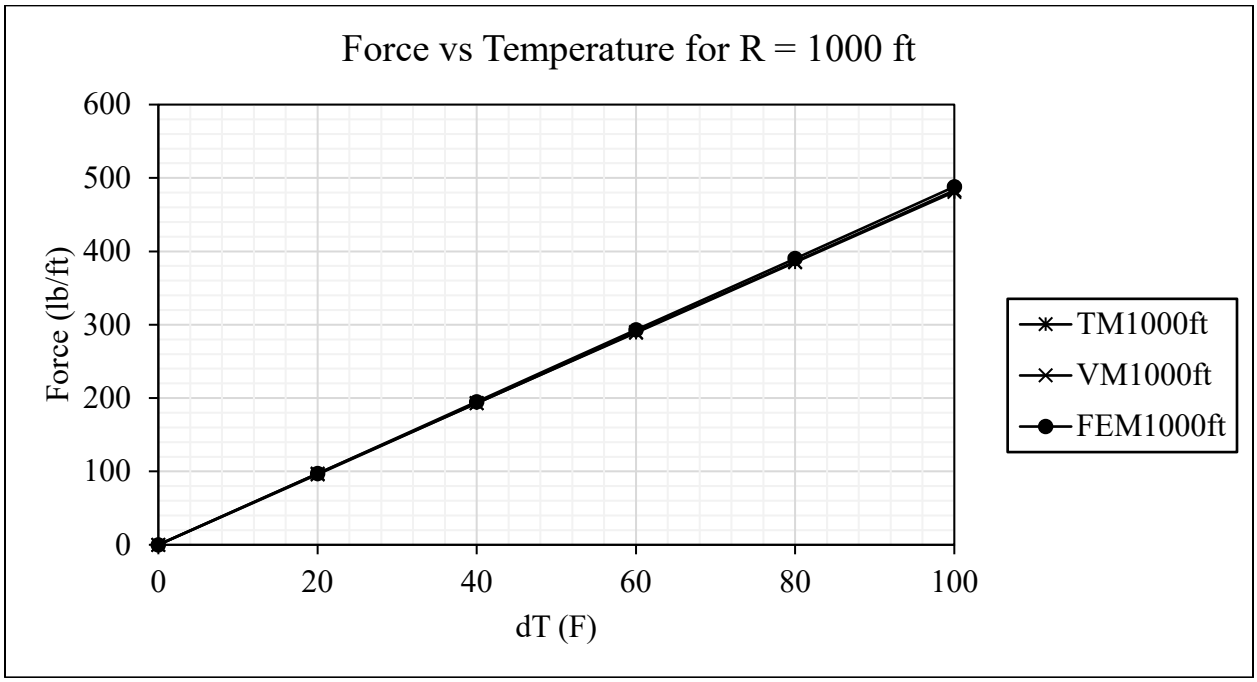

Figure 23: Force per unit length vs temperature difference for different methods (1000 ft)

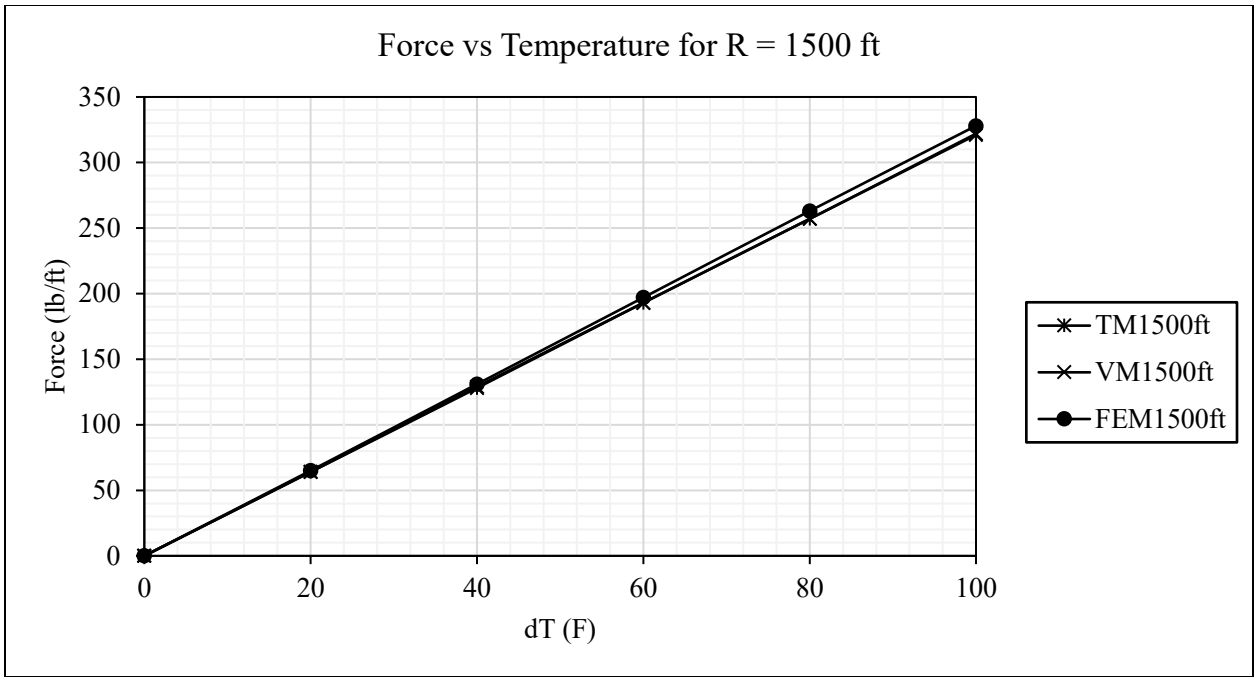

Figure 24: Force per unit length vs temperature difference for different methods (1500 ft)

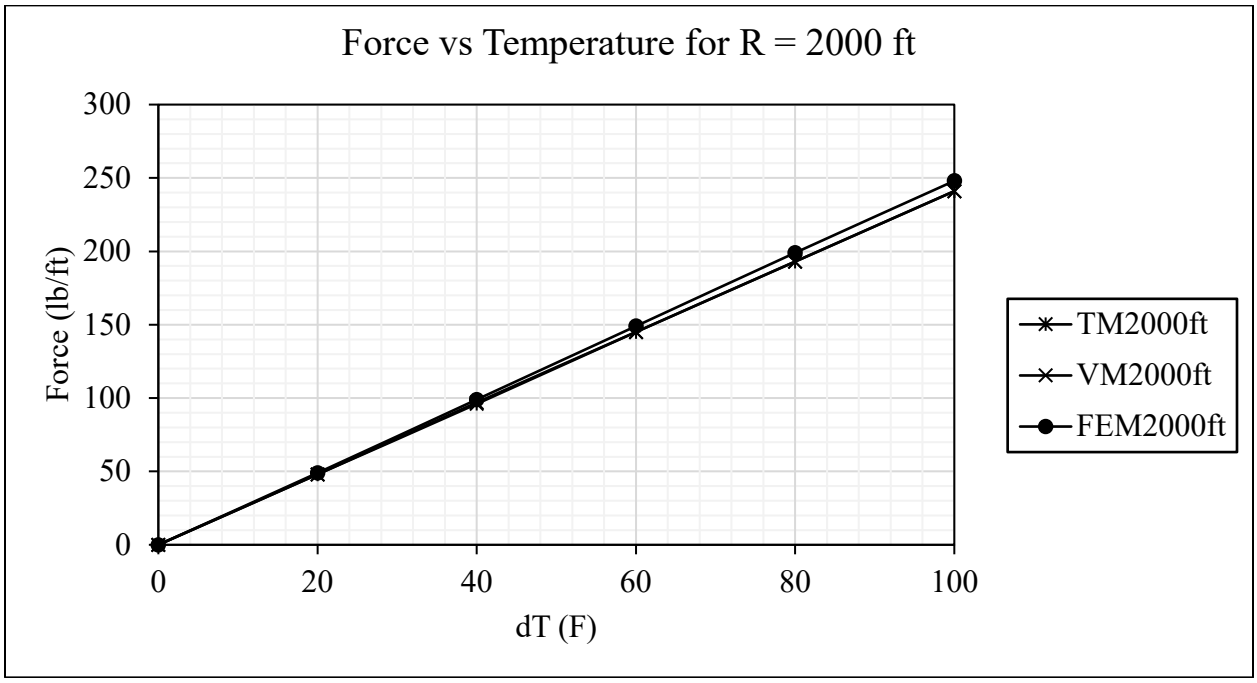

Figure 25: Force per unit length vs temperature difference for different methods (2000 ft)

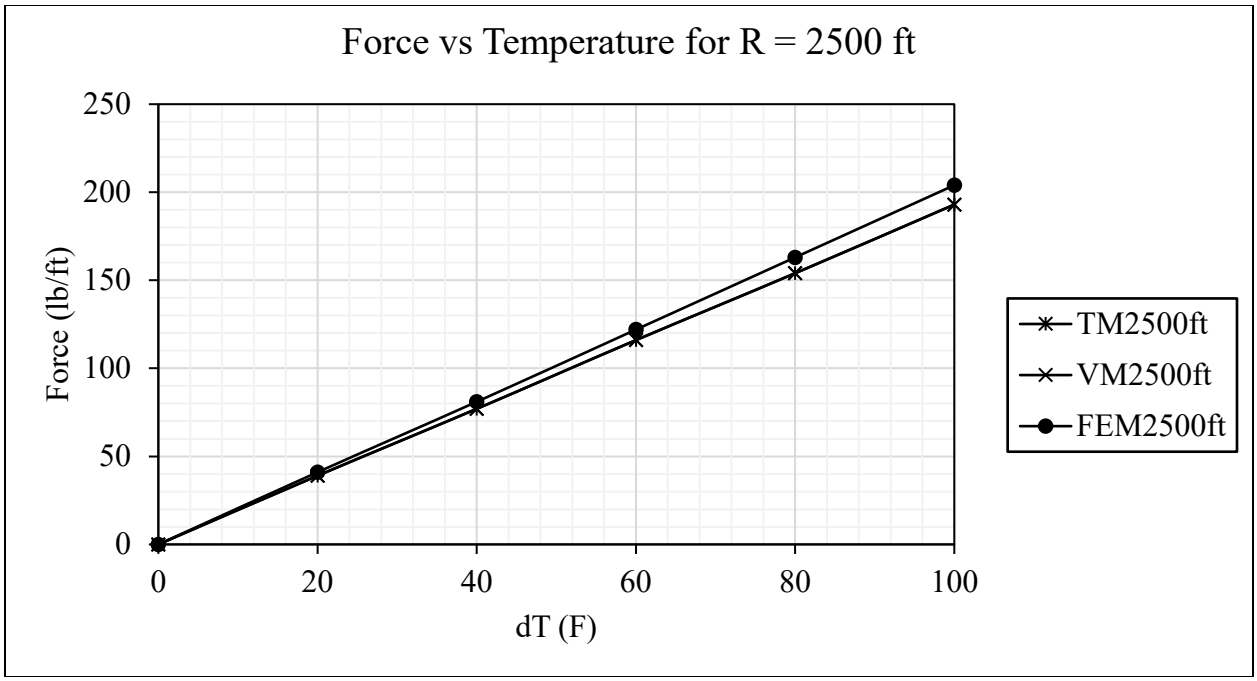

Figure 26: Force per unit length vs temperature difference for different methods (2500 ft)

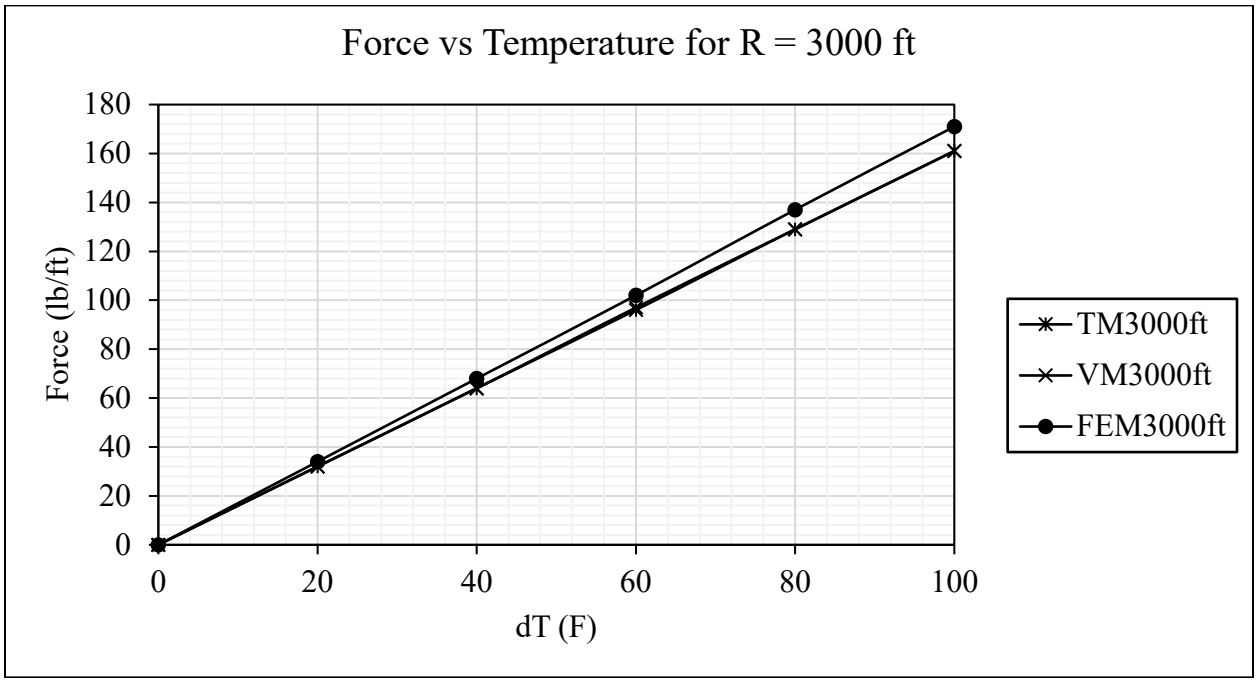

Figure 27: Force per unit length vs temperature difference for different methods (3000 ft)

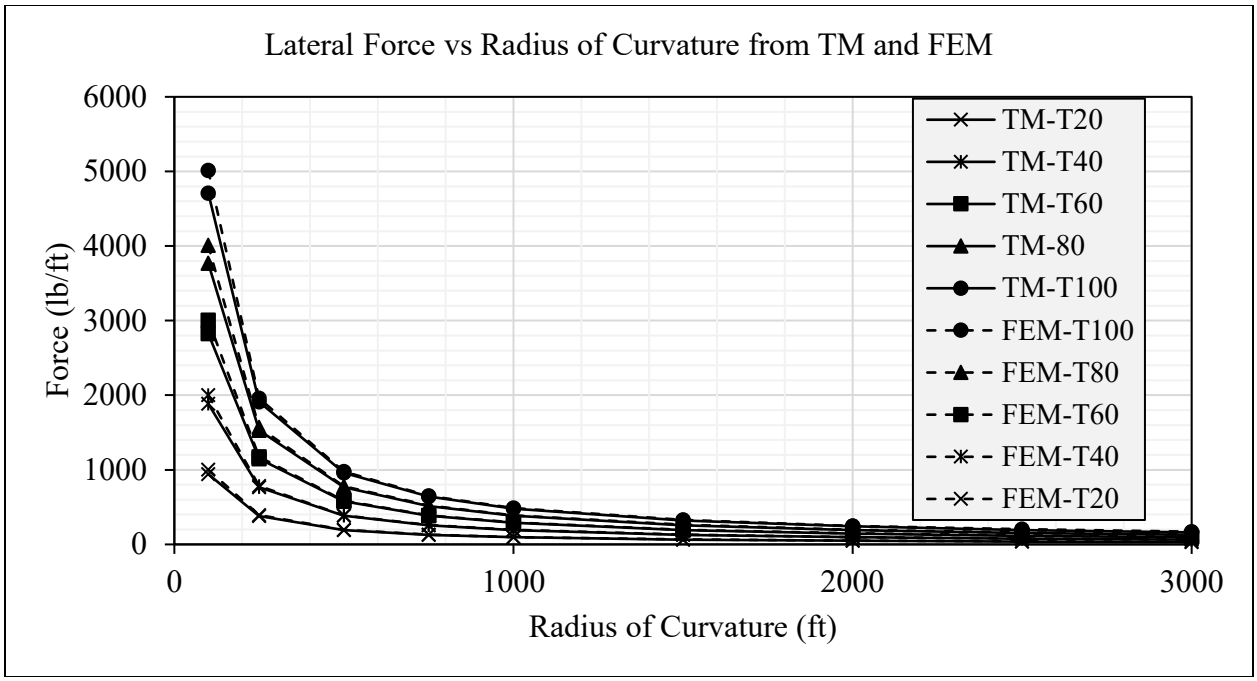

Figure 28: Lateral force per unit length vs radius of curvature for TM vs FEM

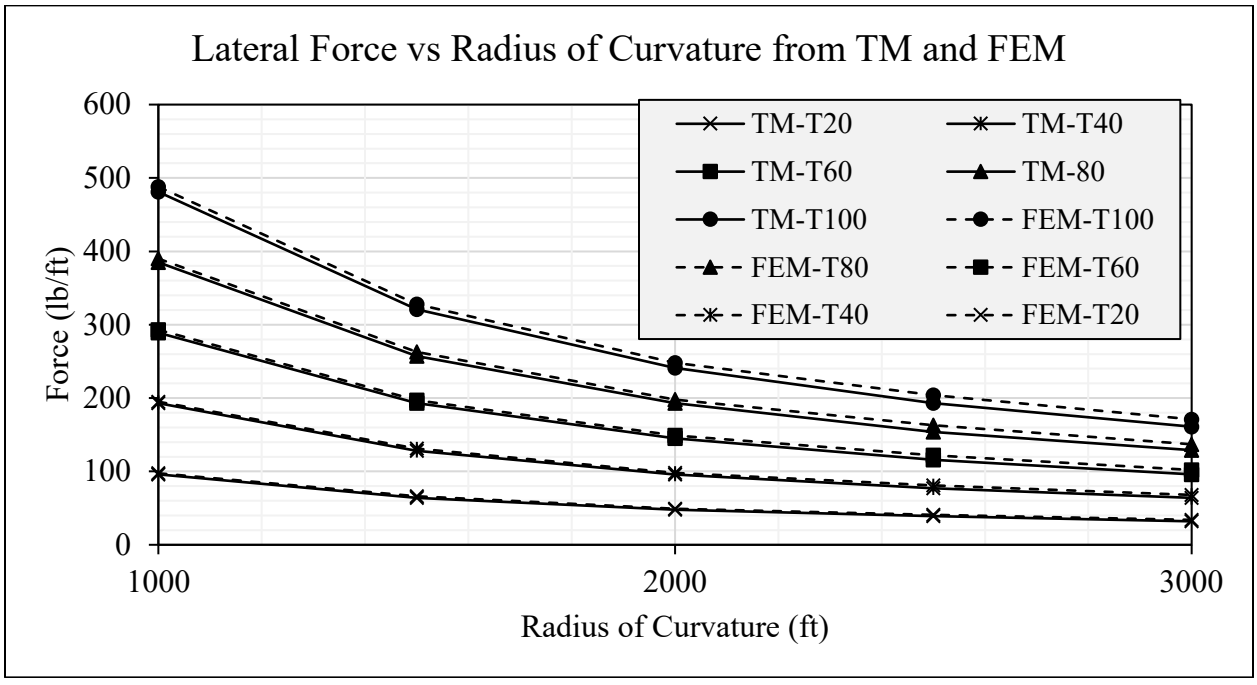

Figure 29: Lateral force per unit length vs radius of curvature for TM vs FEM (larger radii only)

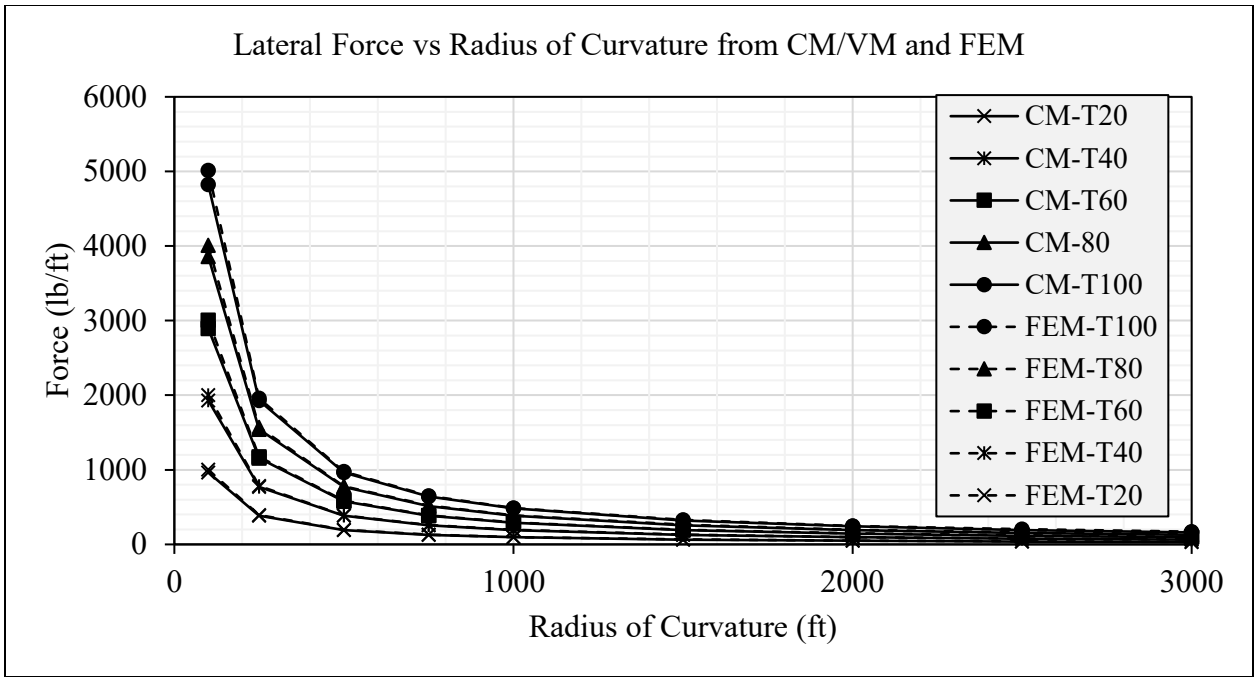

Figure 30: Lateral force per unit length vs radius of curvature for CM/VM vs FEM

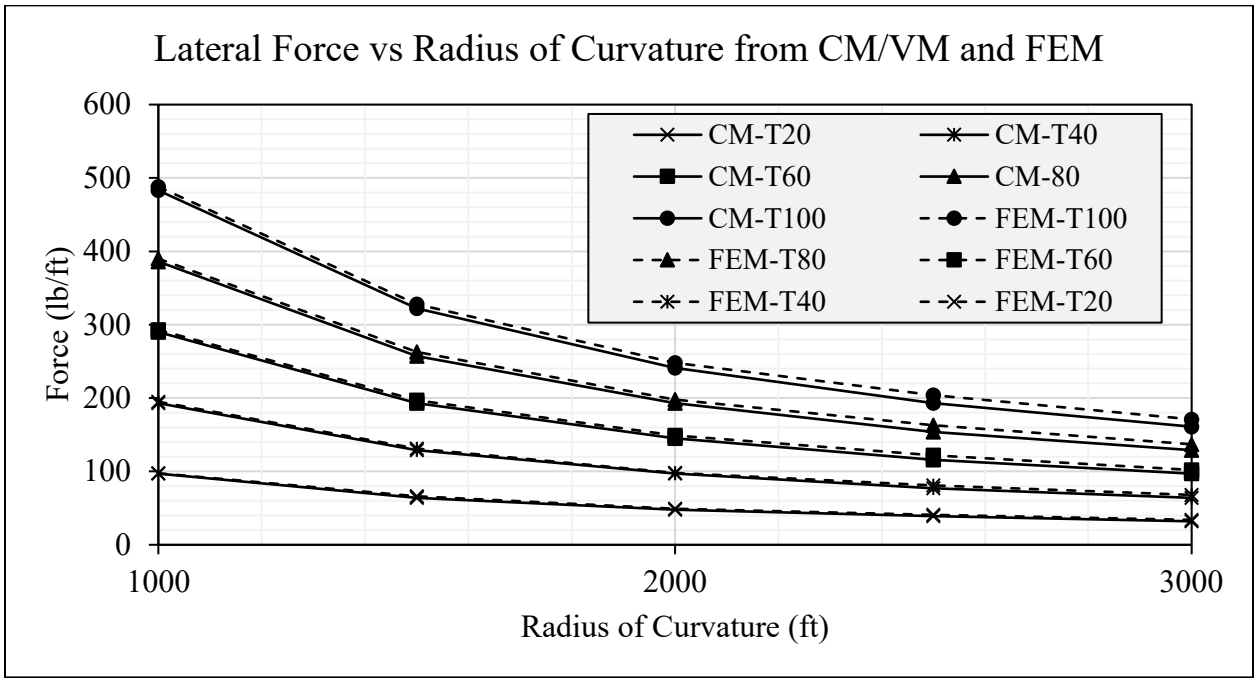

Figure 31: Lateral force per unit length vs radius of curvature for CM/VM vs FEM (larger radii only)

Analyzing A Quarter Ring Model

In addition to analyzing a full idealized ring, an arc section of the ring is also analyzed using the finite element software. Its results are compared with that of analytical models (Figure 32). As it

can be observed from the figure, apart from the end sections (boundaries), the results for the arcs are the similar to that of a full idealized ring. The reason the solution degrades at the boundaries for the arc section is because when a stable system (e.g. a circular ring) is cut, unless a purpose-designed boundary (some sort of adaptive elastic support) is used to simulate the exact behavior of the system, the available supports (fixed, pin, free, hinge, etc.) in the software do not represent the correct behavior, resulting in a concentration of unrealistic stresses at the boundaries. Since the values at the boundaries of the arc section are not valid, a certain length from the boundaries towards the internal region of the arc should be established where high concentrated stresses can be ignored. When the regions of high stresses are ignored, the behavior for the rest of the arc is similar to its full ring equivalent.

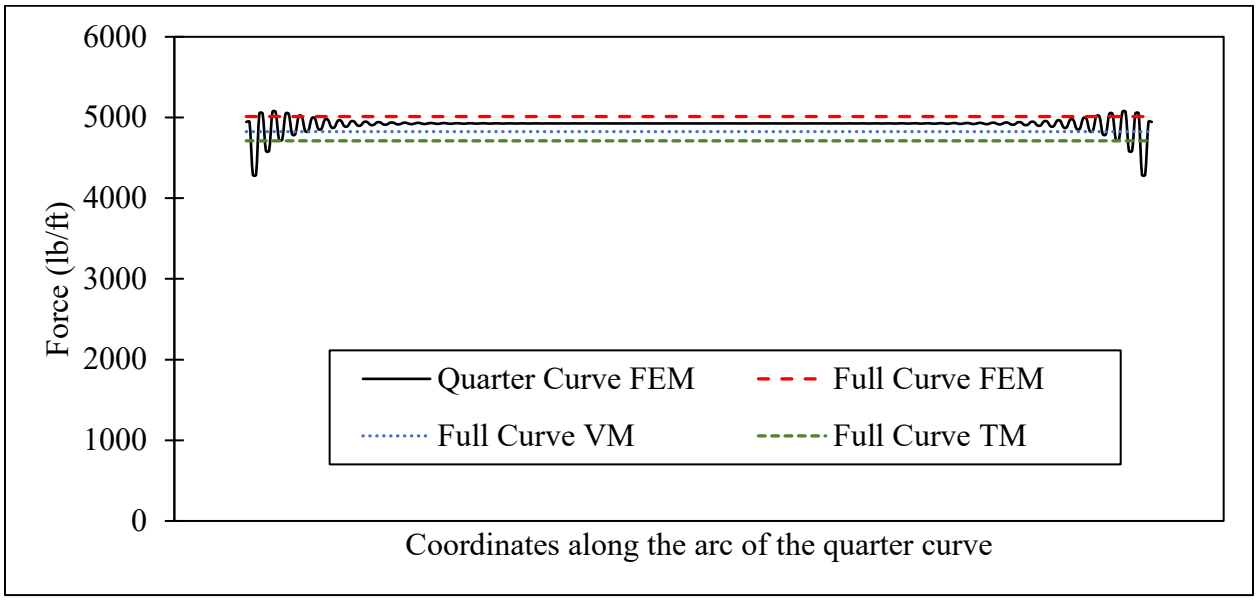

Figure 32: Uniformly distributed lateral forces per unit length for the quarter curve compared with analytical and FEM models

Figure 32 compares uniformly distributed lateral forces per unit length for the quarter curve with analytical and FEM models. For this specific example, the radius of curvature is 100 ft, the temperature difference is 100 degrees F and the data for about 7 ft from each boundary of the arc (about 10% of the total arc length) is ignored to get rid of unrealistic stress concentration.

CONCLUDING REMARKS

In this research activity, three analytical and one finite element models were developed to determine track-induced lateral thermal expansion forces on a curved bridge. The models are tested through a parametric study, the result of which are presented graphically in the results and discussion of this report. The range for the temperature difference is taken between 0 to 100 degrees Fahrenheit while the range for radius of curvature is considered from 100 ft to 3000 ft. As can be observed from Figure 19 to Figure 27, the relationship between the uniformly distributed lateral thermal expansion forces is directly proportional to the increase in temperature. Based on the presented results, for a 100 ft radius curve for instance, a temperature of 100-degree Fahrenheit

could generate up to 5000 lb/ft of uniformly distributed lateral thermal expansion force and if a 2 ft tie spacing for a typical track is assumed, this will translate to about 10,000 lbs. of lateral force, acting on a single fastener.

It should be noted that if a single rail is considered, the roughly 10,000 lbs. of force will be divided by the two fasteners, however since the analysis conducted for this study considers the track, as a unit, the 10,000 lb force should be taken per fastener. In comparison, the same force for a 3000 ft curve track drastically drops to only about 350 lbs. per sleeper in the lateral direction.

Likewise, the relationship between the uniformly distributed lateral thermal expansion force and the radius of curvature are presented from Figure 28 to Figure 31. As it can be seen from these figures, the uniformly distributed lateral force due to thermal expansion is inversely proportional to the radius of curvature, again confirming the fact that as the radius increases, the curvature effects are reduced and there is a corresponding decrease in the lateral force.

REFERENCES

1. Deng, Y., Phares, B., Greimann, L., Shryack, G. and Hoffman, J., (2015), *Behavior of curved and skewed bridges with integral abutments*. Journal of Constructional Steel Research, 109, pp.115-136.
2. Unsworth, J., (2010), *Design of Modern Steel Railway Bridges*. Florida: CRC Press.
3. Nakai, H.i, and Yoo, C.H. (1988), *Analysis and Design of Curved Steel Bridges*. New York: McGraw-Hill.
4. Heins, C. P., and Firmage, D.A. (1979), *Design of Modern Steel Highway Bridges*. New York: Wiley.
5. Shanmugam, N.E., Mahendrakumar, M., and Thevendran, V. (2003), *Ultimate Load Behavior of Horizontally Curved Plate Girders. Journal of Constructional Steel Research* 59.4: 509-29. Web.
6. *Practical Guide to Railway Engineering*. (2003). Landover, MD. American Railway Engineering and Maintenance of Way Association
7. Timoshenko, S. and Goodier, J., (1951), *Theory of Elasticity*. New York. Mc Graw-Hill.
8. Boresi, P.A., Chong, K. P., and Lee, J.D., 3rd Edition. (2011). *Elasticity in Engineering Mechanics*. New Jersey. John Wiley and Sons.
9. Barron, B. and Barron, R., (2013). *Design for Thermal Stresses*. New Jersey. John Wiley and Sons.
10. Eslami, M.R.. Hetnarski, R.B., Ignaczak. J., Noda, N., Sumi, N., and Tanigawa. Y., (2018), *Theory of Elasticity and Thermal Stresses Explanations, Problems and Solutions.* New York. Springer
11. Blosser, M.L., (1988), *Thermal Stress in High Temperature Cylindrical Fasteners*. NASA Technical Memorandum 100611. Langley Research Center. Hampton, Virginia
12. Fukui, K. and Fukui, T., (1969), *Stresses around Circular Ring Inclusion Due to Uniform Thermal Gradient*. Bulletin of JSME, 12(51), pp.437-444.
13. Hibbeler, R., (2011), *Mechanics of Materials*. 8th ed. Singapore: Prentice Hall.
14. Sinclair, G., and Helms, J. (2015), *A review of simple formulae for elastic hoop stresses in cylindrical and spherical pressure vessels: What can be used when*. International Journal of Pressure Vessels and Piping, 128, 1-7. doi: 10.1016/j.ijpvp.2015.01.006

15. Campos, U., and Hall, D. (2019). *Simplified Lamé's equations to determine contact pressure and hoop stress in thin-walled press-fits*. Thin-Walled Structures, 138, 199-207. doi: 10.1016/j.tws.2019.02.008
16. Donley, M., & Kerr, A. (1987). *Thermal buckling of curved railroad tracks*. International Journal of Non-Linear Mechanics, 22(3), 175-192. doi: 10.1016/0020-7462(87)90001-1
17. Donley, M. (1981). *Thermal Buckling of Curved Railway Track* (Master's Thesis). University of Delaware.

APPENDIX A

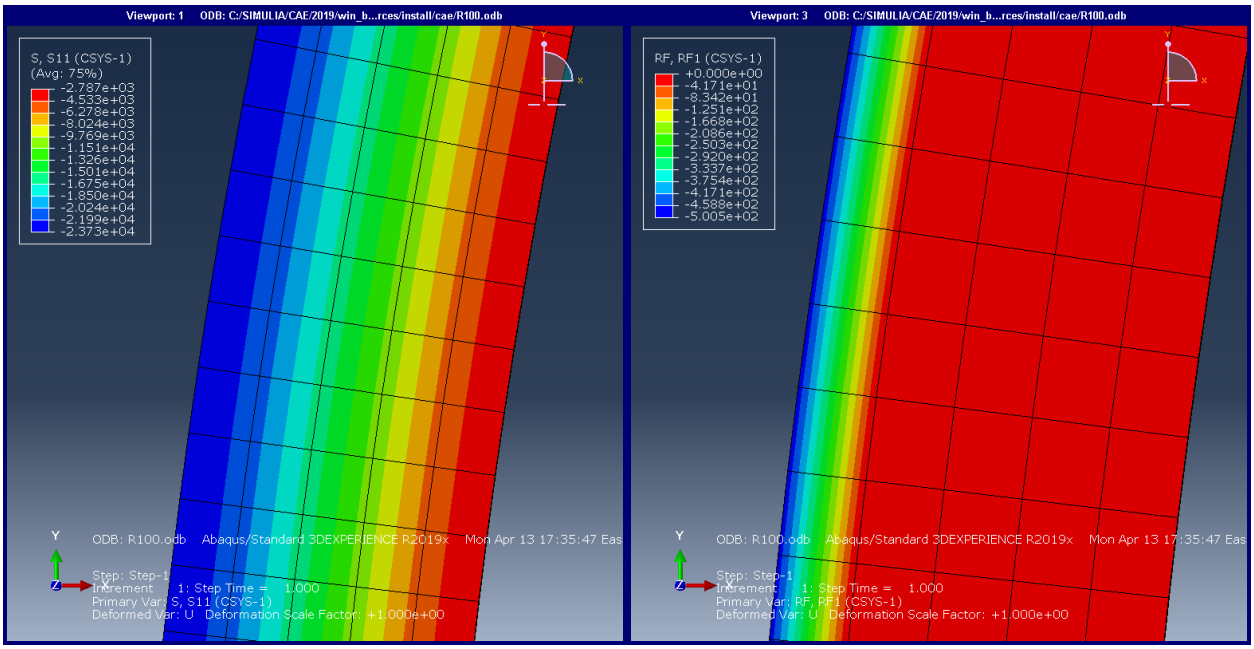

Figure A - 1: FEM Ring Model for R = 100 ft and T = 20 F

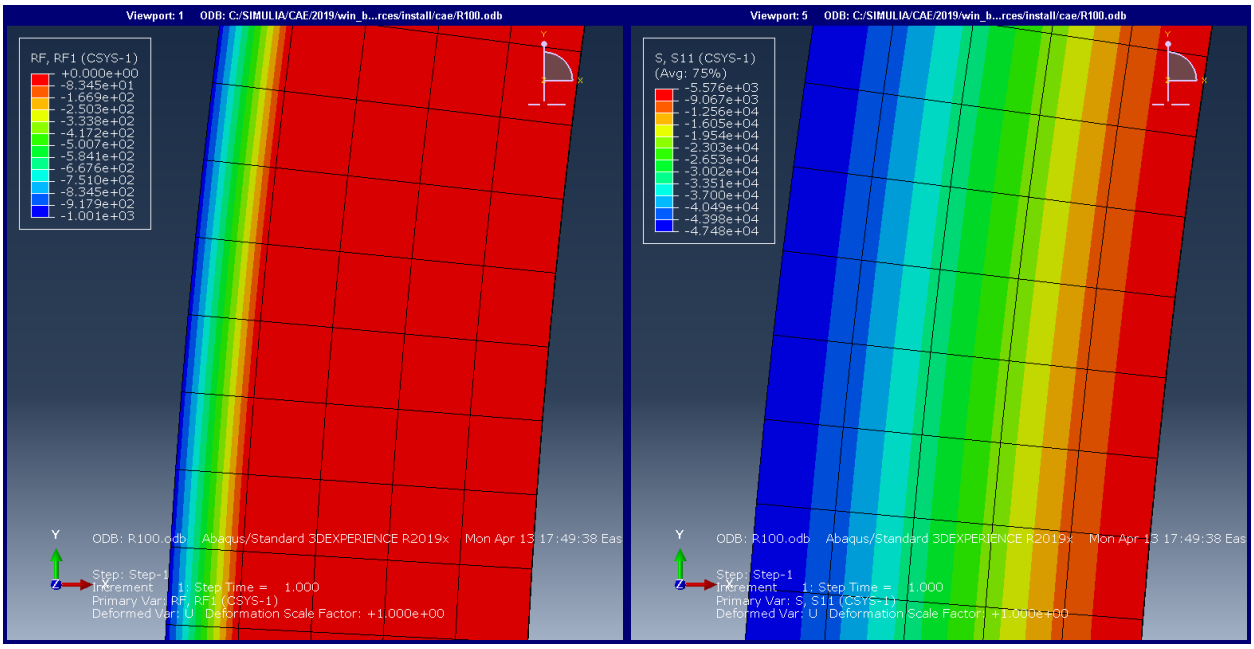

Figure A - 2: FEM Ring Model for R = 100 ft and T = 40 F

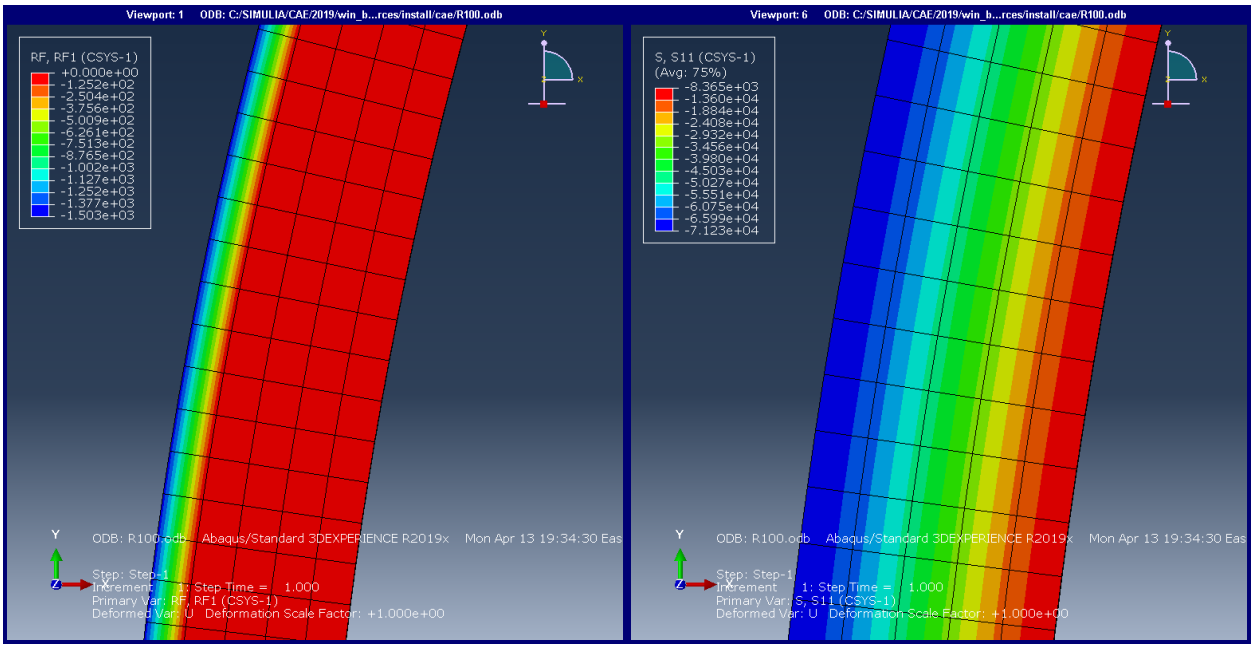

Figure A - 3: FEM Ring Model for R = 100 ft and T = 60 F

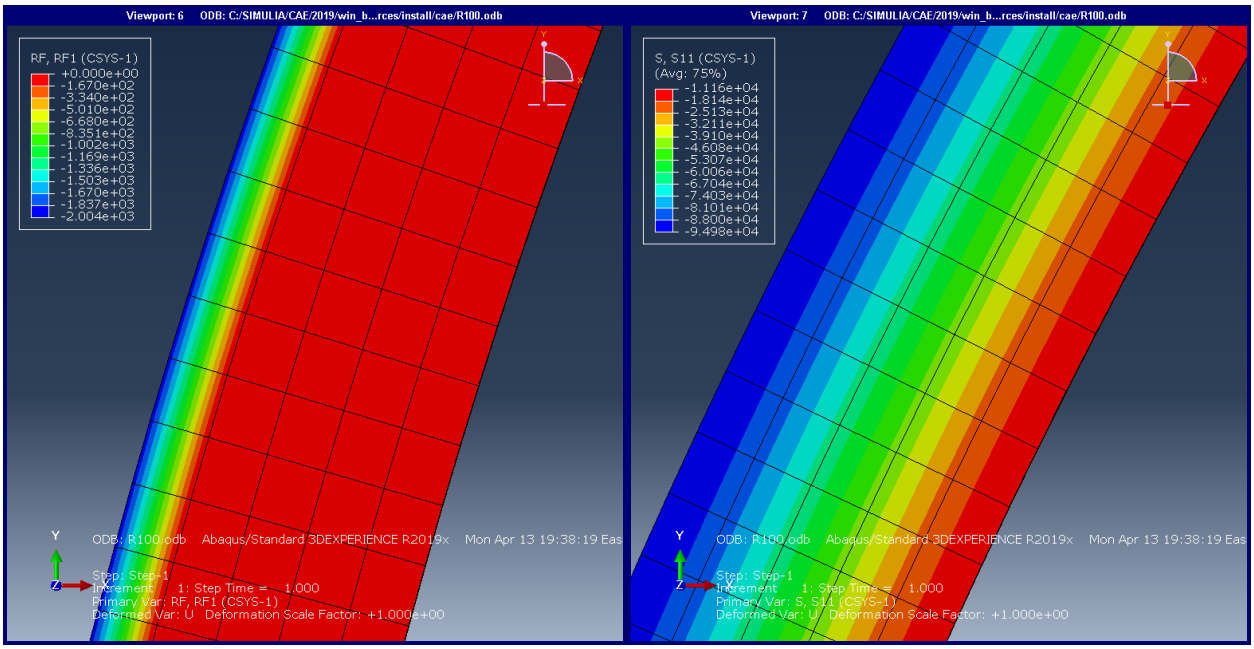

Figure A - 4: FEM Ring Model for R = 100 ft and T = 80 F

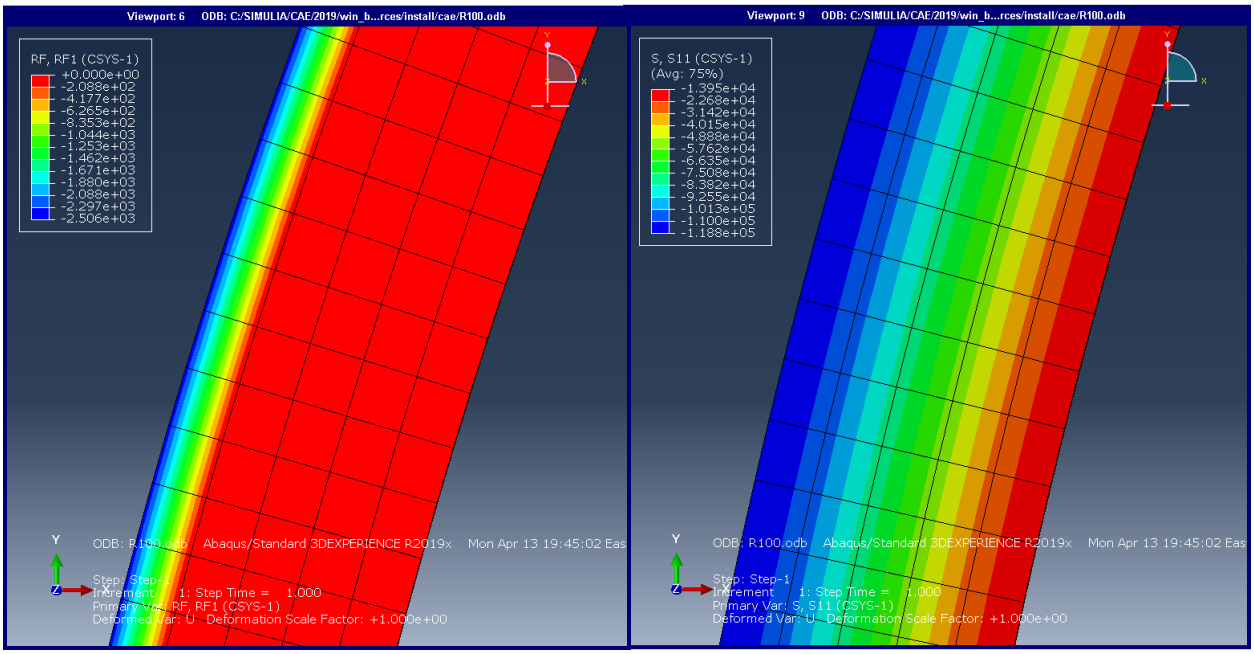

Figure A - 5: FEM Ring Model for R = 100 ft and T = 100 F

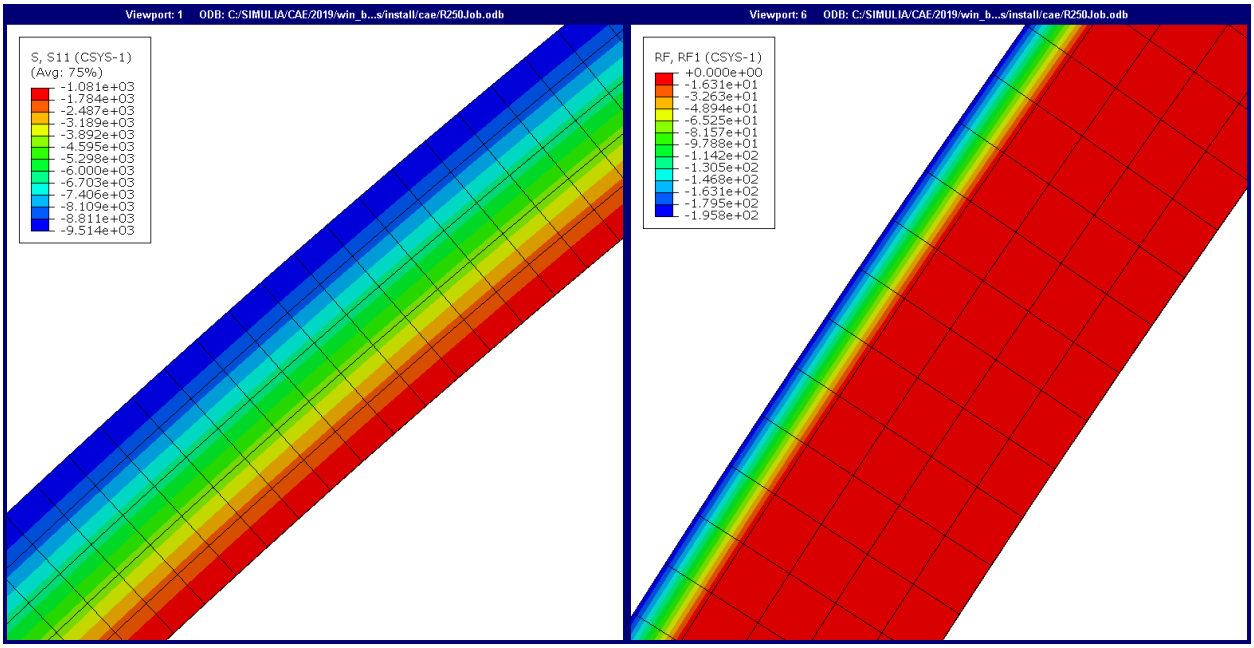

Figure A - 6: FEM Ring Model for R = 250 ft and T = 20 F

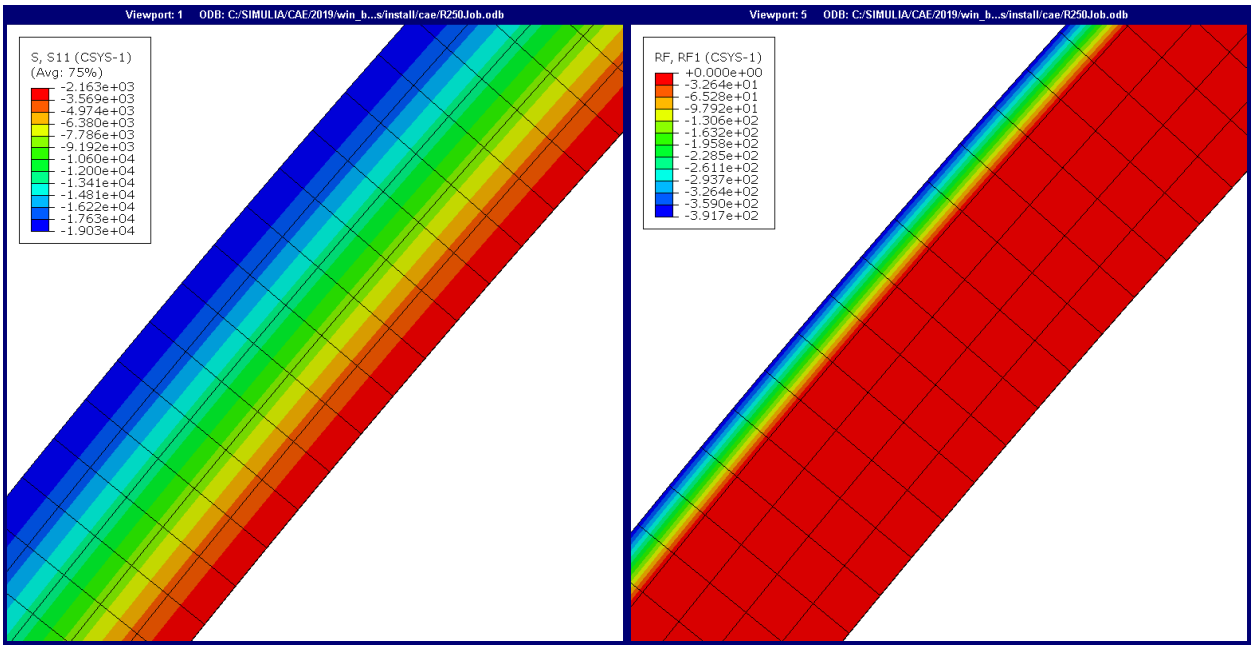

Figure A - 7: FEM Ring Model for R = 250 ft and T = 40 F

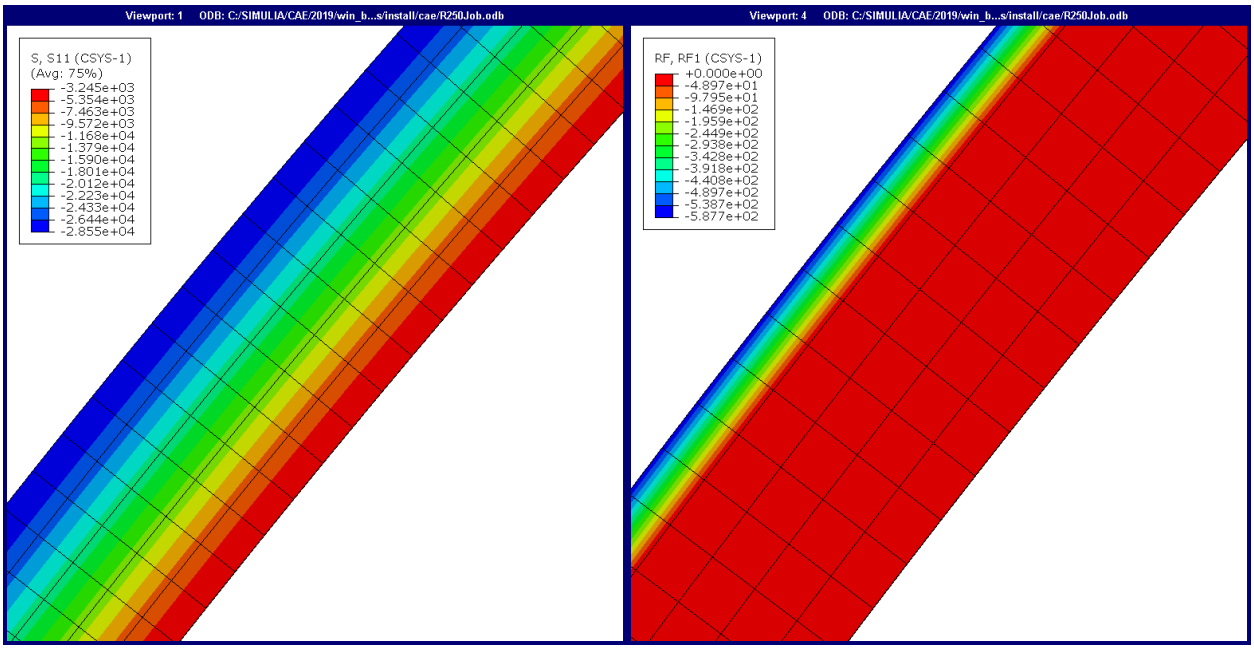

Figure A - 8: FEM Ring Model for R = 250 ft and T = 60 F

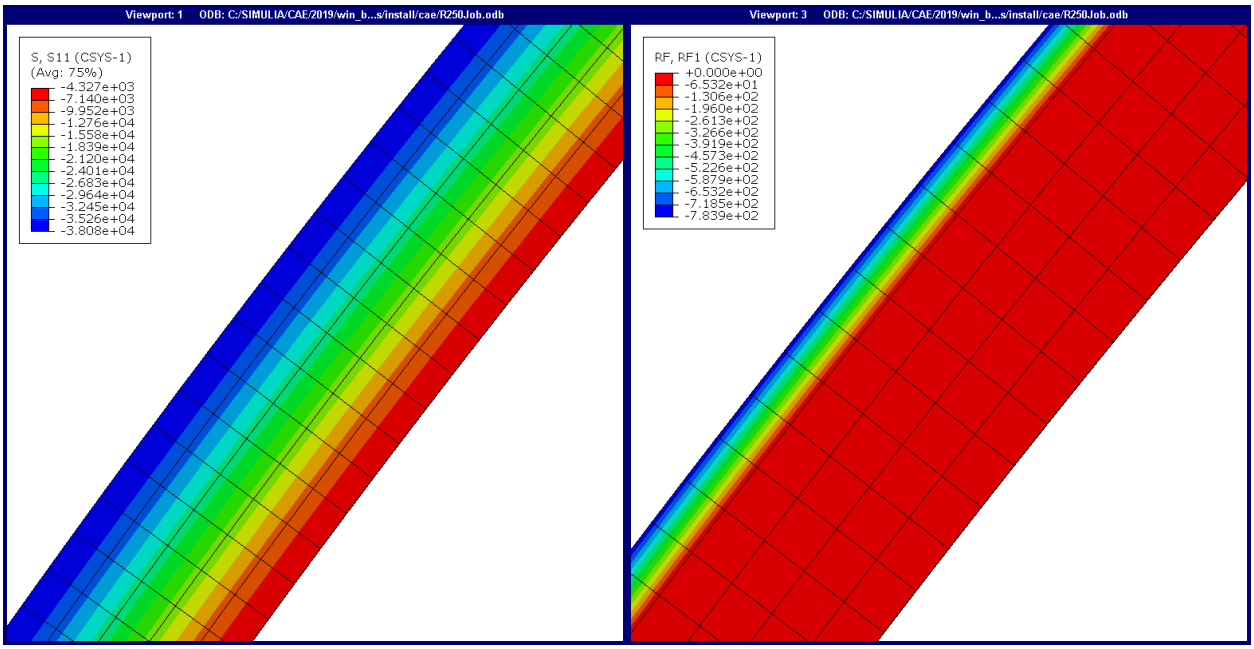

Figure A - 9: FEM Ring Model for R = 250 ft and T = 80 F

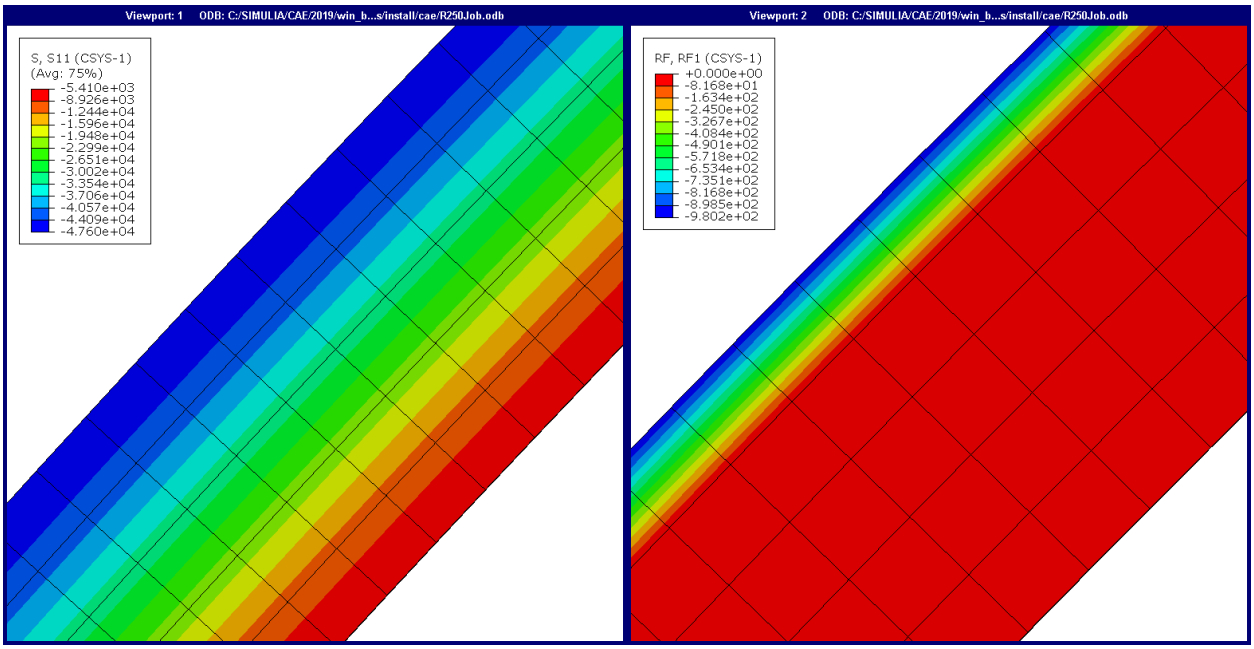

Figure A - 10: FEM Ring Model for R = 250 ft and T = 100 F

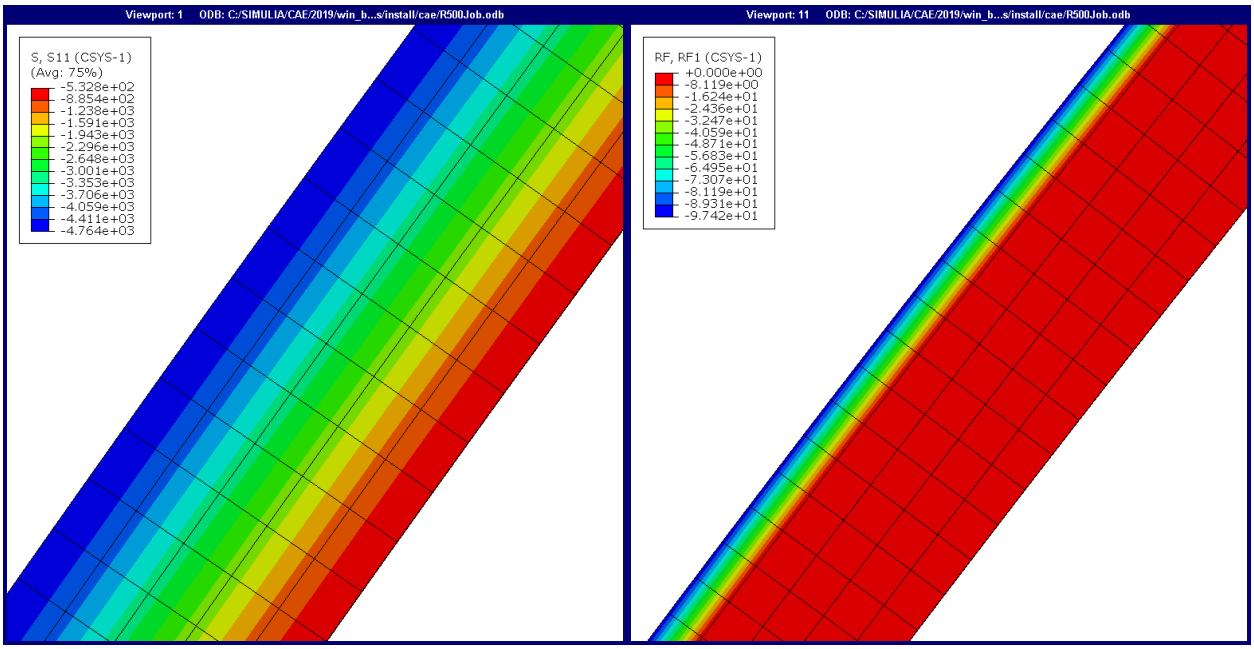

Figure A - 11: FEM Ring Model for R = 500 ft and T = 20 F

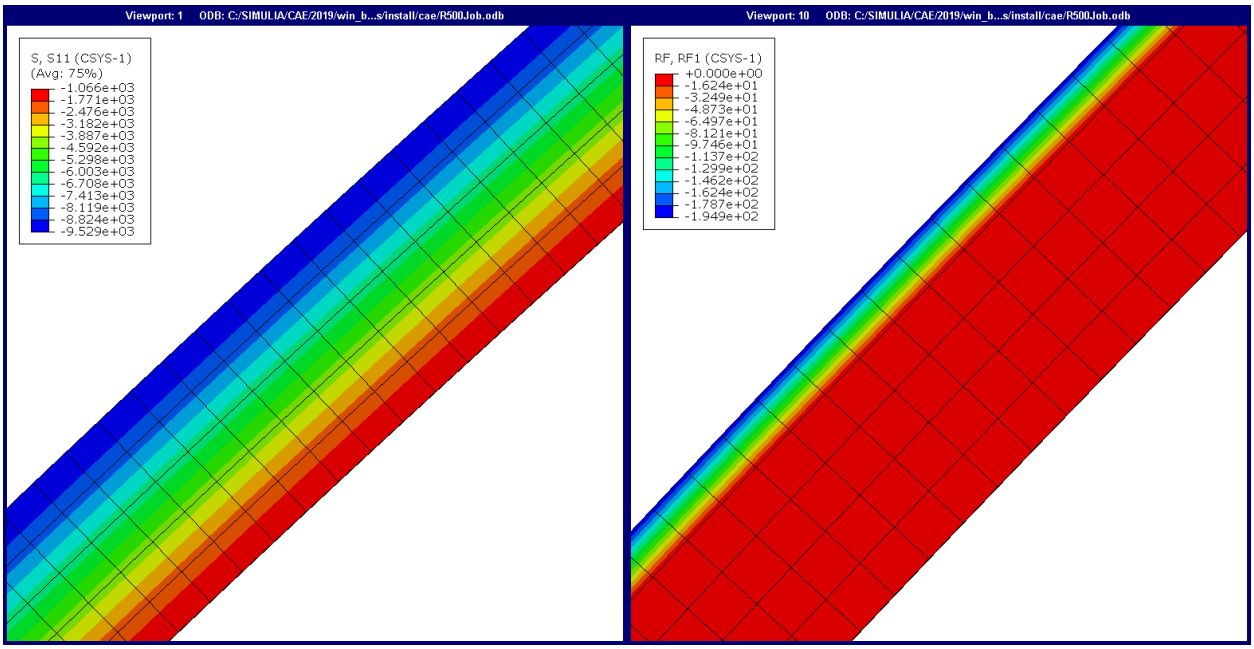

Figure A - 12: FEM Ring Model for R = 500 ft and T = 40 F

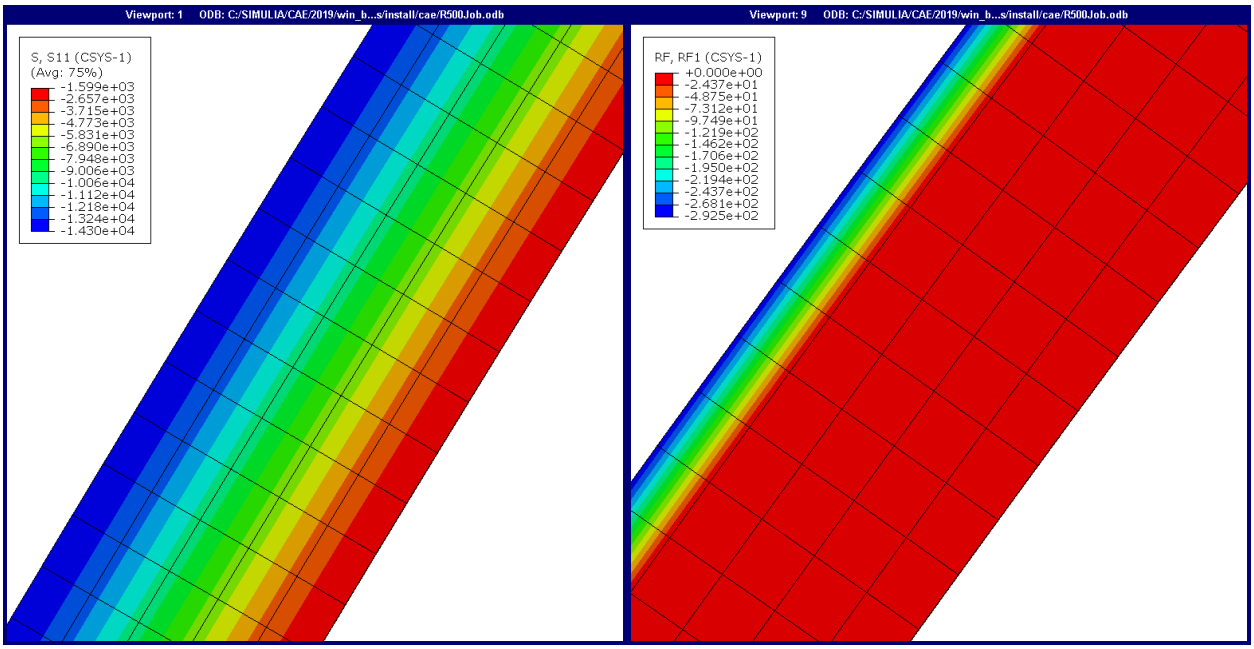

Figure A - 13: FEM Ring Model for R = 500 ft and T = 60 F

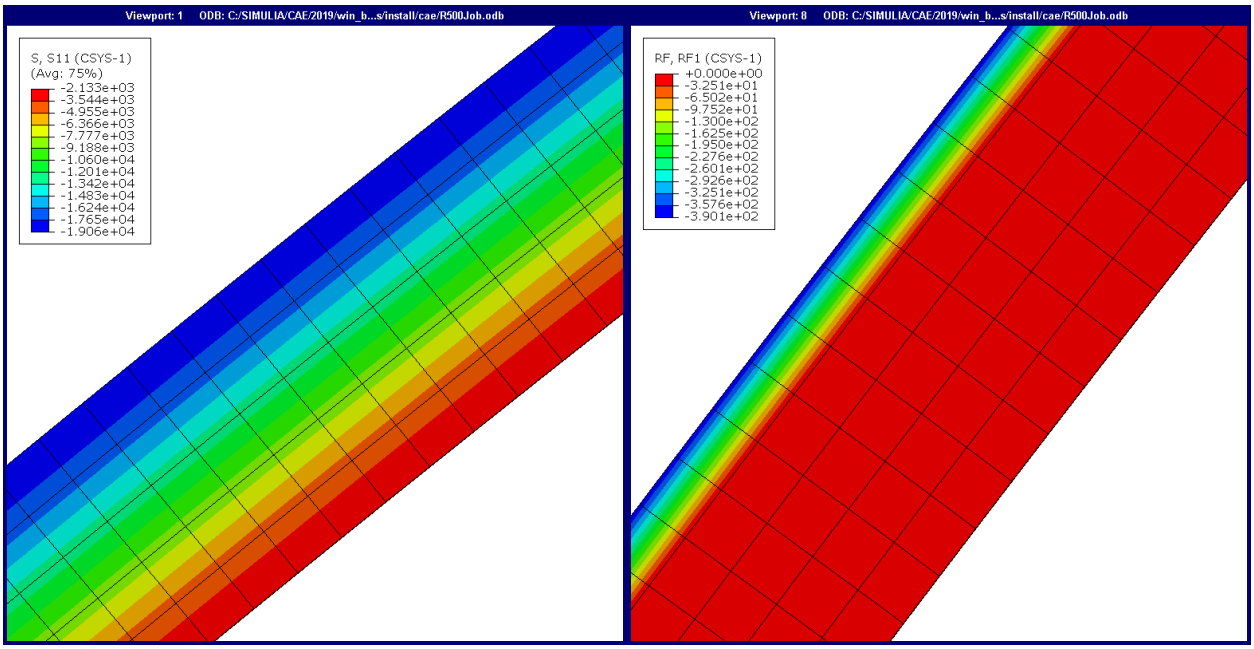

Figure A - 14: FEM Ring Model for R = 500 ft and T = 80 F

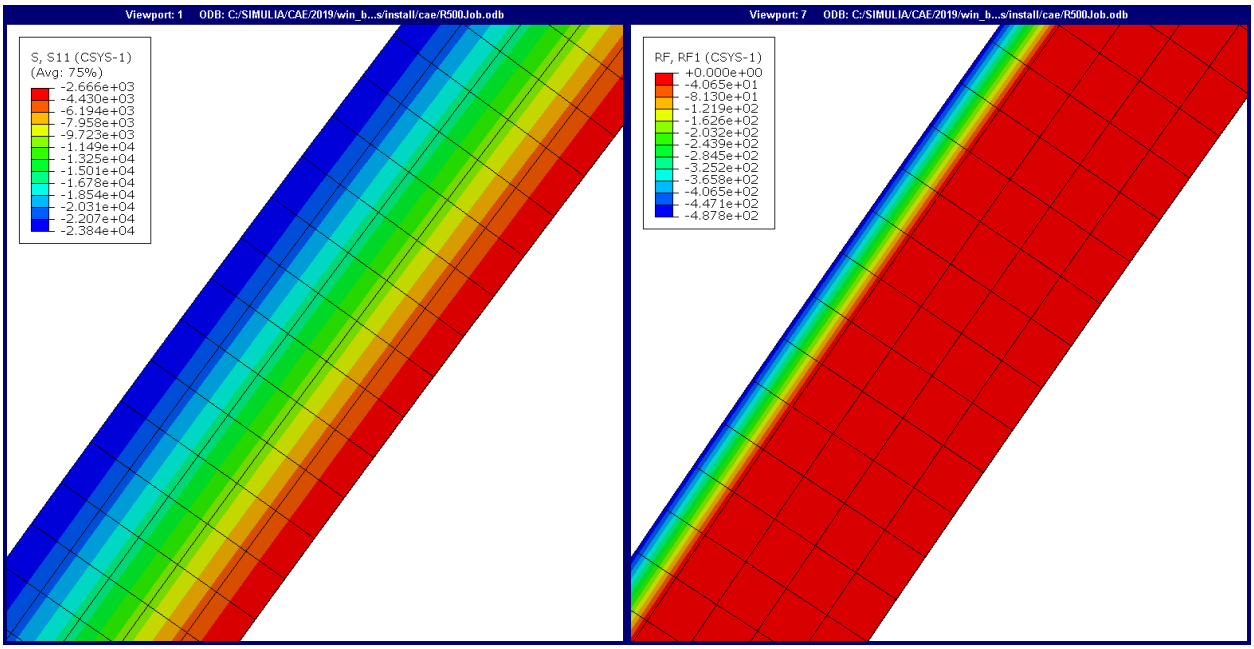

Figure A - 15: FEM Ring Model for R = 500 ft and T = 100 F

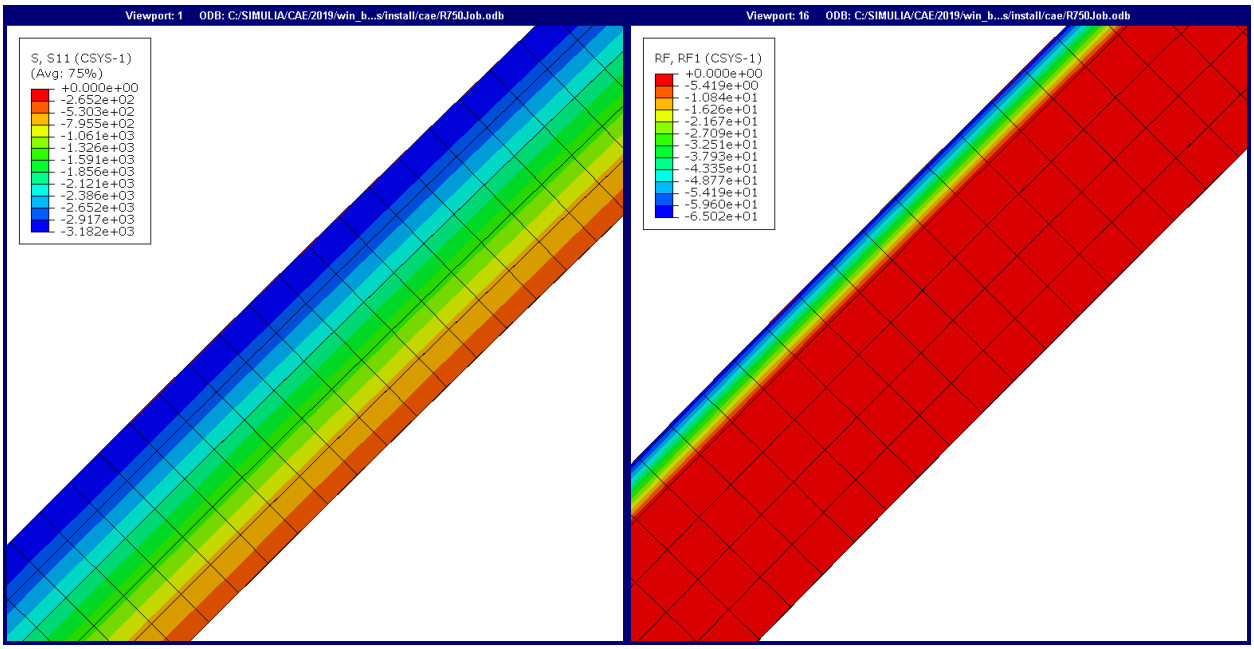

Figure A - 16: FEM Ring Model for R = 750 ft and T = 20 F

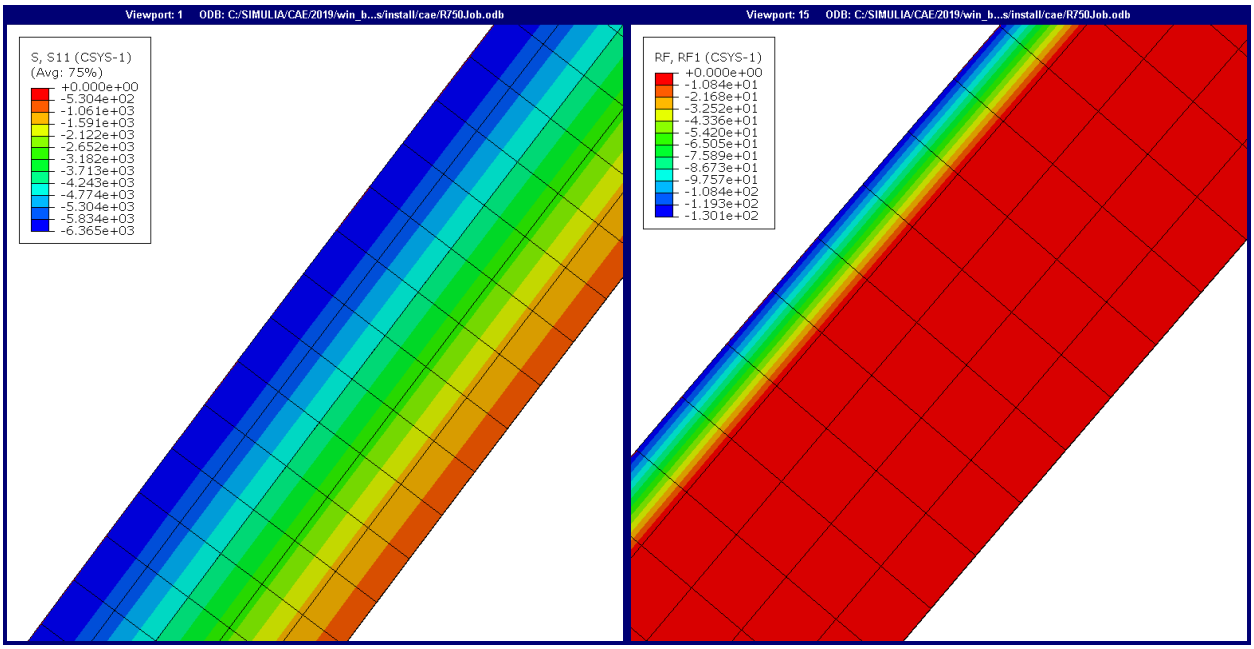

Figure A - 17: FEM Ring Model for R = 750 ft and T = 40 F

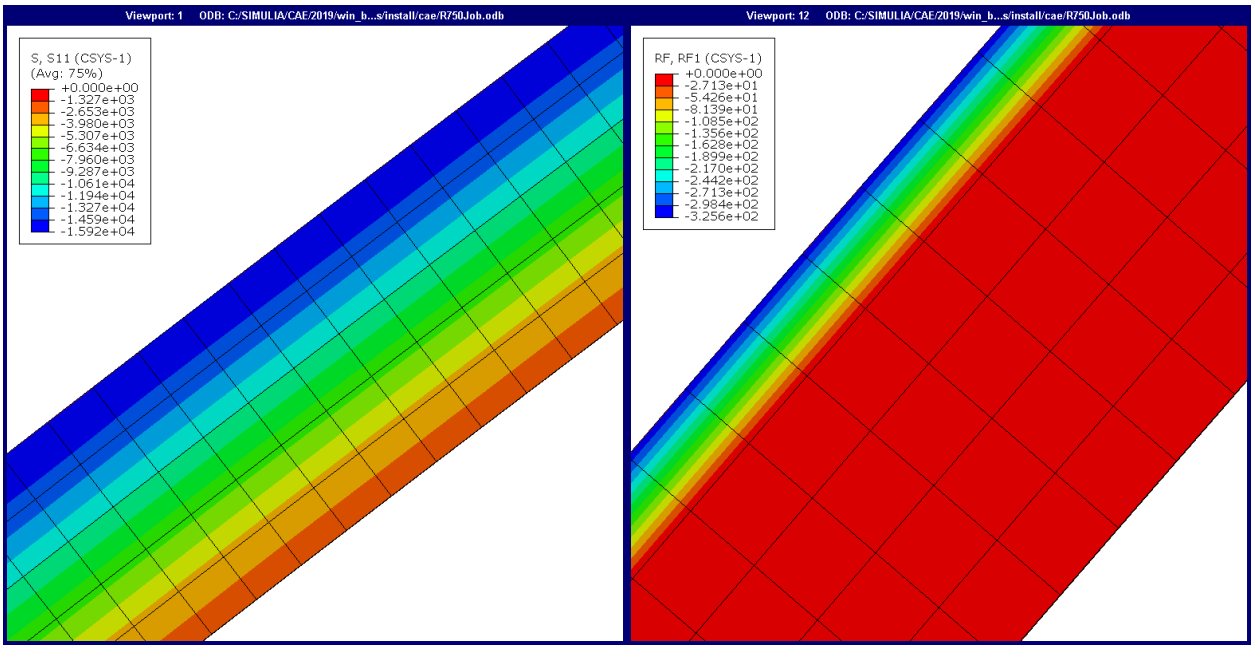

F
igure A - 18: FEM Ring Model for R = 750 ft and T = 60 F

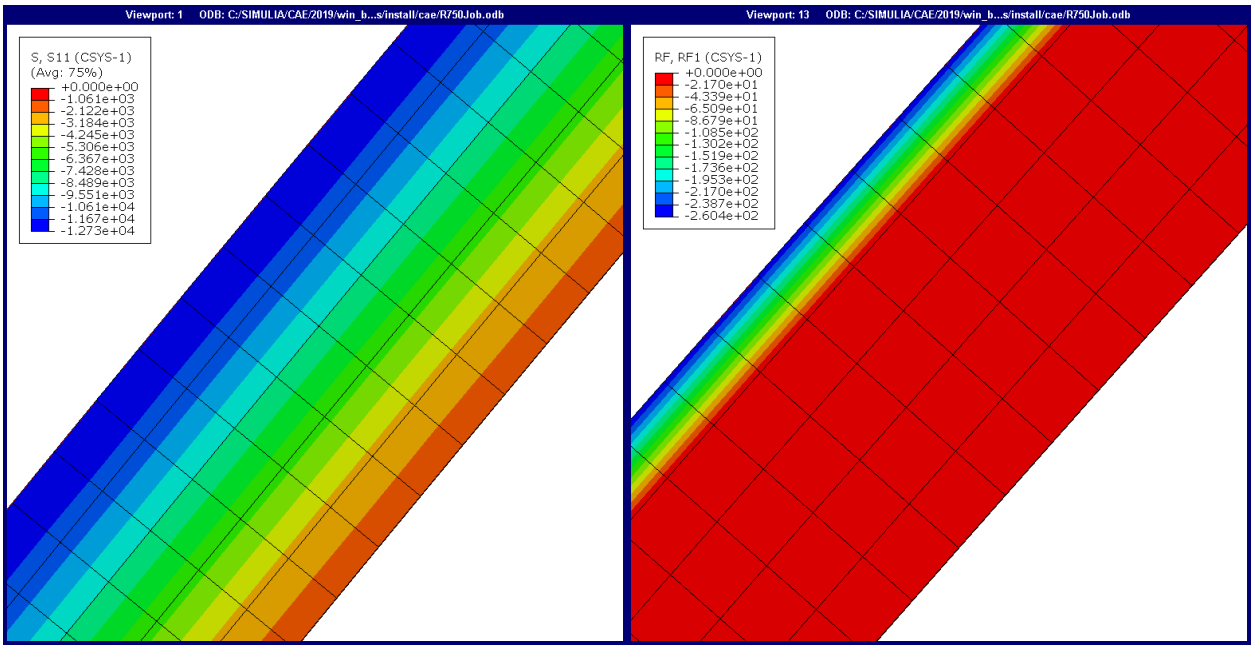

Figure A - 19: FEM Ring Model for R = 750 ft and T = 80 F

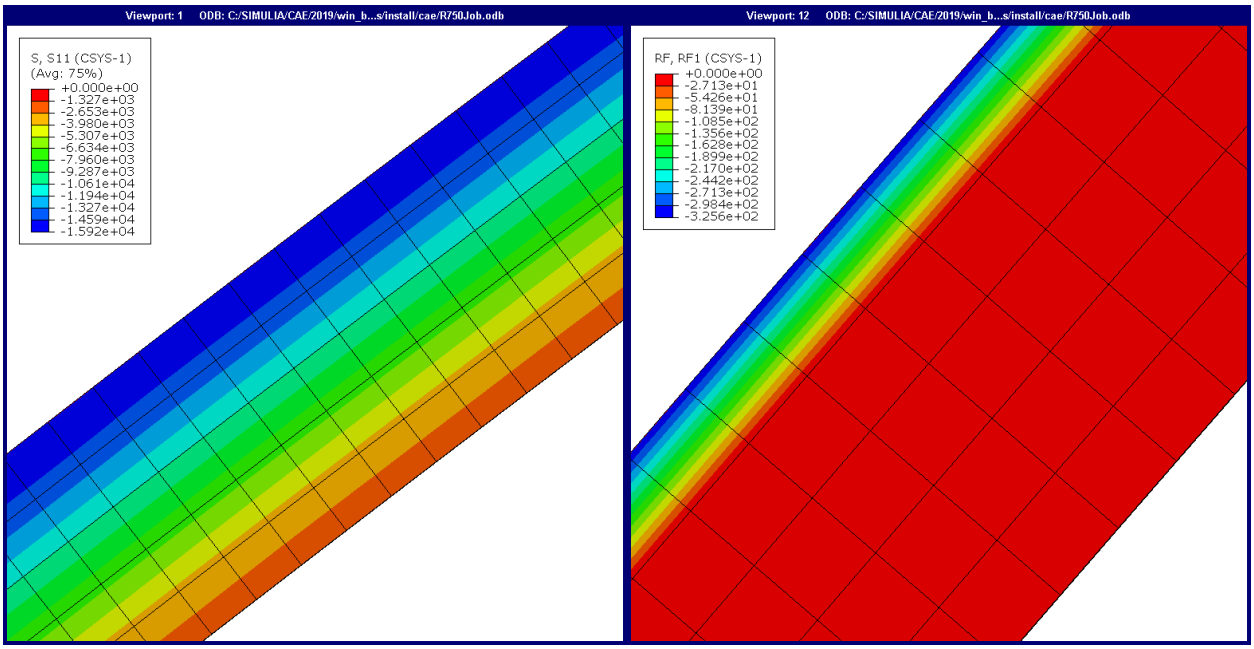

Figure A - 20: FEM Ring Model for R = 750 ft and T = 100 F

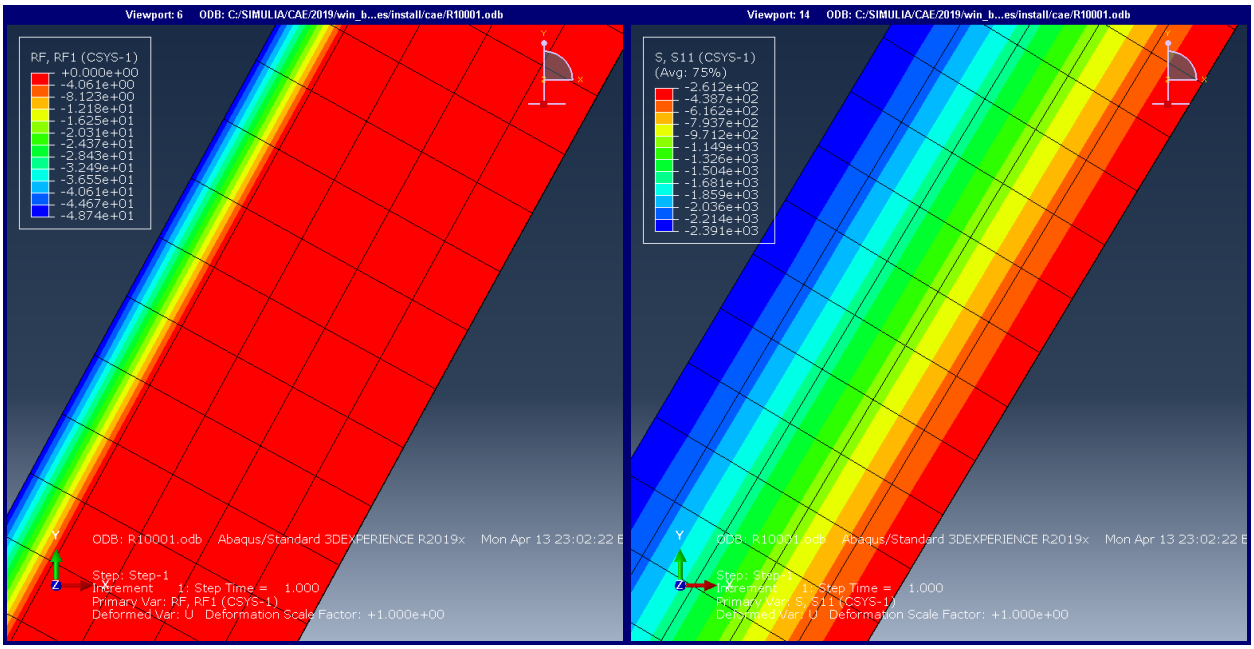

Figure A - 21: FEM Ring Model for R = 1000 ft and T = 20 F

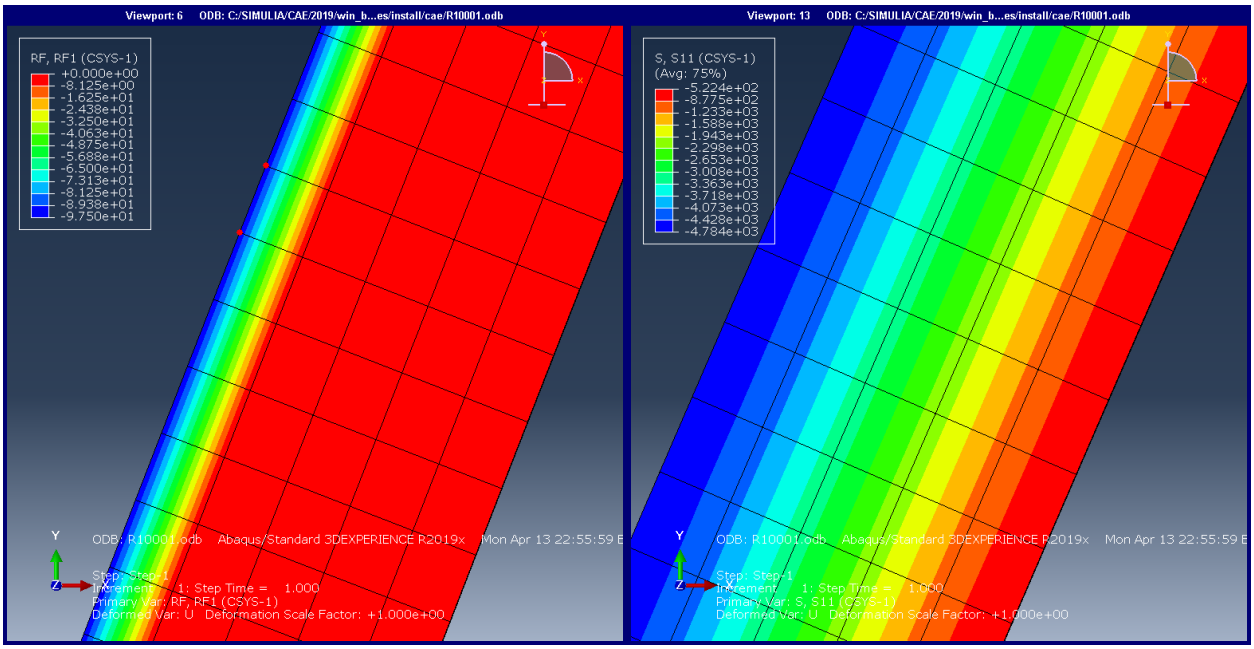

Figure A - 22: FEM Ring Model for R = 1000 ft and T = 40 F

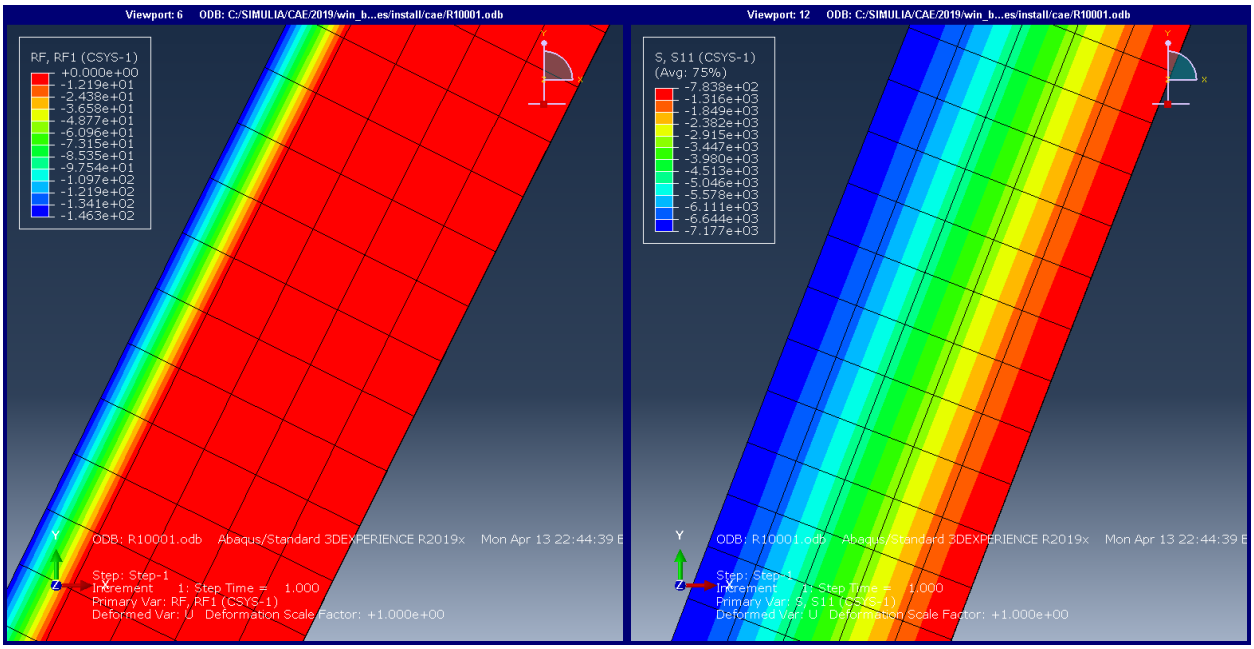

Figure A - 23: FEM Ring Model for R = 1000 ft and T = 60 F

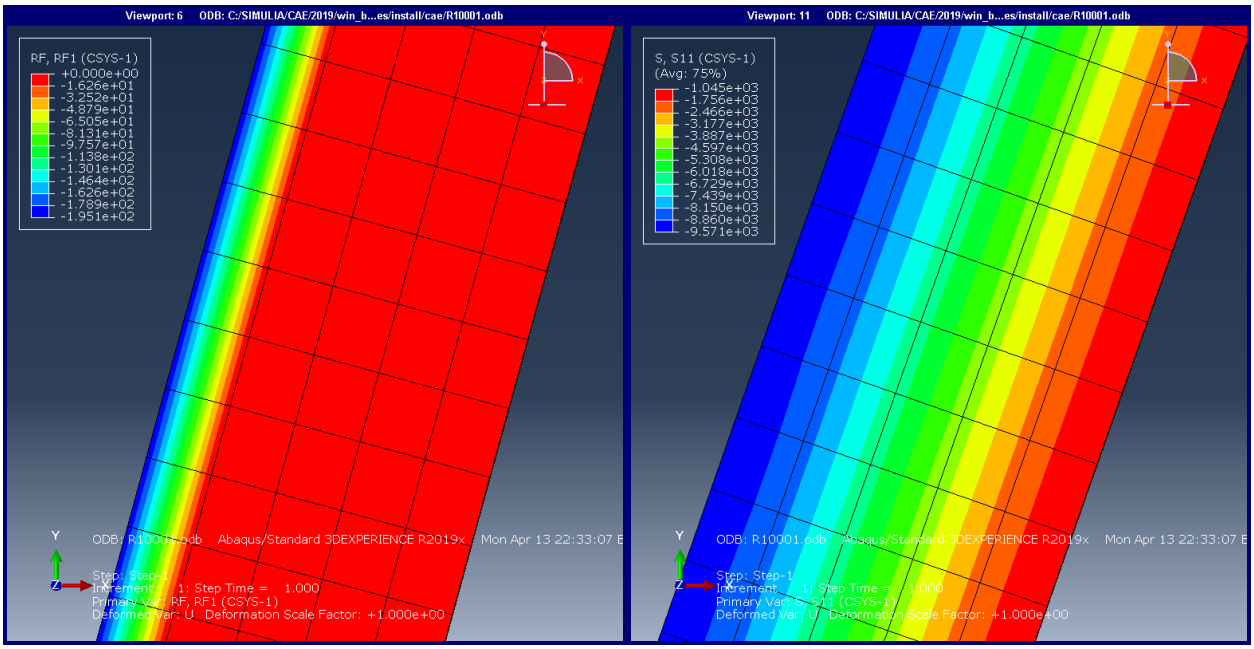

Figure A - 24: FEM Ring Model for R = 1000 ft and T = 80 F

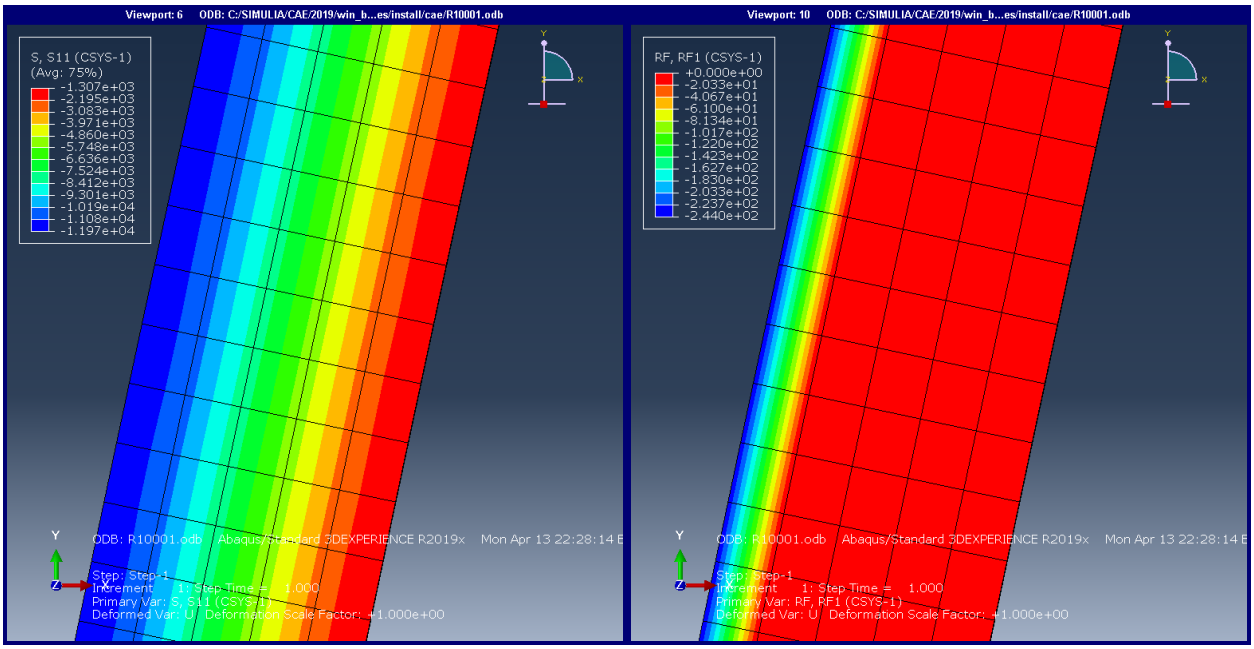

Figure A - 25: FEM Ring Model for R = 1000 ft and T = 100 F

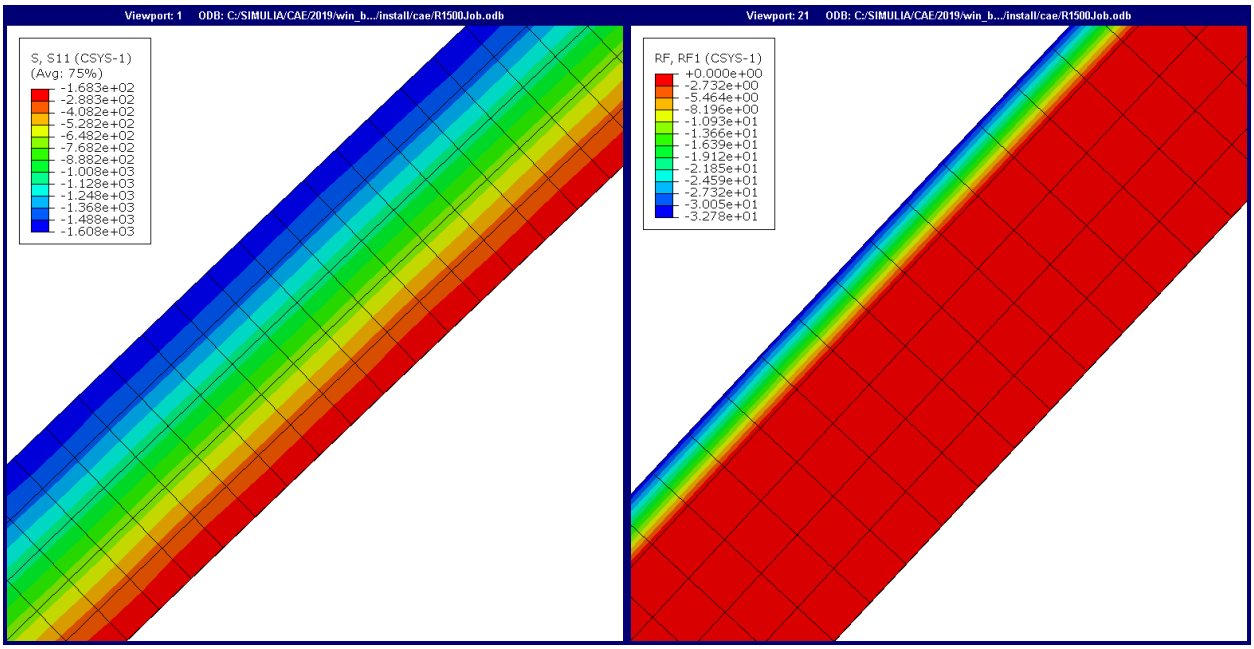

Figure A - 26: FEM Ring Model for R = 1500 ft and T = 20 F

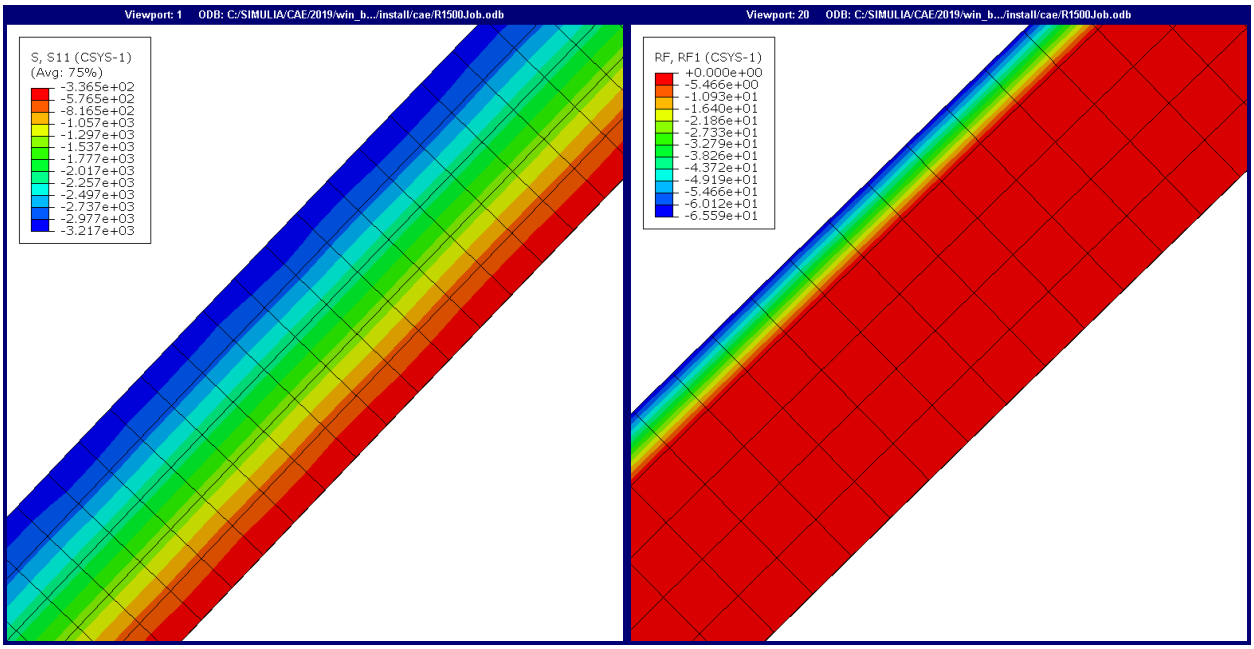

Figure A - 27: FEM Ring Model for R = 1500 ft and T = 40 F

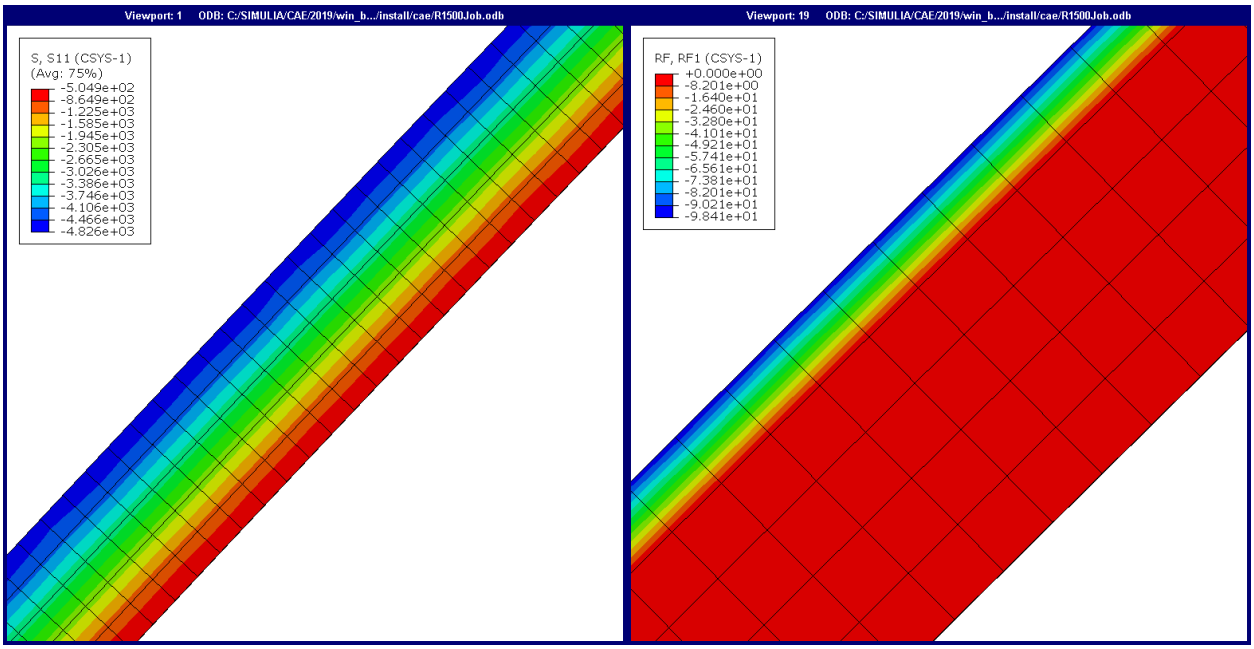

Figure A - 28: FEM Ring Model for R = 1500 ft and T = 60 F

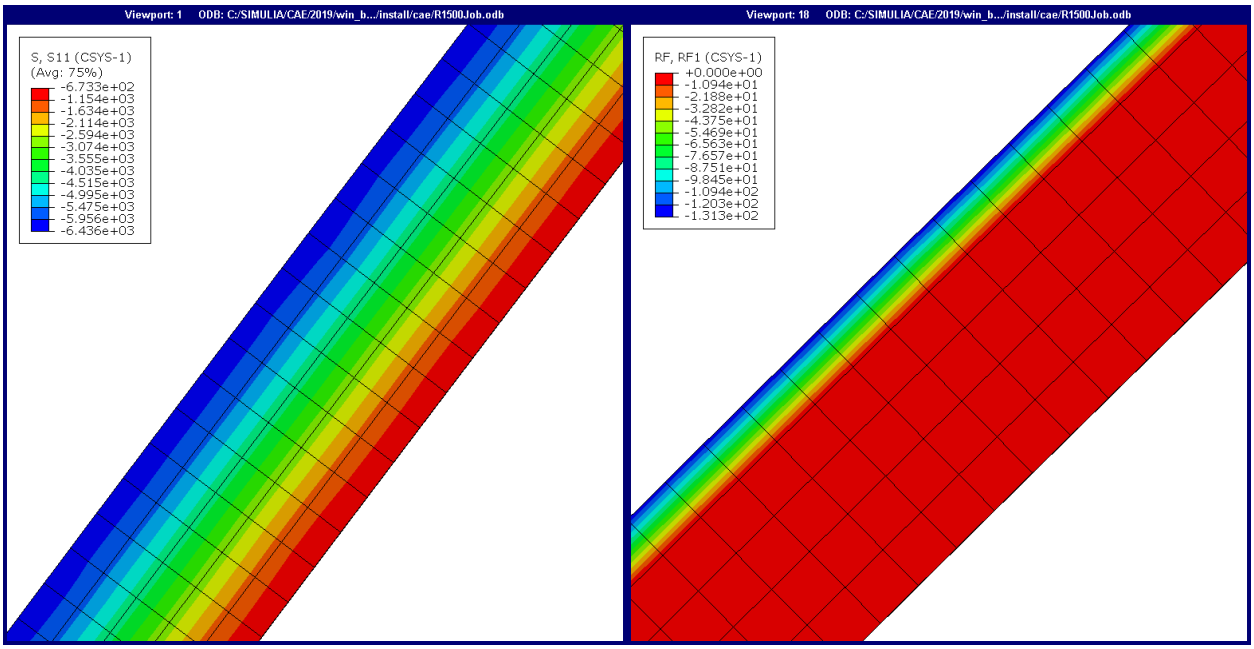

Figure A - 29: FEM Ring Model for R = 1500 ft and T = 80 F

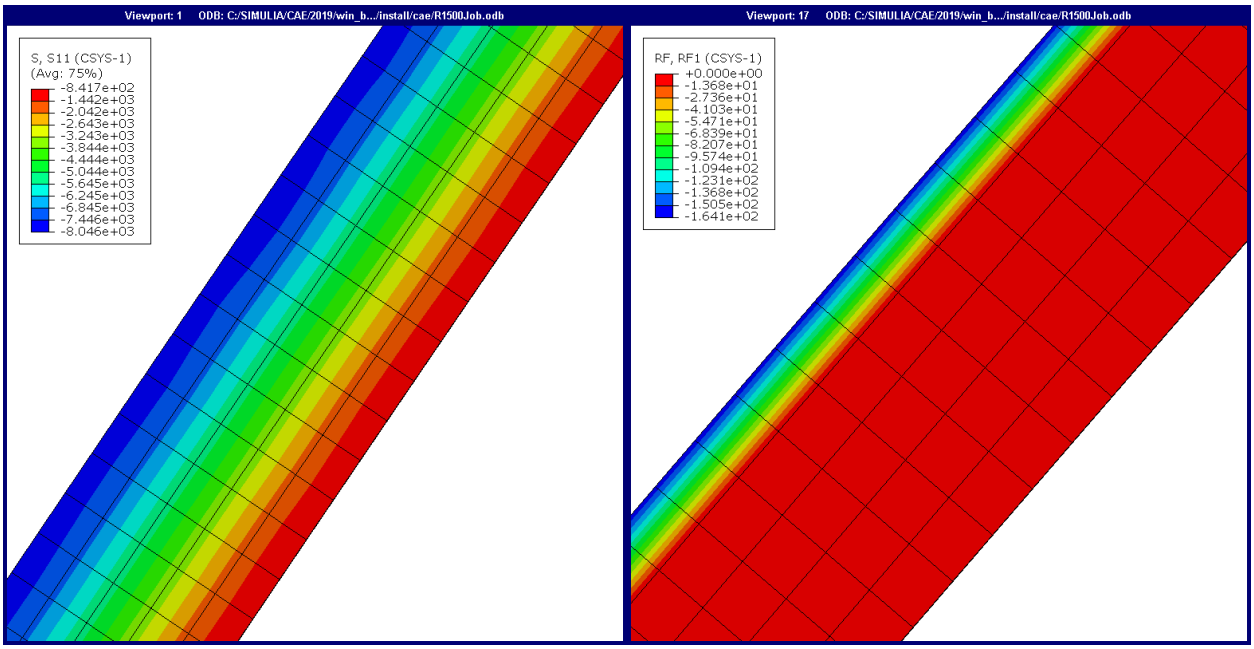

Figure A - 30: FEM Ring Model for R = 1500 ft and T = 100 F

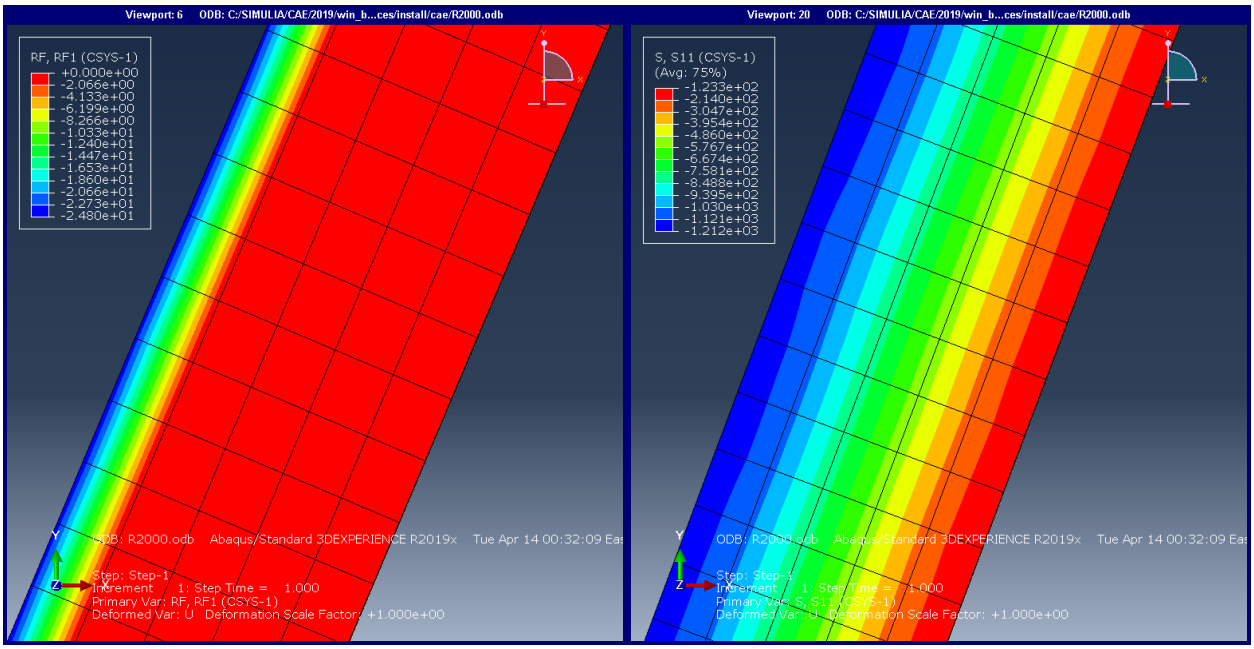

Figure A - 31: FEM Ring Model for R = 2000 ft and T = 20 F

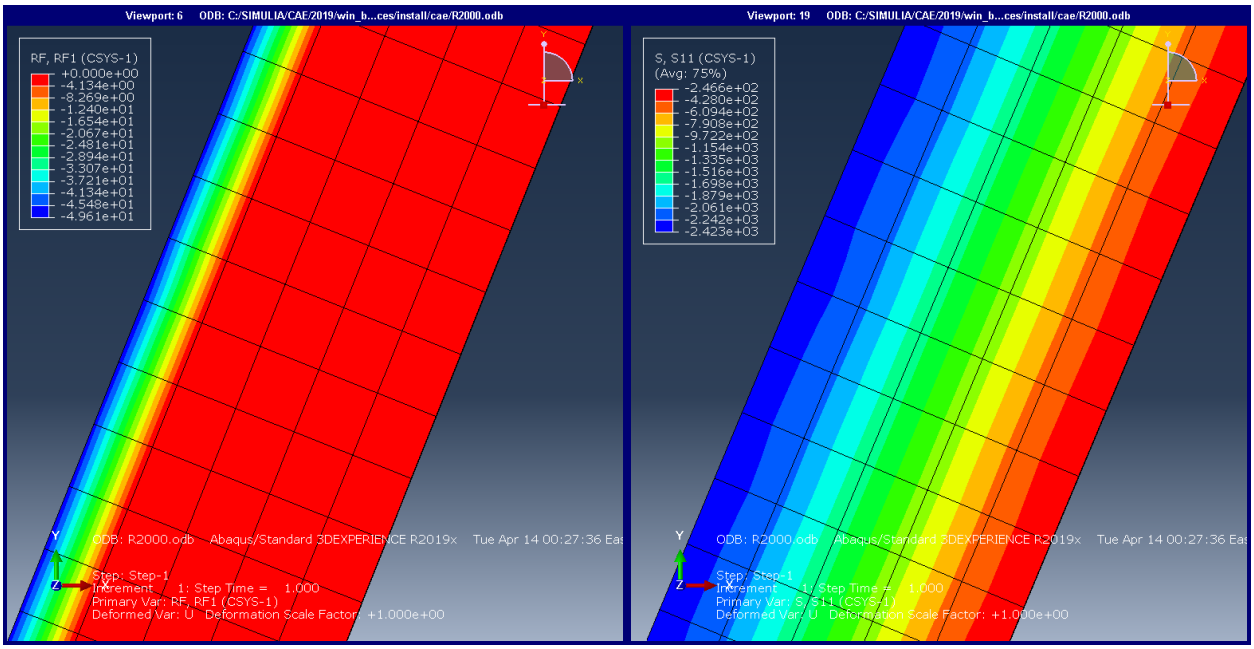

Figure A - 32: FEM Ring Model for R = 2000 ft and T = 40 F

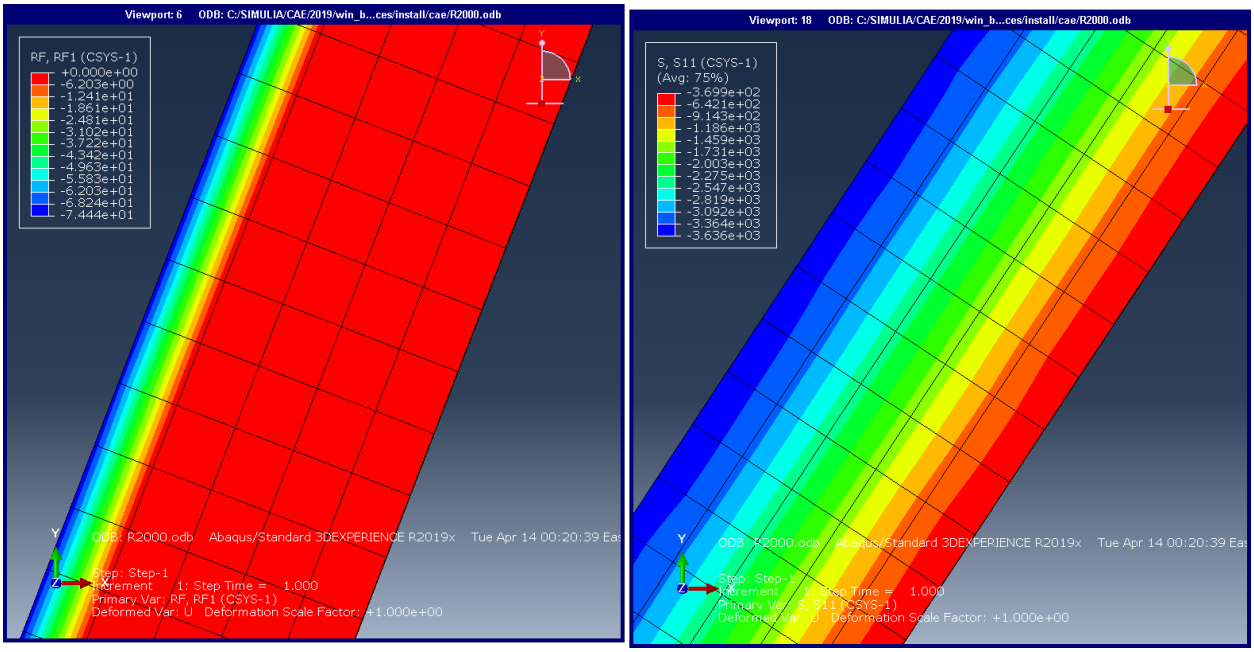

Figure A - 33: FEM Ring Model for R = 2000 ft and T = 60 F

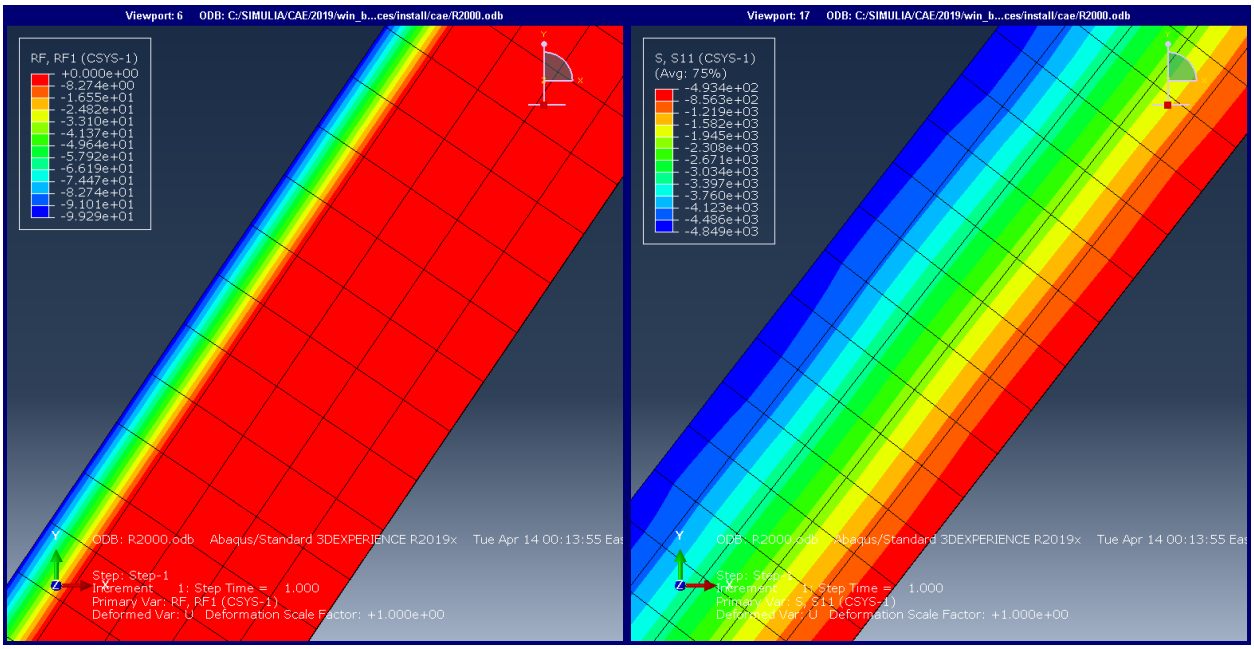

Figure A - 34: FEM Ring Model for R = 2000 ft and T = 60 F

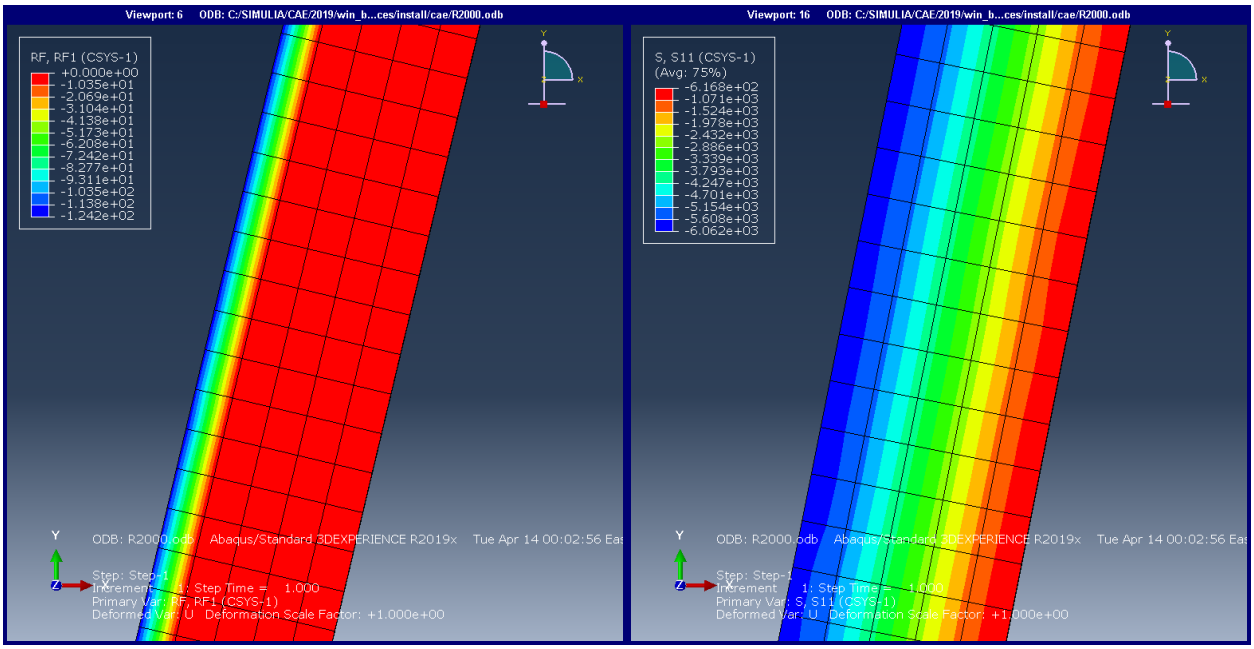

Figure A - 35: FEM Ring Model for R = 2000 ft and T = 80 F

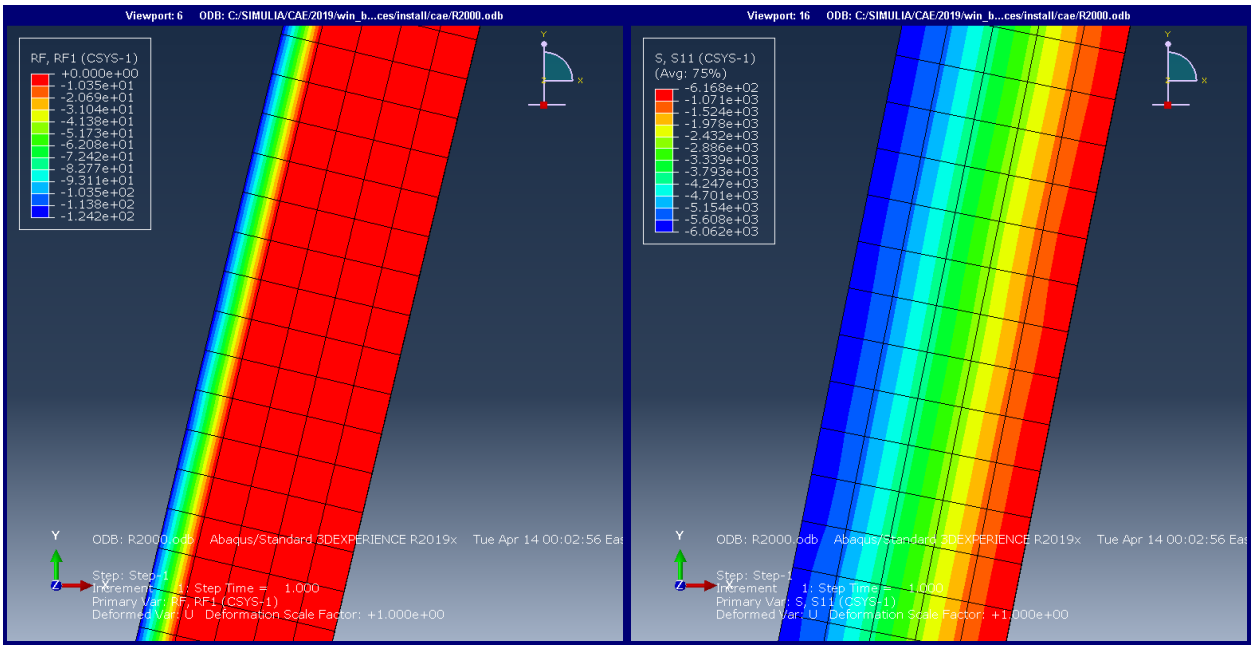

Figure A - 36: FEM Ring Model for R = 2000 ft and T = 100 F

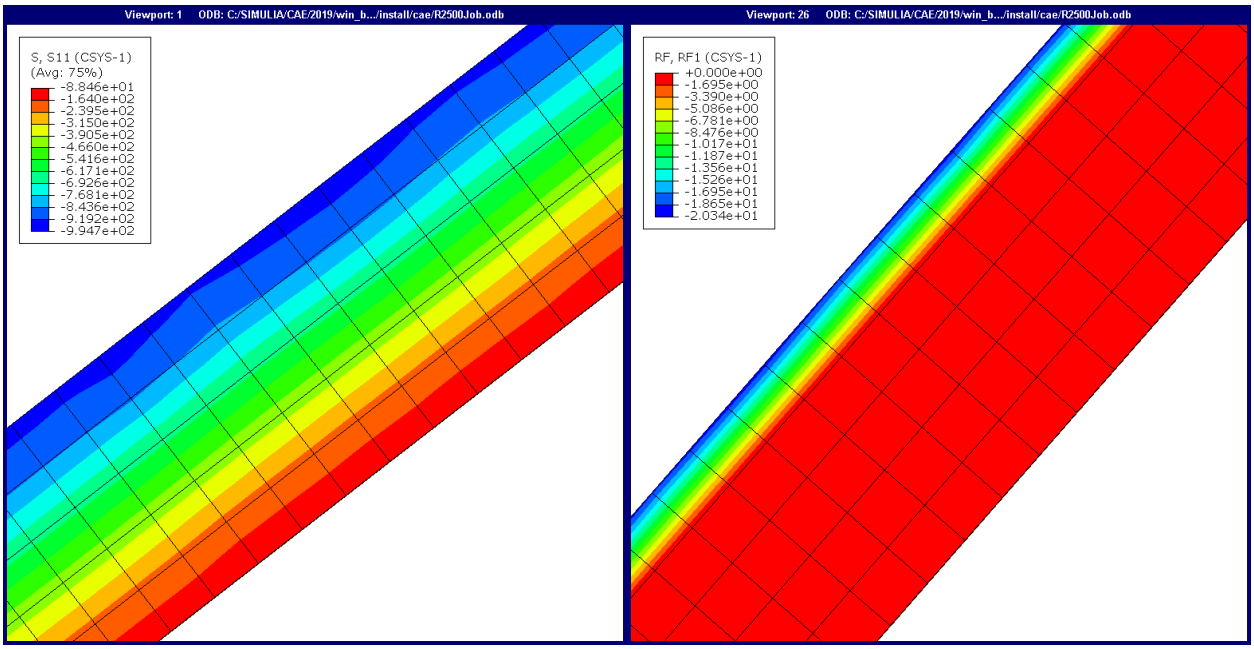

Figure A - 37: FEM Ring Model for R = 2500 ft and T = 20 F

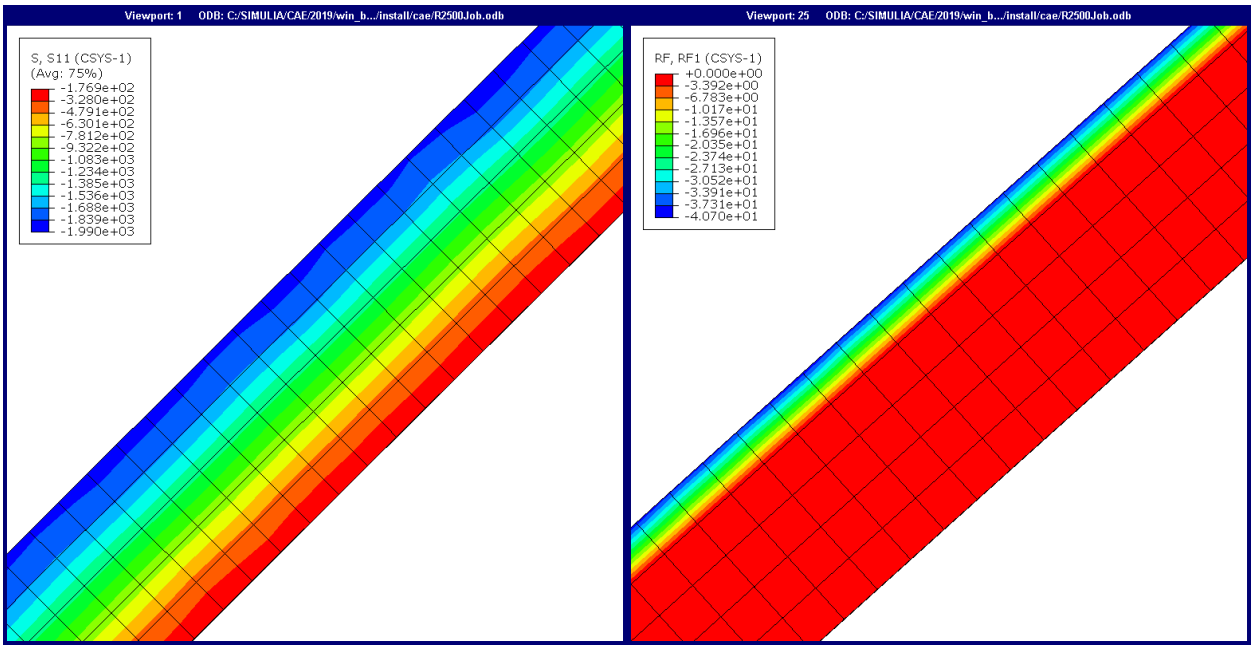

Figure A - 38: FEM Ring Model for R = 2500 ft and T = 40 F

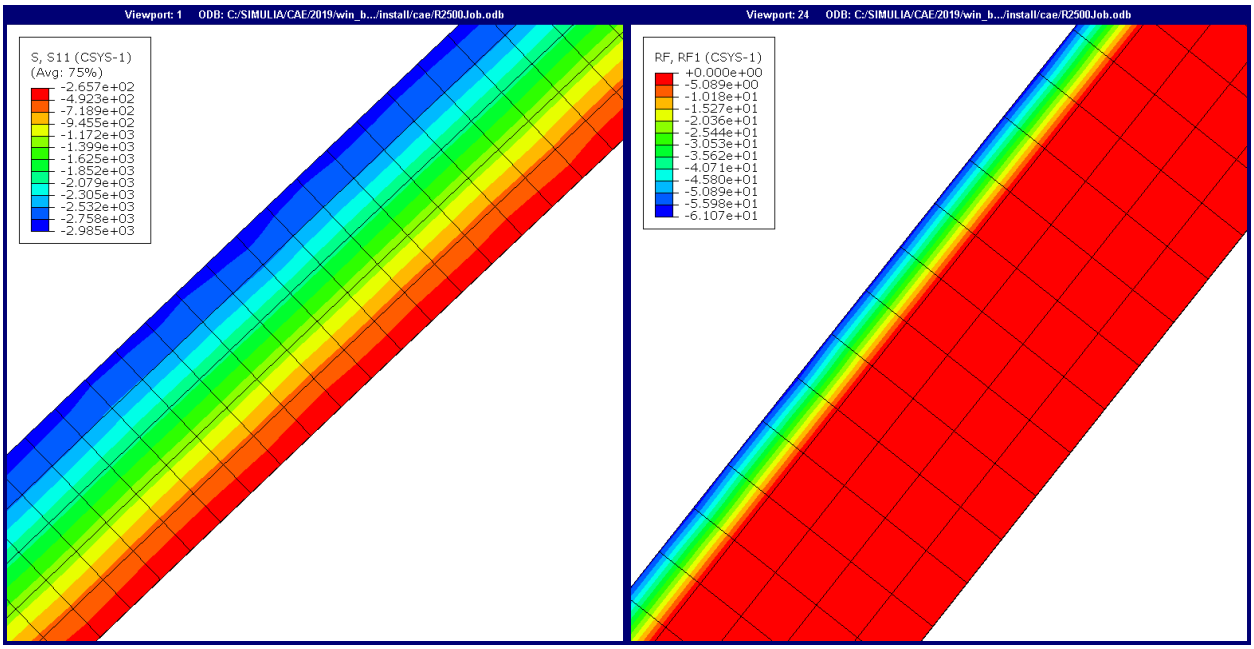

Figure A - 39: FEM Ring Model for R = 2500 ft and T = 60 F

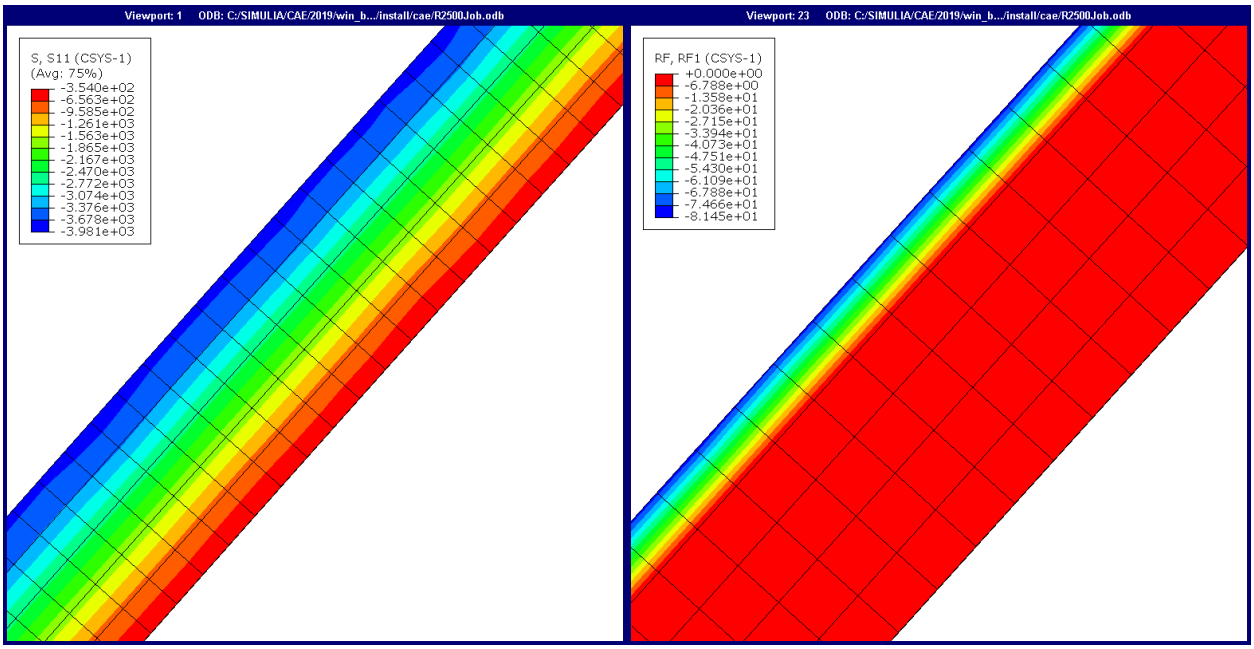

Figure A - 40: FEM Ring Model for R = 2500 ft and T = 80 F

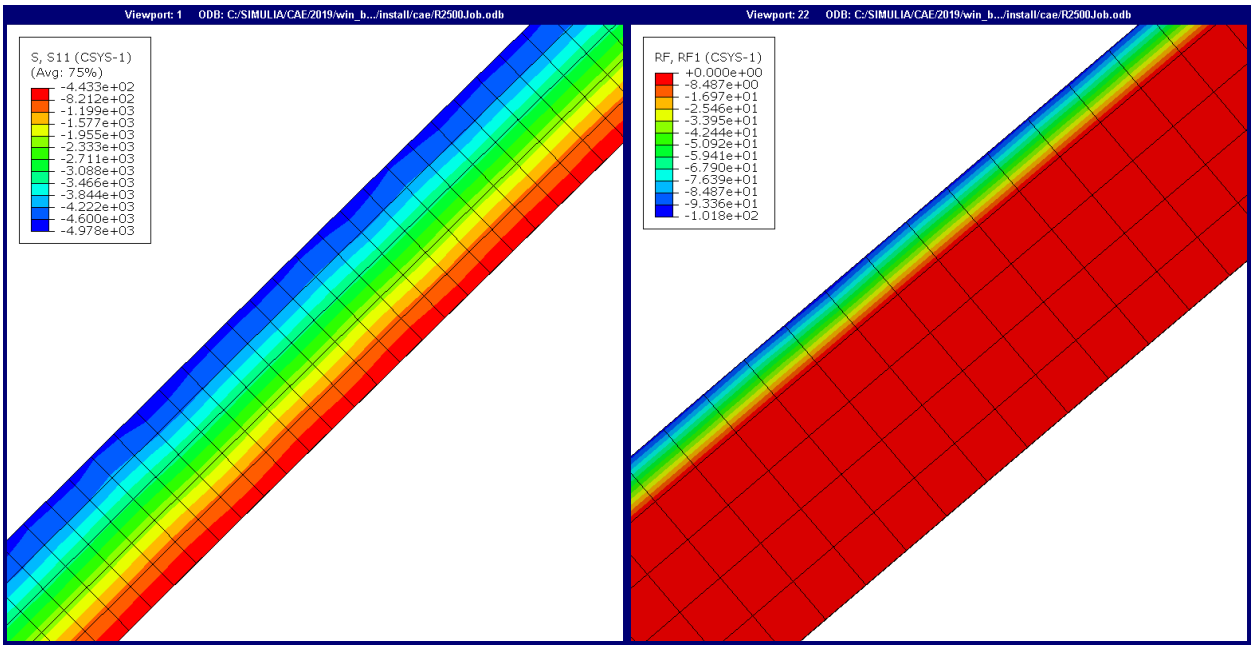

Figure A - 41: FEM Ring Model for R = 2500 ft and T = 100 F

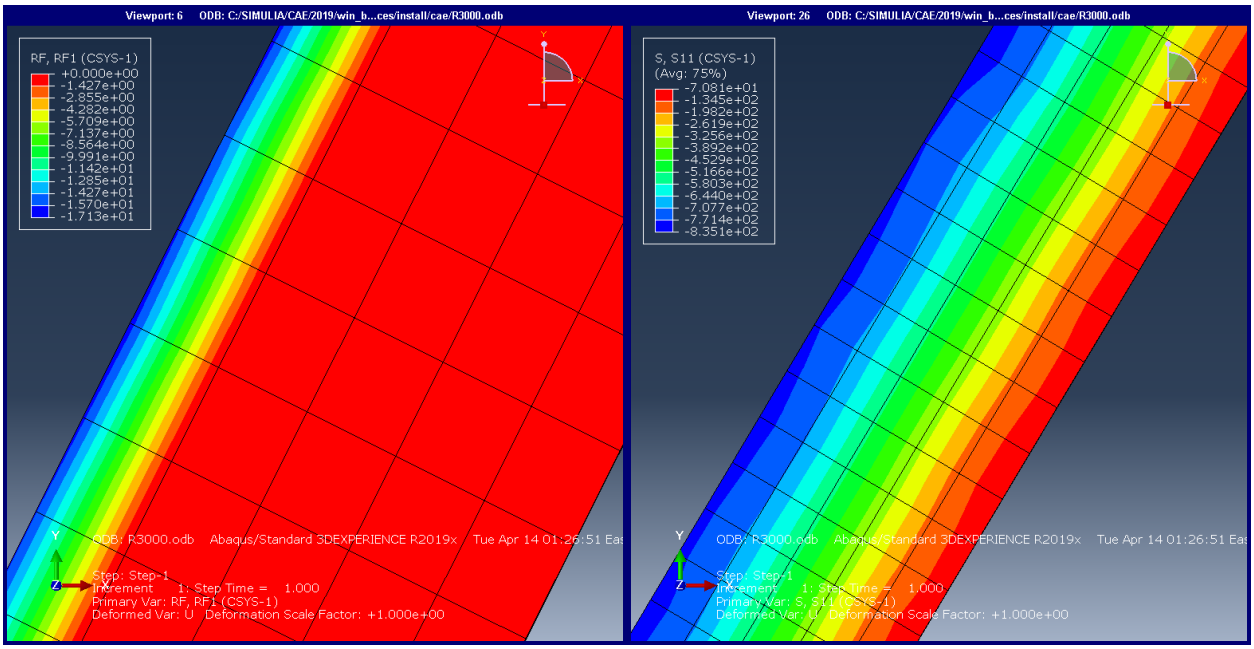

Figure A - 42: FEM Ring Model for R = 3000 ft and T = 20 F

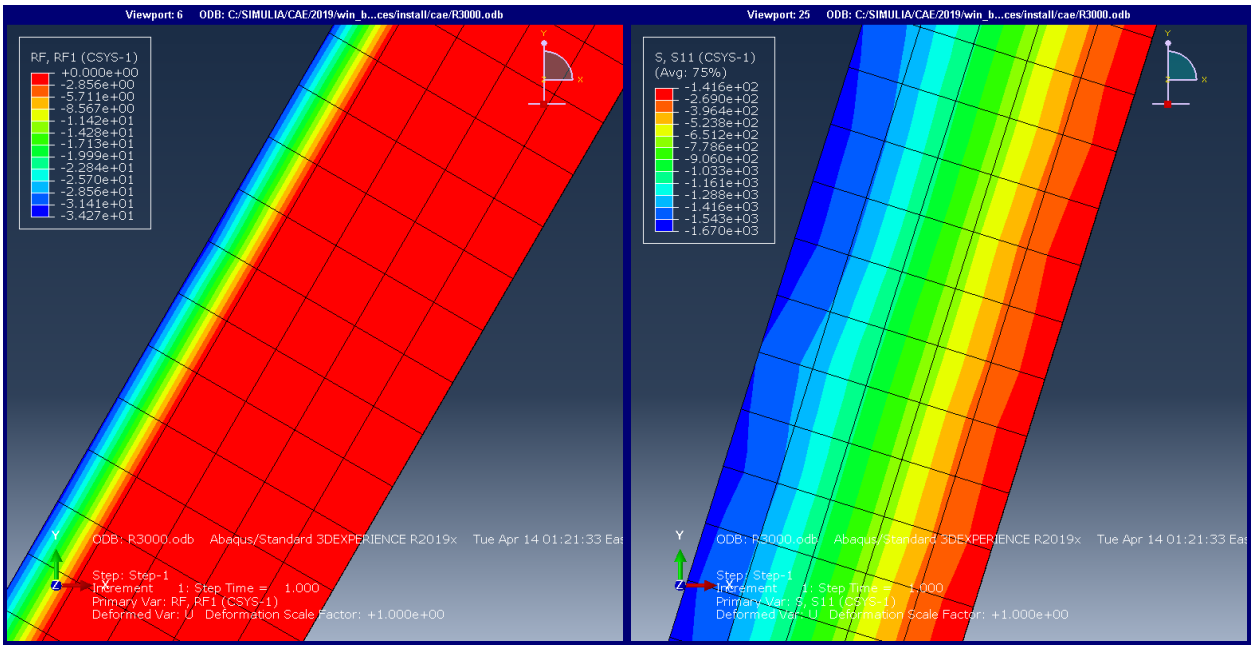

Figure A - 43: FEM Ring Model for R = 3000 ft and T = 40 F

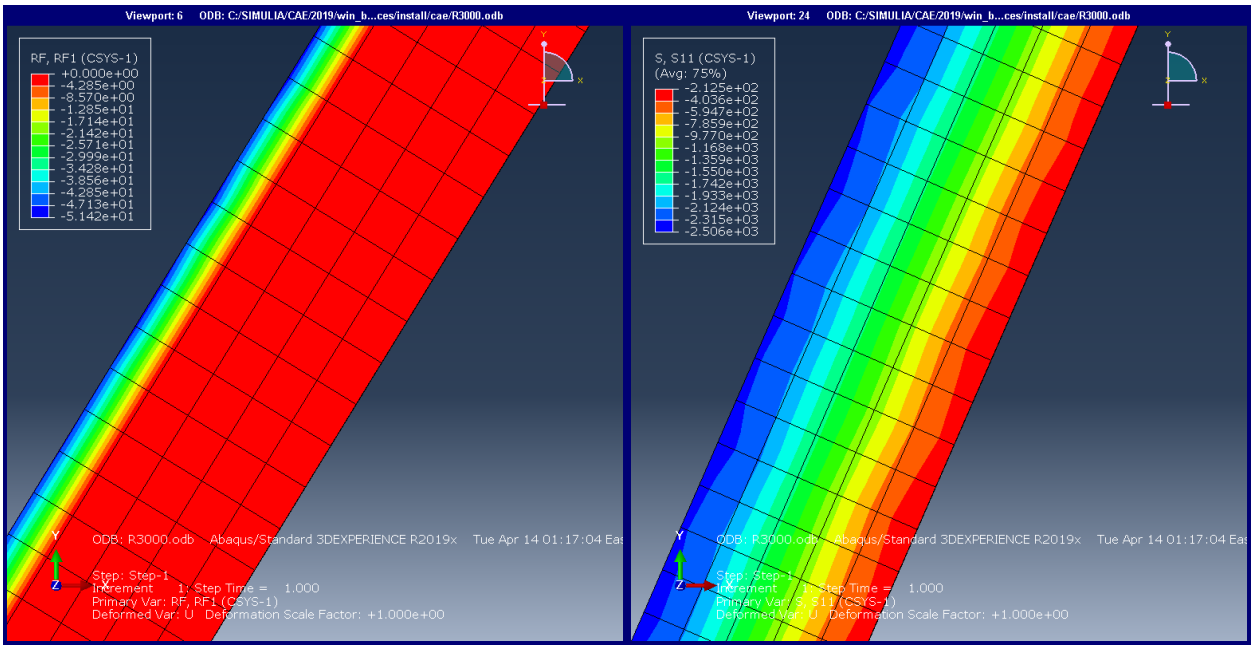

Figure A - 44: FEM Ring Model for R = 3000 ft and T = 60 F

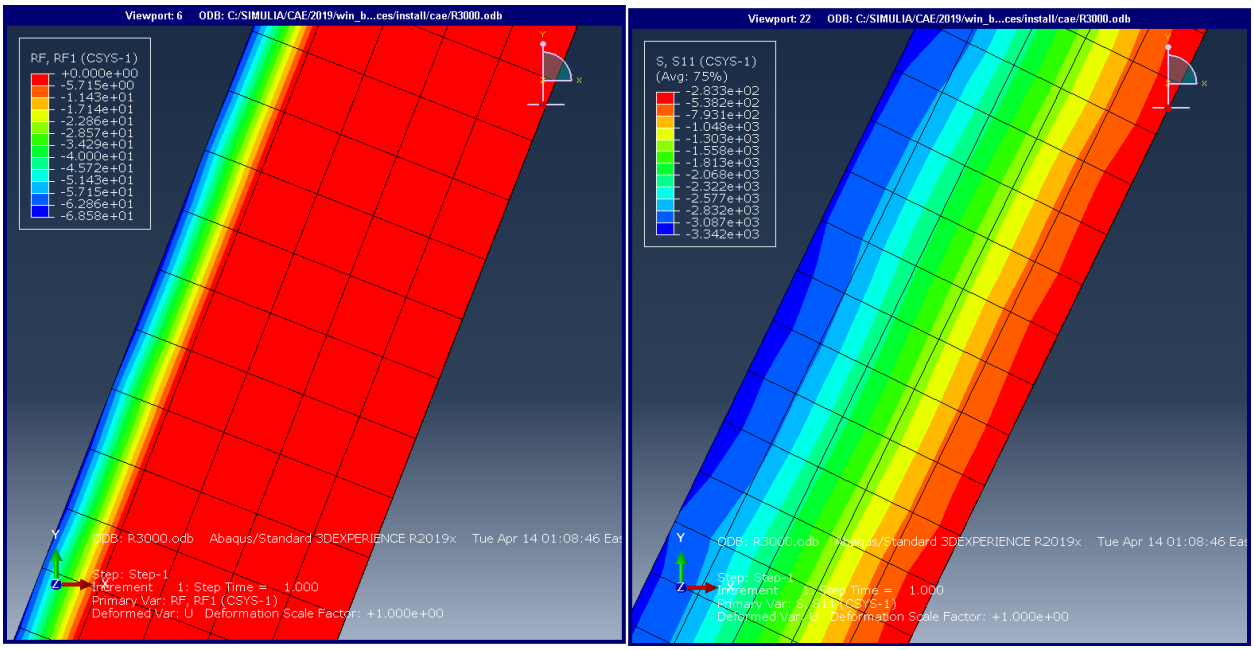

Figure A - 45: FEM Ring Model for R = 3000 ft and T = 80 F

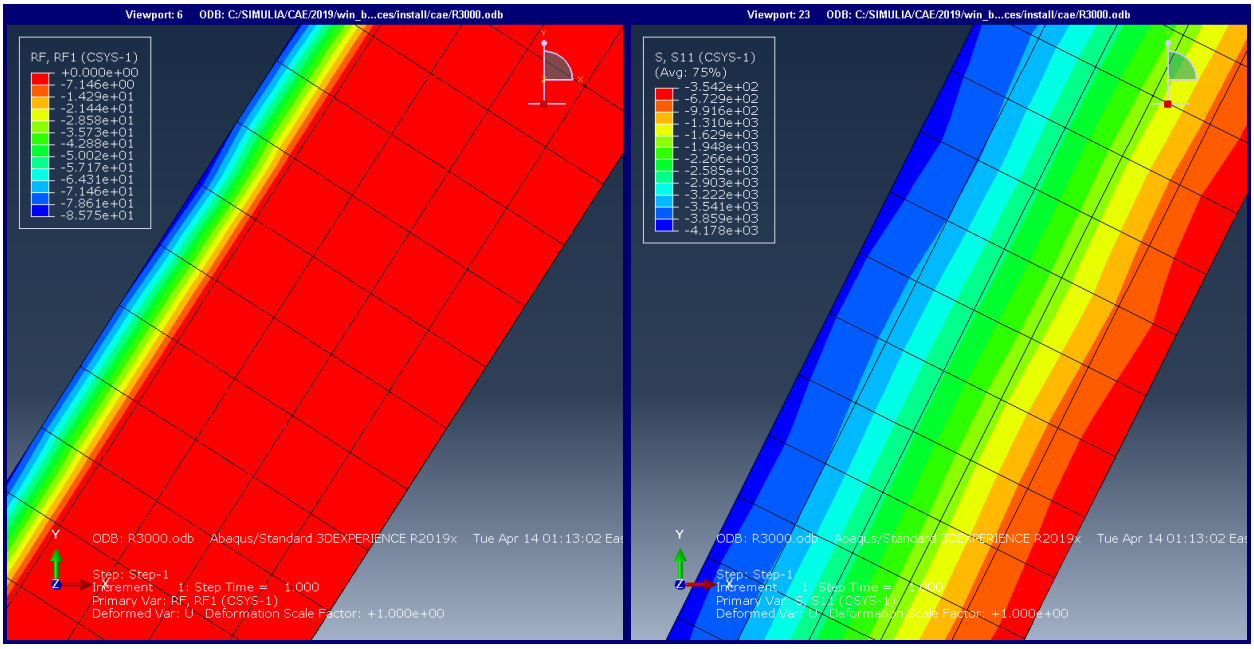

Figure A - 46: FEM Ring Model for R = 3000 ft and T = 100 F

APPENDIX B

Table B - 1: Data from Timoshenko Stress Analysis Method

Radius (ft)	TM-T0	TM-T20	TM-T40	TM-T60	TM-80	TM-T100
100	0	942	1885	2827	3769	4711
250	0	382	765	1147	1530	1912
500	0	192	384	576	768	961
750	0	128	257	385	513	641
1000	0	96	193	289	385	481
1500	0	64	128	193	257	321
2000	0	48	96	145	193	241
2500	0	39	77	116	154	193
3000	0	32	64	96	129	161

Table B - 2: Data from Thin Walled Cylinder Method

Radius (ft)	CM-T0	CM-T20	CM-T40	CM-T60	CM-80	CM-T100
100	0	965	1930	2895	3860	4825
250	0	386	772	1158	1544	1930
500	0	193	386	579	772	965
750	0	129	257	386	515	643
1000	0	97	193	290	386	483
1500	0	64	129	193	257	322
2000	0	48	97	145	193	241
2500	0	39	77	116	154	193
3000	0	32	64	97	129	161

Table B - 3: Data from Variational Formulation Method

Radius (ft)	VM-T0	VM-T20	VM-T40	VM-T60	VM-80	VM-T100
100	0	965	1930	2895	3860	4825
250	0	386	772	1158	1544	1930
500	0	193	386	579	772	965
750	0	129	257	386	515	643
1000	0	97	193	290	386	483
1500	0	64	129	193	257	322
2000	0	48	97	145	193	241
2500	0	39	77	116	154	193
3000	0	32	64	97	129	161

Table B - 4: Data from Finite Element Analysis Method

Radius (ft)	FEM-T0	FEM-T20	FEM-T40	FEM-T60	FEM-T80	FEM-T100
100	0	1001	2002	3006	4008	5012
250	0	392	783	1175	1568	1960
500	0	195	390	585	780	976
750	0	130	260	390	521	651
1000	0	98	195	293	390	488
1500	0	66	131	197	263	328
2000	0	49	98	149	198	248
2500	0	41	81	122	163	204
3000	0	34	68	102	137	171

ACKNOWLEDGEMENT

This study was conducted with the support from the USDOT Tier 1 University Transportation Center on Railroad Sustainability and Durability.

ABOUT THE AUTHORS

Jubair Ahmad Musazay, MCE

Jubair Ahmad Musazay is currently a graduate research assistant at the University of Delaware under the guidance of Professor Allan Zarembski. His research is focused on determination of track-induced net lateral forces on curved railway tracks. Hailing from Afghanistan, he has briefly worked in both industry and academia in his country of origin in the field of railroad engineering. He has obtained a Master of Civil Engineering with concentration in structure and a Graduate Certificate in Railroad Engineering from the University of Delaware in 2017.

Dr. Allan M. Zarembski, P.E., Hon. Mbr. AREMA, FASME

Dr. Zarembski is an internationally recognized authority in the fields of track and vehicle/track system analysis, railway component failure analysis, track strength, and maintenance planning. Dr. Zarembski is currently Professor of Practice and Director of the Railroad Engineering and Safety Program at the University of Delaware's Department of Civil and Environmental Engineering, where he has been since 2012. Prior to that he was President of ZETA-TECH, Associates, Inc. a railway technical consulting and applied technology company, he established in 1984. He also served as Director of R&D for Pandrol Inc., Director of R&D for Speno Rail Services Co. and Manager, Track Research for the Association of American Railroads. He has been active in the railroad industry for over 40 years.

Dr. Zarembski has PhD (1975) and M.A (1974) in Civil Engineering from Princeton University, an M.S. in Engineering Mechanics (1973) and a B.S. in Aeronautics and Astronautics from New York University (1971). He is a registered Professional Engineer in five states. Dr. Zarembski is an Honorary Member of American Railway Engineering and Maintenance of way Association (AREMA), a Fellow of American Society of Mechanical Engineers (ASME), and a Life Member of American Society of Civil Engineers (ASCE). He served as Deputy Director of the Track Train Dynamics Program and was the recipient of the American Society of Mechanical Engineer's Rail Transportation Award in 1992 and the US Federal Railroad Administration's Special Act Award in 2001. He was awarded The Fumio Tatsuoka Best Paper Award in 2017 by the Journal of Transportation Infrastructure Geotechnology.

He is the organizer and initiator of the Big Data in Railroad Maintenance Planning Conference held annually at the University of Delaware. He has authored or co-authored over 200 technical papers, over 120 technical articles, two book chapters and two books.

Joseph W. Palese, PhD, MBA, PE

Dr. Palese is a Senior Scientist and Program Manager: Railroad Engineering and Safety Program at the University of Delaware. He has over 30 years of experience in track component design and analysis, failure analysis and component life forecasting algorithm specifications, and development of inspection systems. Throughout his career, Dr. Palese has focused on acquiring and utilizing large amounts of track component condition data for planning railway maintenance

activities. Dr. Palese has completed his Bachelor's, Master's and Doctorate in Civil Engineering from the University of Delaware, along with a MBA from Rowan University. He is a registered Professional Engineer in the state of New Jersey.